Journal for ImmunoTherapy of Cancer

BYON4228 is a pan-allelic antagonistic SIRPα antibody that potentiates destruction of antibody-opsonized tumor cells and lacks binding to SIRPγ on T cells

Mary J van Helden ,[1] Seline A Zwarthoff,[1] Roel J Arends,[1] Inge M J Reinieren-Beeren,[1] Marc C B C Paradé,[1] Lilian Driessen-Engels,[1] Karin de Laat-Arts,[1] Désirée Damming,[1] Ellen W H Santegoeds-Lenssen,[1] Daphne W J van Kuppeveld,[1] Imke Lodewijks,[1] Hugo Olsman,[2] Hanke L Matlung,[2] Katka Franke,[2] Ellen Mattaar-Hepp,[1] Marloes E M Stokman,[1] Benny de Wit,[1] Dirk H R F Glaudemans,[1] Daniëlle E J W van Wijk,[1] Lonnie Joosten-Stoffels,[1] Jan Schouten,[1] Paul J Boersema,[1] Monique van der Vleuten,[1] Jorien W H Sanderink,[1] Wendela A Kappers,[1] Diels van den Dobbelsteen,[1] Marco Timmers,[1] Ruud Ubink,[1] Gerard J A Rouwendal,[1] Gijs Verheijden,[1] Miranda M C van der Lee,[1] Wim H A Dokter,[1] Timo K van den Berg[1,2]

To cite: van Helden MJ, Zwarthoff SA, Arends RJ, *et al*. BYON4228 is a pan-allelic antagonistic SIRPα antibody that potentiates destruction of antibody-opsonized tumor cells and lacks binding to SIRPγ on T cells. *Journal for ImmunoTherapy of Cancer* 2023;**11**:e006567. doi:10.1136/jitc-2022-006567

► Additional supplemental material is published online only. To view, please visit the journal online (http://dx.doi.org/10.1136/jitc-2022-006567).

Accepted 26 March 2023

[1]Byondis BV, Nijmegen, Gelderland, The Netherlands
[2]Sanquin Research, Amsterdam, The Netherlands

Correspondence to
Dr Timo K van den Berg; Timo.vandenBerg@byondis.com

ABSTRACT

Background Preclinical studies have firmly established the CD47-signal-regulatory protein (SIRP)α axis as a myeloid immune checkpoint in cancer, and this is corroborated by available evidence from the first clinical studies with CD47 blockers. However, CD47 is ubiquitously expressed and mediates functional interactions with other ligands as well, and therefore targeting of the primarily myeloid cell-restricted inhibitory immunoreceptor SIRPα may represent a better strategy.

Method We generated BYON4228, a novel SIRPα-directed antibody. An extensive preclinical characterization was performed, including direct comparisons to previously reported anti-SIRPα antibodies.

Results BYON4228 is an antibody directed against SIRPα that recognizes both allelic variants of SIRPα in the human population, thereby maximizing its potential clinical applicability. Notably, BYON4228 does not recognize the closely related T-cell expressed SIRPγ that mediates interactions with CD47 as well, which are known to be instrumental in T-cell extravasation and activation. BYON4228 binds to the N-terminal Ig-like domain of SIRPα and its epitope largely overlaps with the CD47-binding site. BYON4228 blocks binding of CD47 to SIRPα and inhibits signaling through the CD47-SIRPα axis. Functional studies show that BYON4228 potentiates macrophage-mediated and neutrophil-mediated killing of hematologic and solid cancer cells in vitro in the presence of a variety of tumor-targeting antibodies, including trastuzumab, rituximab, daratumumab and cetuximab. The silenced Fc region of BYON4228 precludes immune cell-mediated elimination of SIRPα-positive myeloid cells, implying anticipated preservation of myeloid immune effector cells in patients. The unique profile of BYON4228 clearly distinguishes it from previously reported antibodies representative of agents in clinical development, which either lack recognition of one of the two SIRPα polymorphic variants (HEFLB), or cross-react with SIRPγ and inhibit CD47-SIRPγ interactions (SIRPAB-11-K322A, 1H9), and/or have functional Fc regions thereby displaying myeloid cell depletion activity (SIRPAB-11-K322A). In vivo, BYON4228 increases the antitumor activity of rituximab in a B-cell Raji xenograft model in human $SIRP\alpha_{BIT}$ transgenic mice. Finally, BYON4228 shows a favorable safety profile in cynomolgus monkeys.

Conclusions Collectively, this defines BYON4228 as a preclinically highly differentiating pan-allelic SIRPα

WHAT IS ALREADY KNOWN ON THIS TOPIC

⇒ The CD47-signal-regulatory protein (SIRP)α axis functions as a myeloid immune checkpoint and agents targeting this pathway have shown encouraging results in early clinical trials in patients with cancer.

WHAT THIS STUDY ADDS

⇒ We report the generation and preclinical characterization of a novel SIRPα blocking antibody, BYON4228. Side-by-side comparisons with other previously described SIRPα blocking antibodies show that BYON4228 has a unique and favorable preclinical profile.

HOW THIS STUDY MIGHT AFFECT RESEARCH, PRACTICE OR POLICY

⇒ BYON4228 has the potential to become a best-in-class CD47-SIRPα antagonist.

antibody without T-cell SIRPγ recognition that promotes the destruction of antibody-opsonized cancer cells. Clinical studies are planned to start in 2023.

BACKGROUND

Antibodies against tumor-associated antigens (anti-TAAs) play a prominent role in the treatment of a broad range of solid and hematologic cancers.[1] Some of the most commonly used examples of anti-TAAs include trastuzumab directed against Her2 (over)expressed on breast and other types of cancer cells, cetuximab directed against the epidermal growth factor receptor (EGFR) on various carcinoma cells, rituximab directed against CD20 expressed on malignant B cells, and daratumumab directed against CD38 on multiple myeloma cells. Generally, anti-TAAs act by a combination of target-related direct and immune-mediated mechanisms. The immune-mediated mechanisms include complement-dependent cytotoxicity (CDC), effector cell-mediated antibody-dependent cellular cytotoxicity (ADCC) performed by natural killer (NK) cells and granulocytes, and antibody-dependent cellular phagocytosis (ADCP) exerted by macrophages.[2–6] Furthermore, anti-TAAs can also effectively trigger adaptive T cell-mediated immunity by facilitating cross-presentation of tumor antigens to cytotoxic T lymphocytes.[7] All these immune effector cell responses are triggered by the Fc regions of anti-TAAs that ligate activating Fc receptors and thereby initiate intracellular signaling and (direct or indirect) downstream tumor cell elimination. Despite this multitude of mechanisms, there remains a pertinent need to improve anti-TAAs clinical efficacy.

The CD47-signal-regulatory protein (SIRP)α axis has been firmly established as a myeloid immune checkpoint in preclinical and in early stage clinical studies.[8–12] SIRPα is a typical inhibitory immunoreceptor primarily expressed on myeloid cells, including monocytes, macrophages, granulocytes and dendritic cell subsets.[13–16] Two polymorphic variants are present in the human population, named $SIRP\alpha_{BIT}$ (also known as V1) and $SIRP\alpha_{1}$ (also known as V2). SIRPα is the only inhibitory member of a multigene receptor family with the closest homologs in humans and other primates being SIRPβ1v1, SIRPβ1v2 and SIRPγ.[17] CD47, also known as integrin-associated protein, is the cellular ligand for SIRPα and SIRPγ, but not for the two SIRPβ1 receptors.[18–22] CD47 is broadly expressed on most if not all cells in the body and is often found to be overexpressed on cancer cells.[9 10] Cellular CD47 binding to SIRPα triggers inhibitory intracellular signaling via immunoreceptor tyrosine-based inhibitory motifs in the SIRPα cytoplasmic tail involving the recruitment and activation of the tyrosine phosphatases SH2 domain-containing protein-tyrosine phosphatases (SHP)-1 and/or SHP-2, which restricts myeloid effector function.[13 15 16 23–26] Consequently, blockade of CD47-SIRPα signaling can promote macrophage-mediated and neutrophil-mediated tumor cell destruction in the presence of cancer-opsonizing antibodies, or other pro-phagocytic signals.[9–11 27–30] In addition, there is accumulating evidence that disruption of the CD47-SIRPα signaling axis promotes adaptive anticancer immunity[31 32] in combination with programmed cell death protein-1 (PD-1)/programmed death ligand-1 checkpoint inhibitors,[33 34] or other approaches such as radiotherapy that can also trigger antitumor immunity.[35]

Around 35 therapeutics directed towards the CD47-SIRPα axis have entered clinical trials in recent years.[36–38] The first clinical studies were performed with CD47-targeting agents, used as single agents or in combination with anti-TAAs or anti-PD-1, and have shown limited toxicity and promising initial efficacy.[36 37 39–41] However, conceptually there appear to be several disadvantages of targeting CD47 per se. First, CD47 is not specific for tumor cells. In fact, CD47 is widely distributed, therefore forming a large 'antigen sink' requiring high doses of drug for saturation. Furthermore, many CD47-targeting agents have Fc tails with normal effector functions, including Fc receptor binding, and this may opsonize normal cells and cause toxicity, for instance, by promoting the immune-mediated destruction of such healthy cells. Indeed, anemia and thrombocytopenia are common side effects of CD47 targeting agents with functional Fc regions, often requiring red blood cell transfusion, even though a low-dose priming strategy has been adopted to mitigate this to some extend.[36 39] Finally, CD47 does not only bind SIRPα but it also mediates functional interactions with integrins,[22 42] vascular endothelial growth factor-2[43] thrombospondin-1[44] and SIRPγ,[45] and these may be affected by CD47-targeting agents too. The most notable of these other CD47 ligands is SIRPγ, a close homolog of SIRPα present only in primates, which is expressed on T cells and activated NK cells.[45] CD47-SIRPγ interactions are pivotal for T-cell extravasation and activation and their disruption might therefore curtail durable antitumor immunity.[34 46–48] Thus, targeting of CD47 may not be the most optimal way to selectively antagonize CD47-SIRPα interactions and therefore therapeutic targeting of the myeloid cell-restricted SIRPα may represent a better strategy.

Currently, four therapeutic SIRPα-targeting antibodies have entered clinical development in cancer indications: BI 765063 (NCT03990233, NCT04653142, NCT05249426, NCT05446129), BI 770371 (NCT05327946; no details on the antibody nor its properties have been disclosed yet), BMS-986351 (NCT03783403, NCT05168202), and GS-0189 (NCT04502706) (also see table 1). However, most of the anti-SIRPα antibodies HEFLB, 1H9, and SIRPAB-11, which in all probability are representative for three of the clinical stage SIRPα antibodies (see table 1), have been reported to lack binding to both polymorphic SIRPα variants that are present in the human population, or they also recognize the related SIRPγ.[29 34 49–54]

Here we report the preclinical characterization of BYON4228 and a direct in vitro comparison with the three anti-SIRPα antibodies HEFLB, 1H9 and SIRPAB-11.

Table 1 Properties of anti-SIRPα antibodies used for in vitro comparisons

mAb	Source of sequences	Fc tail	Names of corresponding agent in clinical trials*
HEFLB	WO 2017/178653	IgG4-S228P/L445P	BI-765063 OSE-172
SIRPAB-11-K322A	WO 2020/068752	IgG1-K322A	BMS-986351 Anzurstobart CC-95251
1H9	WO 2019/023347	IgG1-N297A	GS-0189 FSI-189

*Based on data provided in Gauttier *et al*,[34] WO 2017/178653[54] and WO 2019/175218,[70] HEFLB most likely corresponds to BI-765063/OSE-172; based on identity of amino acid sequences in the publication of the International Non-proprietary Name (WHO Drug Information Vol 36 No 2 2022, p319) and WO 2020/068752,[58] SIRPAB-11-K322A corresponds to anzurstobart/BMS-986351/CC-95251; based on data provided in Liu *et al*[49] and a Forty Seven Inc. Corporate presentation of 2020,[71] 1H9 most likely corresponds to GS-0189/FSI-189.
mAb, monoclonal antibody ; SIRP, signal-regulatory protein.

BYON4228 is a pan-allelic SIRPα antibody that lacks binding to SIRPγ present on T cells. BYON4228 binds to a region overlapping with the CD47 binding site on SIRPα, thereby preventing binding of CD47 to SIRPα and blocking inhibitory signaling. BYON4228 potentiates killing and phagocytosis by human neutrophils and macrophages, respectively, of hematologic and solid tumor cells opsonized with various anti-TAAs. Silencing of the BYON4228 Fc tail prevents unwanted destruction of SIRPα-positive myeloid cells. In a human $SIRP\alpha_{BIT}$ transgenic mouse model, BYON4228 promotes rituximab-dependent elimination of Raji cells. Finally, intravenous single dose infusion of up to 100 mg/kg and repeated dose infusion of up to 30 mg/kg BYON4228 to cynomolgus monkeys is well tolerated. These data support further development of BYON4228 in clinical trials.

METHODS

Detailed methods can be found in the online supplemental materials.

BYON4228 antibody development and humanization

BYON4228 was generated by immunization of rabbits with the extracellular domains (ECDs) of SIRPα allelic variants, sequencing PCR products from selected B cells and humanization.

HEFLB, SIRPAB-11-K322A, 1H9 antibody sequences

The sources of the antibody amino acid sequences of HEFLB, SIRPAB-11-K322A (referred as SIRPAB-11 in this paper) and 1H9 (the latter generated as a G1m17,1 allotype) (also see online supplemental materials) and their presumed equivalents in clinical trials are shown in table 1.

Anti-TAAs

The following anti-TAAs were used: rituximab (MabThera, Roche), daratumumab (DARZALEX, Janssen Biologics), panitumumab (Vectibix, Amgen), cetuximab (Erbitux, Merck) and trastuzumab (Herceptin, Roche).

Cellular binding to SIRP-expressing Expi Chinese hamster ovary-S cells and primary granulocytes

Transiently transfected Expi Chinese hamster ovary-S (ExpiCHO-S) cells were first incubated for 30 min with primary antibodies and then with AF647-conjugated or R-phycoerythrin (PE)-conjugated anti-human IgG antibodies. Median fluorescent intensities were determined by flow cytometry (FACSympony or FACSVerse, BD Bioscience) or relative fluorescence units were determined (EnVision, PerkinElmer).

CD47-bead and mAb binding to U937 cells and primary cells

Peripheral blood mononuclear cells (PBMCs) or U937 cells were stained with Alexa Fluor 647-labeled antibodies and then incubated with CD47-Fc-coated fluorescent beads plus anti-CD3 allophycocyanin-H7 and anti-CD14 PerCp-Cy5.5. After 30 min and washing, the cells were analyzed using flow cytometry (FACSympony or FACSVerse, BD Bioscience).

ADCP and ADCC

ADCP was performed using confocal microscopy (CD20-positive target cells) or live cell imaging (CD20-negative target cells). Monocytes were differentiated to macrophages with macrophage colony-stimulating factor) for 7 days. Fluorescently labeled or pHrodo-labeled target cells and antibodies were added for 3–8 hours at 37°C in the presence of 100 µg/mL intra-venous immunoglobulins (IVIg). For confocal ADCP, the cells were counterstained with anti-CD19-PE and Hoechst 33342 to determine phagocytosis (ImageXpress, Molecular Devices). For live cell imaging based ADCP, images were taken every 30 or 60 min using a real-time fluorescence imager (IncuCyte, Sartorius). For ADCC, human neutrophils were isolated, activated for 30 min with 10 ng/mL granulocyte-macrophage colony-stimulating factor (GM-CSF), incubated for 4 or 20 hours with 100 µCi Cr-51 labeled target cells (effector:target ratio of 50:1), and killing was determined by analyzing the supernatant in

a scintillation counter (MicroBeta[2] Microplate Counter, PerkinElmer).

Raji xenograft in human SIRPα$_{BIT}$-severe combined immunodeficiency transgenic mice

Tumors were induced by subcutaneous (SC) injection of 2×10^7 Raji cells into the flank of female human SIRPα$_{BIT}$-severe combined immunodeficiency (scid) animals. BYON4228 was administered intraperitoneal (IP) three times a week for 4 weeks at a dose of 5 mg/kg. Rituximab was administered at 1 mg/kg IP.

Graphical representation, curve fitting and statistical analysis

Dose-response curves were fitted by non-linear regression with a variable slope (four parameters) in GraphPad Prism 9. EC_{50} or IC_{50} values were calculated in GraphPad Prism as the concentration that gives a response halfway between bottom and top of the curve. Statistical testing was performed in GraphPad Prism 9 as indicated in the figure legends. For functional assays (ADCC, ADCP), statistical analysis was performed on the 'fold enhancement' graphs. Since no values could be calculated for non-/poor-responsive donors, statistical tests were not performed on EC_{50} and IC_{50} summarizing graphs or figures 3B and 4C.

RESULTS

BYON4228 is a high affinity pan-allelic SIRPα antibody

We aimed to generate a blocking antibody against the inhibitory receptor SIRPα that binds to both the SIRPα$_{BIT}$ and SIRPα$_1$ polymorphic variants, but lacks binding to SIRPγ on human T cells. The blocking antibody should disrupt the binding of CD47 to SIRPα and inhibit CD47-induced SIRPα signaling. Rabbits were immunized with a mixture of proteins representing the ECDs of both SIRPα allelic variants and cynomolgus SIRPα. B cells from these rabbits were screened for antibody production levels, antigen binding and blocking to select B-cell clones producing antibodies that met our criteria. The variable domains of these B-cell clones were used to produce chimeric antibodies with hIgG1 backbone to allow further selection rounds. Ultimately, we selected BYON4228, a humanized antibody that met all our pre-set criteria, and compared it to three SIRPα antibodies that are considered to be representative of three clinical stage SIRPα antibodies (table 1). BYON4228 bound to both SIRPα$_{BIT}$ and SIRPα$_1$ with high affinity (table 2, figure 1A,B). Clearly, this pan-allelic characteristic was not a common property of all other SIRPα-antibodies tested. In particular we found, in line with earlier publications,[51 55] that the SIRPα antibody HEFLB did not display binding to SIRPα$_1$ (figure 1A,B). All four anti-SIRPα monoclonal antibodies (mAbs) tested (ie, BYON4228, HEFLB, SIRPAB-11 and 1H9) showed binding to SIRPβ1v1 and SIRPβ1v2, although with variable EC_{50} values (figure 1A,B). In line with its binding specificity, BYON4228 potently bound to primary SIRPα-expressing immune cells irrespective of their SIRPα-genotype (figure 1C,D). Overall, these results show that BYON4228 is a high-affinity pan-allelic SIRPα antibody that binds its native antigen on myeloid cells.

Table 2 Overview of observed affinities of BYON4228

Ligand for BYON4228	Observed affinities (K_D-obs)	
	Antigen on surface set-up	Antibody on surface set-up
Human SIRPα$_1$ ECD	<0.010 nM	1.94 nM
Human SIRPα$_{BIT}$ ECD	0.123 nM	24.3 nM
Human SIRPβ1v1 ECD	0.040 nM	8.66 nM*
Human SIRPβ1v2 ECD	3.16 nM	>100 nM†

*Kinetic parameters were estimated using a C1 chip instead of a CM5 chip (used for the other measurements).
†Fast on, fast off binding, no kinetic parameters could be estimated.
ECD, extracellular domain; NB, no binding; SIRP, signal-regulatory protein .

BYON4228 binds to a conserved epitope on the CD47-binding domain of SIRPα and blocks signaling

The extracellular region of SIRPα consists of three immunoglobulin superfamily (IgSF) domains and the first N-terminal V-set IgSF domain mediates binding to CD47.[21] To identify the domain to which BYON4228 binds, we took advantage of the finding that BYON4228 lacks binding to SIRPγ (online supplemental figure S1A, table 3) and generated various chimeric SIRPα-SIRPγ domain swapped proteins. Binding of BYON4228 to these chimeric proteins could only be detected when domain 1 was derived from SIRPα, but not from SIRPγ. The origin of domain 2 and 3 was irrelevant for BYON4228 binding, showing that SIRPα domain 1 is both essential as well as sufficient for BYON4228 binding. Therefore, the BYON4228 epitope is present within this domain (online supplemental figure S1A). To define in more detail the epitope of BYON4228, we employed hydrogen deuterium exchange mass spectrometry technology. This method relies on the hydrogen to deuterium exchange, which occurs when molecules are incubated in heavy water. When a protein is complexed with an antibody, the deuterium uptake is hampered in the binding region, which can be measured using mass spectrometry. Using this method, BYON4228 binding signals were detected in the regions between residues 26–40, 50–62 and 95–103 (online supplemental figure S1B) of both SIRPα$_{BIT}$ and SIRPα$_1$. For visualization, the epitope was projected onto the N-terminal Ig-like CD47-binding domain of SIRPα$_{BIT}$ and SIRPα$_1$, previously resolved by X-ray crystallography.[21 56] A large overlap with the CD47 binding site was noted (figure 2). The binding site covered almost exclusively non-polymorphic amino acid residues (online supplemental figure S1C), in line with the potent binding of BYON4228 to both SIRPα$_{BIT}$ and SIRPα$_1$. In conclusion, these results show that the BYON4228 epitope maps

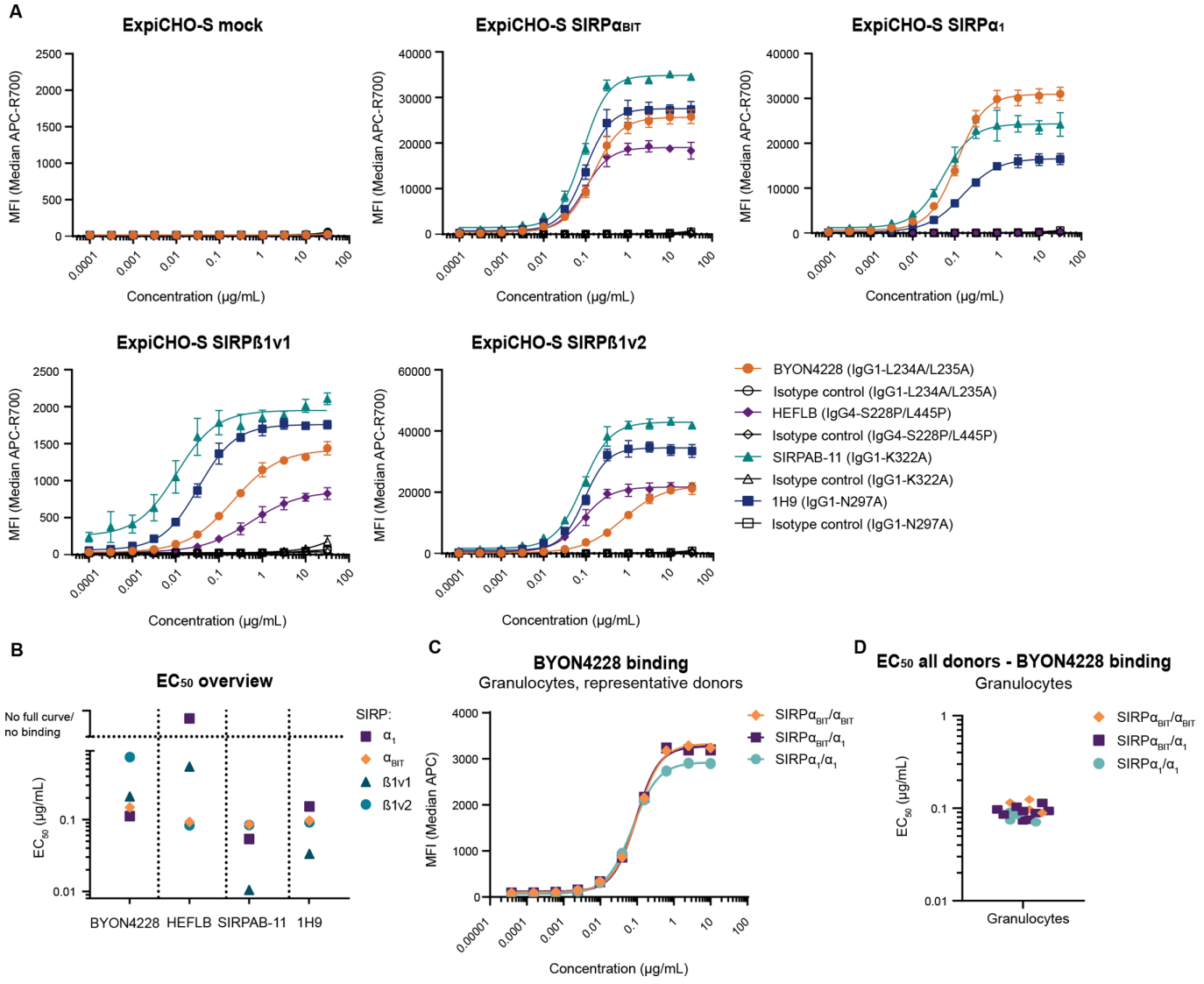

Figure 1 BYON4228 is a high affinity pan-allelic SIRPα binding antibody. (A,B) Binding of indicated SIRPα antibodies and respective isotype control antibodies to ExpiCHO-S cells that transiently expressed indicated SIRP molecules or were mock transfected. (A) Average median fluorescence intensity (MFI) ±SD of N=3 independent experiments are depicted. (B) Overview of the geomean EC_{50} values per antibody. (C,D) Cellular binding of BYON4228 (IgG1-L234A/L235A) to gated erythrocyte-lysed granulocytes from representative healthy donors with indicated SIRPα genotypes (C) and the EC_{50} summary of BYON4228 for all donors (N=17) (D). APC, allophycocyanin; ExpiCHO-S, Expi Chinese hamster ovary-S; SIRP, signal-regulatory protein.

to the CD47 binding site on the membrane distal domain of SIRPα.

To test the ability of BYON4228 to disrupt the interaction between SIRPα and CD47, PBMCs were incubated with fluorescent beads coated with human CD47. The CD47-beads bound to SIRPα-expressing monocytes and BYON4228 was able to inhibit such binding in a dose-dependent manner, irrespective of the SIRPα-genotype (figure 3A,B). While all four tested anti-SIRPα antibodies showed binding to primary monocytes of all SIRPα-genotypes, HEFLB was unable to inhibit CD47 binding to monocytes of $SIRP\alpha_1/\alpha_1$ donors and inhibited CD47-bead binding to monocytes of $SIRP\alpha_{BIT}/\alpha_1$ donors with limited efficacy (figure 3A,B). The binding

Table 3 Observed affinities of BYON4228 for binding to human SIRPγ

	Observed affinities (K_D-obs)	
Ligand for BYON4228	**Antigen on surface set-up**	**Antibody on surface set-up**
Human SIRPγ ECD	NB	*

*Dose-dependent very low binding responses were observed; no K_D could be estimated.
ECD, extracellular domain; NB, no binding; SIRP, signal-regulatory protein.

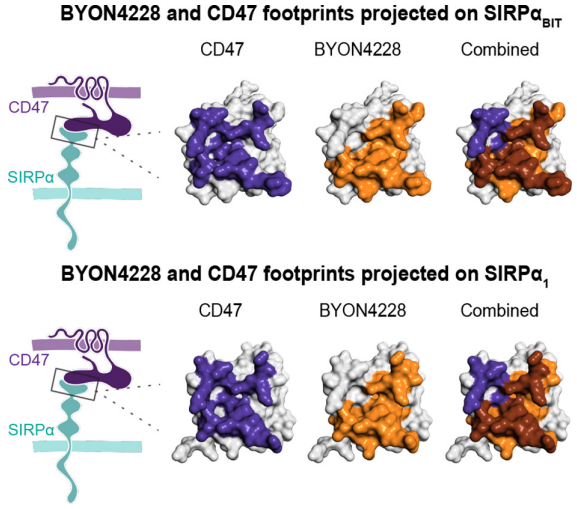

Figure 2 BYON4228 binds to the CD47-binding domain of SIRPα. (A) The BYON4228 epitope was mapped using HDX-MS. Projection of the CD47 binding site[21 56] (purple, left), BYON4228 HDX-MS mapped epitope (orange, middle) and overlap (brown, right) onto the N-terminal Ig-like CD47-binding domain of SIRPα$_{BIT}$ and SIRPα$_1$. HDX-MS, hydrogen deuterium exchange mass spectrometry; SIRP, signal-regulatory protein.

of HEFLB to monocytes from SIRPα$_1$/α$_1$ individuals (figure 3A,B) is probably due to SIRPβ1v1 and/or SIRPβ1v2 recognition by HEFLB (figure 1A,B) known to be expressed on these cells.[57] In addition, 1H9 was also found to be a poor inhibitor of CD47-bead binding to monocytes of SIRPα$_1$/α$_1$ origin (figure 3A,B). BYON4228 also inhibited the interaction between SIRPα and CD47 to background levels when using the promonocytic human cell line U937 expressing endogenous SIRPα (figure 3C).

To study the effect of BYON4228 binding on CD47-induced SIRPα-signaling, the DiscoverX PathHunter SIRPα Signaling Bioassay was used. This technology uses CD47-deficient Jurkat cells that express SIRPα$_{BIT}$ linked to an β-galactosidase enzyme donor. On ligation with cellular CD47 the enzyme acceptor-linked SHP-1 protein is recruited to SIRPα, and an active β-galactosidase enzyme is formed. Thus, the degree of SIRPα signaling can be measured in a quantitative fashion. We used Raji, SK-BR-3 and A431 cancer cells as a source of cellular CD47-ligand and found that all these cells induced a chemiluminescent signal on co-incubation with the PathHunter SIRPα-expressing Jurkat cells (figure 3D and online supplemental figure S1D). All antibodies tested were able to dose-dependently inhibit SIRPα$_{BIT}$ signaling induced by all three tested CD47-expressing cell lines to background levels (figure 3D and online supplemental figure S1D). Overall, these results show that BYON4228 binds to a conserved epitope that overlaps with the CD47-binding site on SIRPα, and constitutes a pan-allelic SIRPα blocking antibody that inhibits CD47 binding and CD47-induced SIRPα-signaling.

BYON4228 lacks binding to human T-cell expressed SIRPγ

The binding of BYON4228 and other antibodies to SIRPγ was then investigated. BYON4228 displayed no detectable binding to SIRPγ when transiently expressed on ExpiCHO-S cells and negligible/no binding to SIRPγ expressed as a soluble protein (figure 4A, table 3). In line with earlier reports,[54] HEFLB also lacked binding to SIRPγ, whereas SIRPAB-11 showed potent binding to SIRPγ-expressing cells (figure 4A). We furthermore noted, in contrast to an earlier report,[49] that 1H9 also displayed SIRPγ binding when expressed on ExpiCHO-S cells. In line with this, 1H9 also demonstrated binding to SIRPγ-expressing T cells, although with lower potency than SIRPAB-11 (figure 4B,C). Importantly, BYON4228 lacked binding to T cells altogether (figure 4B,C). CD47 is a known ligand for both SIRPα and SIRPγ[45] and indeed, CD47-coated beads showed binding to T cells of most donors. The antibodies 1H9 and SIRPAB-11 blocked CD47-bead binding to T cells, while BYON4228 and HEFLB did not alter this binding (figure 4B,C). Overall, these results show that BYON4228 lacks binding to T-cell expressed SIRPγ and accordingly does not affect CD47 binding to SIRPγ on T cells.

BYON4228 promotes ADCC and ADCP of therapeutic mAbs in a pan-allelic fashion

We then continued to investigate the functional activity of BYON4228 with respect to tumor cell killing. We first studied the impact of BYON4228 on neutrophil-mediated ADCC induced by anti-TAAs. GM-CSF-activated neutrophils were able to kill SK-BR-3 breast cancer tumor cells opsonized with trastuzumab. Addition of BYON4228 potentiated this killing in a dose-dependent and pan-allelic fashion (figure 5A–C), with an average 2.5-fold to 3.0-fold enhancement (figure 5C) of trastuzumab-induced killing at saturating BYON4228 concentrations. ADCC enhancement by BYON4228 appeared most potent (ie, lower EC$_{50}$ values) when neutrophils were of SIRPα$_1$/α$_1$ origin (EC$_{50}$ geomean of 0.10 µg/mL vs 0.19 and 0.26 for SIRPα$_{BIT}$/α$_1$ and SIRPα$_{BIT}$/α$_{BIT}$ donors, respectively). However, at saturating levels of BYON4228, ADCC enhancement was not significantly different between different SIRPα genotyped donors (figure 5C). As expected, the SIRPα$_{BIT}$-specific antibody HEFLB was unable to potentiate trastuzumab-ADCC by SIRPα$_1$/α$_1$ homozygous neutrophils. In addition, trastuzumab-ADCC enhancement of HEFLB by SIRPα$_{BIT}$/α$_1$ neutrophils was limited (1.3-fold by SIRPα$_{BIT}$/α$_1$ donors vs 3.0-fold by SIRPα$_{BIT}$/α$_{BIT}$ donors). 1H9 potentiated ADCC by SIRPα$_1$/α$_1$ neutrophils with limited efficacy (1.5-fold enhancement by SIRPα$_1$/α$_1$ donors vs 3.3-fold enhancement by SIRPα$_{BIT}$/α$_{BIT}$ donors), which was in line with its limited ability to antagonize CD47 binding to monocytes homozygous for SIRPα$_1$ (figure 3A,B). To further evaluate the broadness of its therapeutic applicability, we also determined whether BYON4228 could enhance the ADCC activity of neutrophils towards other target cells, including cetuximab-opsonized and

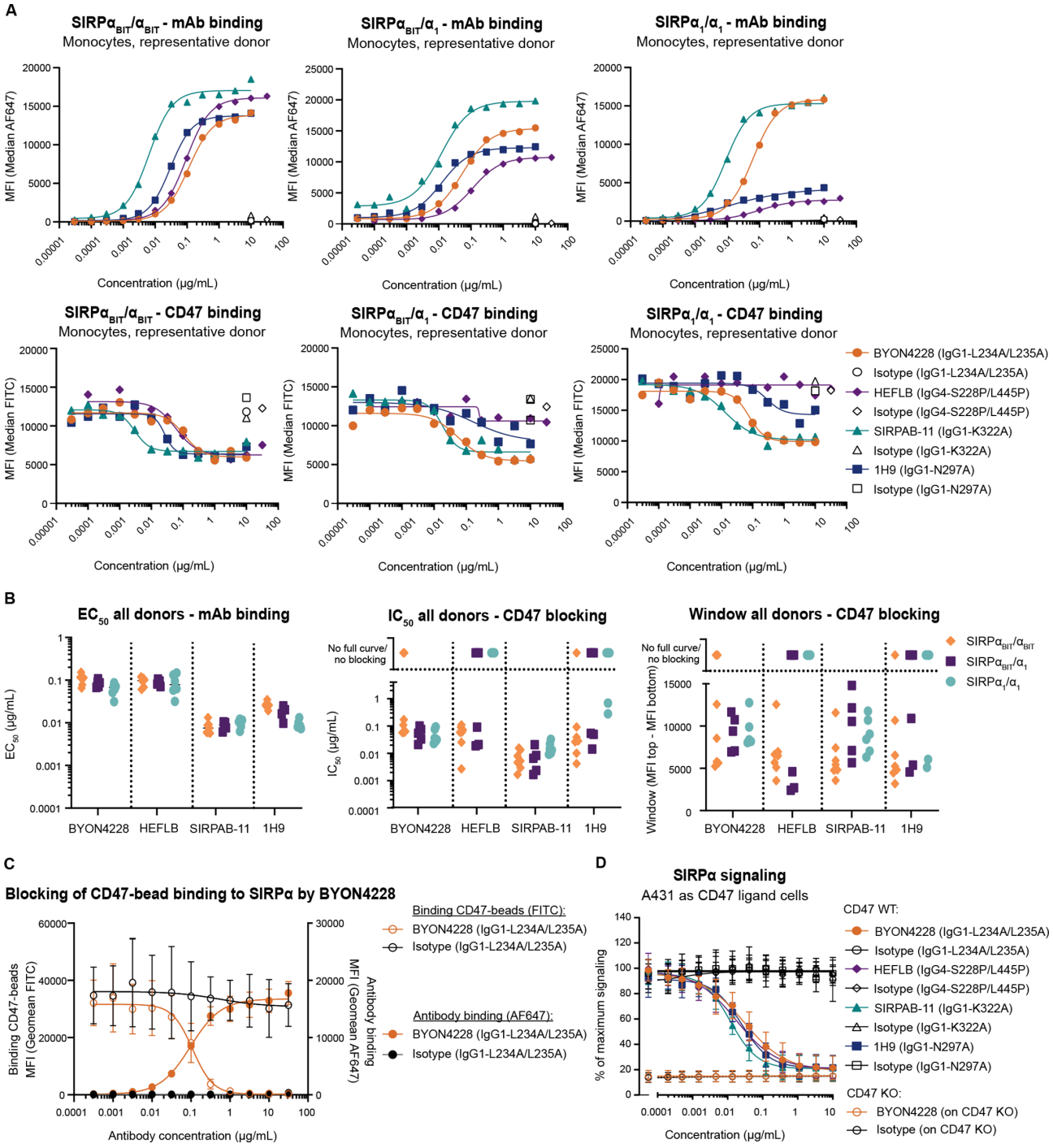

Figure 3 BYON4228 competitively blocks binding of CD47 to SIRPα. (A,B) anti-SIRP mAb binding and blockade of CD47 binding to primary monocytes. Indicated fluorescently labeled antibodies were incubated with primary peripheral blood mononuclear cells for 30 min, and then, fluorescently labeled CD47-coated beads were added. mAb binding and CD47 binding was measured on gated CD14-positive monocytes. (A) Top row depicts mAb binding and bottom row depicts CD47 binding to monocytes of representative donors with indicated SIRPα genotypes. (B) Overview of the mAb binding EC_{50} values (geomeans are depicted), blocking of CD47 binding IC_{50} values, and CD47 blocking windows (Δ MFIs) per antibody of all donors tested (seven SIRPα$_{BIT}$/$_{BIT}$, five SIRPα$_{BIT}$/α$_1$, and six SIRPα$_1$/α$_1$ donors). No IC_{50} values could be calculated from donors with incomplete curve saturation or no response as indicated in the graph. Donors that did not show a window for CD47 blocking were also indicated in the graph. (C) Graph depicts binding of CD47 coated fluorescent beads to U937 cells (left y-axis, open symbols), incubated in the presence of a dose-range of BYON4228-AF647 or AF647-labeled isotype control (right y-axis, closed symbols). Results display average binding MFIs ±SD measured in the FITC or AF647 channel of N=3 independent experiments. (D) SIRPα signaling measured using the PathHunter Jurkat SIRPα signaling reporter cell line (DiscoverX), after co-incubation with CD47-expressing or knock-out (KO) A431 cells, in presence of a concentration-range of indicated antibodies. Results are shown as mean ±SD of N=6 independent experiments. FITC, fluorescein isothiocyanate; mAb, monoclonal antibody; MFI, median fluorescent intensities; SIRP, signal-regulatory protein.

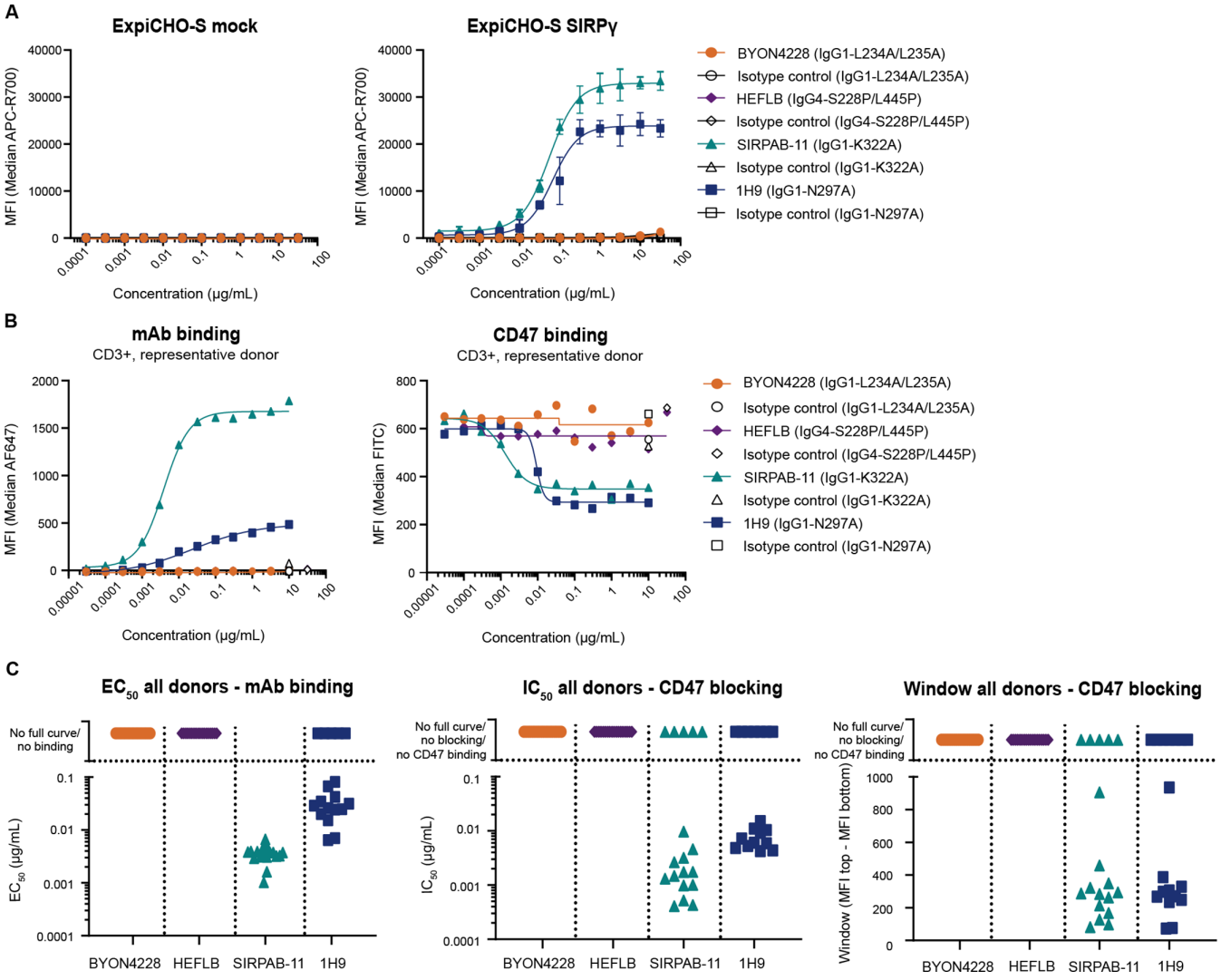

Figure 4 BYON4228 lacks binding to T-cell expressed SIRPγ. (A) Binding of indicated SIRPα antibodies and respective isotype control antibodies to ExpiCHO-S cells that transiently expressed SIRPγ or were mock transfected. Average MFI ±SD of N=3 independent experiments are depicted. (B, C) Anti-SIRP mAb binding and blockade of CD47 binding to primary CD3-positive cells. Indicated fluorescently labeled antibodies were incubated with primary peripheral blood mononuclear cells for 30 min, and then, fluorescently labeled CD47-beads were added. mAb binding and CD47 binding were measured on gated CD3-positive T cells. (B) The left graph depicts mAb binding and the right graph depicts CD47 binding of representative donors. (C) Overview of mAb binding EC_{50} values, CD47 binding IC_{50} values and CD47 blocking windows (Δ MFI) for all donors tested (N=18 donors). No EC_{50} and IC_{50} values could be calculated from donors with incomplete curve saturation or no response as indicated in the graph. While all T-cell donors showed SIRPAB-11 and 1H9 binding and thus most likely expressed SIRPγ, for four of these donors, no T-cell binding of CD47-labeled beads could be demonstrated. Therefore, no IC_{50} value and window could be determined for these four donors and as such they are shown in the top part of the graph (no CD47 binding) together with donors that showed no CD47-blocking or incomplete curve saturation. APC, allophycocyanin; ExpiCHO-S, Expi Chinese hamster ovary-S; mAb, monoclonal antibody; MFI, median fluorescent intensities; SIRP, signal-regulatory protein.

panitumumab-opsonized cancer cell lines (online supplemental figure S2). Both panitumumab (IgG2) and cetuximab (IgG1) alone were able to induce neutrophil ADCC towards the EGFR-expressing epidermoid tumor cell line A431 in a dose-dependent fashion (online supplemental figure S2A–C). BYON4228 enhanced the killing of both anti-EGFR antibodies (online supplemental figure S2E). We also tested panitumumab-induced and cetuximab-induced neutrophil ADCC of the colorectal cancer (CRC) cell line SW48 (online supplemental figure S3). Here, panitumumab consistently led to higher levels of neutrophil-induced killing when compared with cetuximab (4.5-fold vs 1.8-fold, respectively) (online supplemental figure S3C). Again, BYON4228 was able to enhance both panitumumab-induced and cetuximab-induced killing of the CRC cell line SW48 (1.7-fold vs 1.6-fold, respectively) (online supplemental figure S3E). We further tested isogenic SW48 cell lines containing frequently occurring constitutively activating mutations downstream the EGFR signaling pathway (Kirsten rat sarcoma virus (KRAS) G12D, KRAS G13D, rapidly accelerated fibrosarcoma B-type (BRAF) V600E). As expected,

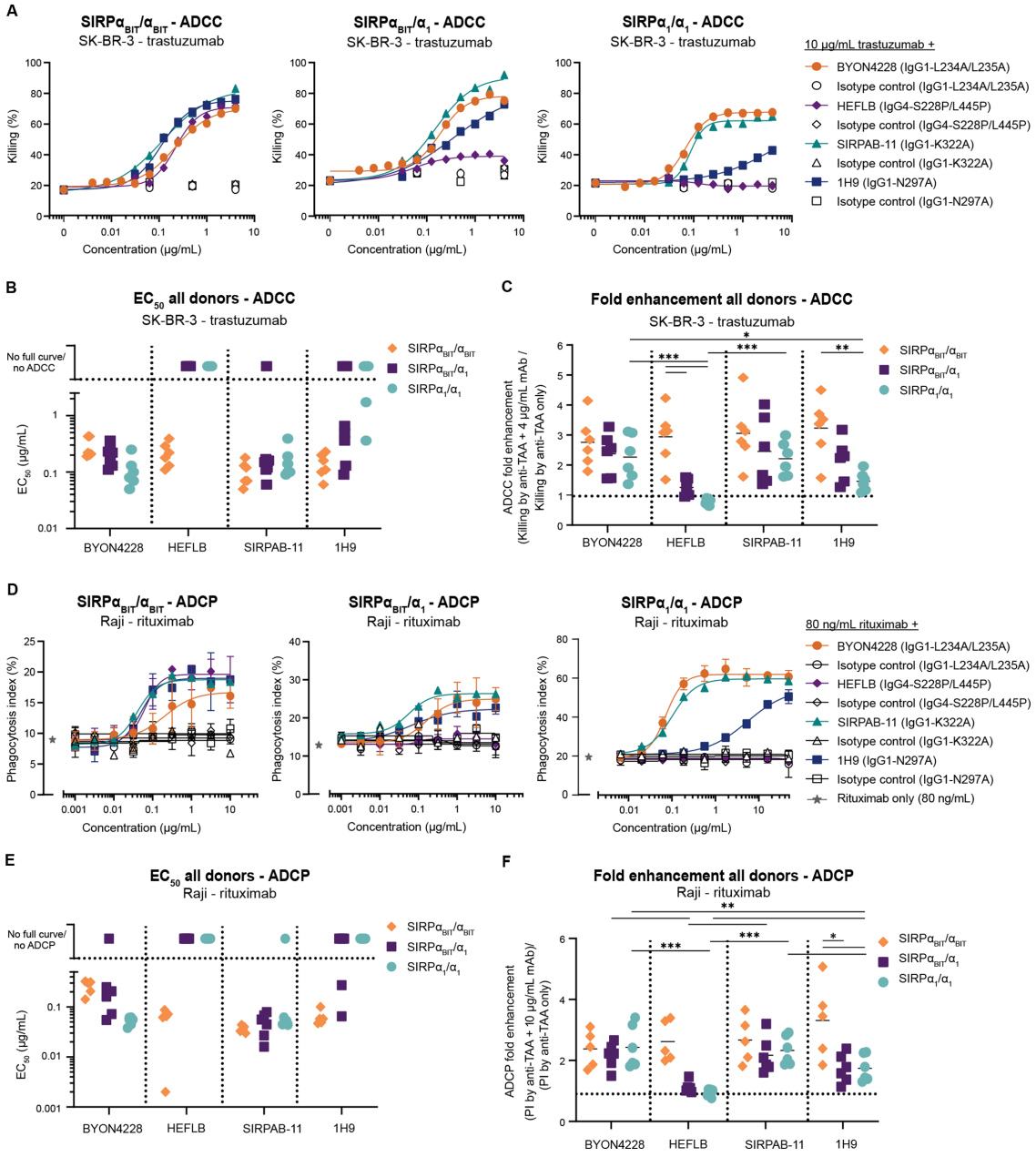

Figure 5 BYON4228 enhanced ADCC and ADCP of therapeutic mAbs in a pan-allelic fashion. (A–C) Neutrophil-mediated ADCC measured using the Cr-51 release assay after 4 hours incubation of target cells (SK-BR-3) and effector cells (primary granulocyte-macrophage colony-stimulating factor activated neutrophils) in the presence of a fixed dose of trastuzumab (10 µg/mL) and a concentration range of indicated antibodies or respective isotype controls. Donors tested: Six SIRPα$_{BIT}$/$_{BIT}$, eight SIRPα$_{BIT}$/α$_{1}$, and six SIRPα$_{1}$/α$_{1}$ donors. (A) Results show concentration-dependent SIRP-mAb induced % killing of SK-BR-3 cells by activated neutrophils of representative donors with indicated SIRPα genotypes. (B) SIRP-mAb induced ADCC EC$_{50}$ values of all donors. No EC$_{50}$ values could be calculated from donors with incomplete curve saturation, no response or incorrect curve-fitting as indicated in the graph. (C) SIRP-mAb induced ADCC fold enhancement of all donors. The means are depicted. The fold enhancement=(% killing at 10 µg/mL trastuzumab + 4 µg/mL anti-SIRPα mAb)/(% killing at 10 µg/mL trastuzumab). (D–F) Macrophage-mediated ADCP measured using confocal microscopy after 3 hours incubation of target cells (Raji) and effector cells (macrophages) in the presence of a fixed dose of rituximab (80 ng/mL) and a concentration range of indicated antibodies or respective isotype controls. Donors tested: Five SIRPα$_{BIT}$/$_{BIT}$, six SIRPα$_{BIT}$/α$_{1}$, and six SIRPα$_{1}$/α$_{1}$ donors. (D) Results show SIRP-mAb induced Phagocytosis Index (PI) of macrophages from representative donors with indicated SIRPα genotypes. (E) SIRP-mAb induced ADCP EC$_{50}$ values of all donors. No EC$_{50}$ values could be calculated from donors with incomplete curve saturation, no response or incorrect curve-fitting as indicated in the graph. (F) SIRP-mAb induced ADCP fold enhancement of all donors. The means are depicted. The fold enhancement=(PI at 80 ng/mL rituximab + 10 µg/mL anti-SIRP mAb)/(PI at 80 ng/mL rituximab). For C and F, * p<0.05, ** p<0.01, ***p<0.001; p>0.05 is not indicated. P values were calculated by one-way analysis of variance (ANOVA) for each genotype (comparing the different mAbs) and for each mAb (comparing the different genotypes) followed by Tukey's multiple comparisons test. ADCC, antibody-dependent cellular cytotoxicity; ADCP, antibody-dependent cellular phagocytosis; mAb, monoclonal antibody; SIRP, signal-regulatory protein; TAA, tumor-associated antigen.

the EGFR pathway mutant cell lines were killed by neutrophils after opsonization with panitumumab and this was further enhanced by BYON4228 (online supplemental figure S3F–H), although overall levels of killing were variable between the different cell lines, probably as a result of differences in EGFR expression levels (online supplemental table S1). The observation that BYON4228 was able to enhance the efficacy (ie, maximum killing) of panitumumab in all tested cell lines (online supplemental figure S3F–H), implies that therapeutic efficacy of a combination of panitumumab and BYON4228 might even be expected in patients that bear the indicated and other known growth-promoting mutations downstream the EGFR signaling pathway, an indication for which cetuximab and panitumumab are currently not registered/recommended.

The capacity of BYON4228 to enhance macrophage-mediated-ADCP induced by anti-TAAs was studied. CD20-expressing CellTrace Far Red labeled Raji cells (Burkitt's lymphoma) were opsonized with rituximab and phagocytosis by monocyte-derived macrophages was assessed using confocal microscopy. To ensure phagocytosis, anti-CD19 was used as a counterstain and only CD19-negative Raji cells entirely engulfed by macrophages (ie, truly phagocytosed) were counted. Rituximab-induced phagocytosis was increased by BYON4228 in a dose-dependent fashion (figure 5D–F). This synergistic effect was detected with all macrophages, irrespective of their SIRPα genotype. We noted that BYON4228 showed higher potency (ie, lower EC_{50}) when macrophages were of $SIRP\alpha_1/\alpha_1$ origin compared with $SIRP\alpha_{BIT}/\alpha_{BIT}$ macrophages (EC_{50} of 0.05 vs 0.25 µg/mL, respectively) (figure 5E). However, the fold enhancement of the Phagocytosis Index of rituximab-induced phagocytosis by $SIRP\alpha_{BIT}/\alpha_{BIT}$ donors at saturating 10 µg/mL was not significantly different when compared with $SIRP\alpha_{BIT}/\alpha_1$ or $SIRP\alpha_1/\alpha_1$ donors (figure 5F). The $SIRP\alpha_{BIT}$-specific blocking antibody HEFLB was again not or only hardly capable of enhancing rituximab-induced phagocytosis by $SIRP\alpha_1$-homozygous or heterozygous macrophages, respectively. Similarly, 1H9 showed limited efficacy and potency for phagocytosis enhancement by $SIRP\alpha_1/\alpha_1$ and $SIRP\alpha_{BIT}/\alpha_1$ macrophages. Remarkably similar results were found when Daudi cells (non-Hodgkin's lymphoma) were used in combination with daratumumab (anti-CD38) (online supplemental figure S4A–C). We also studied phagocytosis in an alternative live-cell imaging-based phagocytosis assay that relied on pHrodo-labeled tumor cells turning bright red on phagocytosis (movie in online supplemental files 7 and 8). The advantage of this method was that no counterstain (anti-CD19) was required to determine phagocytic uptake of the target cell. We again tested daratumumab-induced phagocytosis of Daudi cells and found that BYON4228 strongly enhanced uptake of target cells (online supplemental figure S4D–F). The overall potency of BYON4228 (ie, geomean EC_{50} for all donors, irrespective of the SIRPα genotype) was 0.9 µg/mL in the live-cell imaging pHrodo ADCP assay (N=16) compared with 0.09 µg/mL in the confocal ADCP assay (N=12) (online supplemental figure S4), suggesting the live-cell imaging assay was less sensitive, but was a reproducible orthogonal assay nevertheless. Using the live-cell imaging assay we furthermore studied ADCP of the CRC cell line HT-29 and found that BYON4228 was able to enhance panitumumab-induced and cetuximab-induced phagocytosis (online supplemental figure S5). Altogether, BYON4228 showed functional activity in both neutrophil ADCC and macrophage ADCP assays, indicating its ability to enhance tumor cell killing by myeloid cells.

The BYON4228 silenced Fc tail avoids opsonization and destruction of SIRPα-expressing myeloid cells

With respect to the therapeutic activity of anti-SIRPα antibodies, which relies on anticancer activity of SIRPα-expressing myeloid immune effector cells, it would be undesirable if such SIRPα-expressing cells were depleted through anti-SIRPα Fc mediated processes like CDC, ADCC or ADCP in vivo. Such depletion might compromise both the safety and efficacy of the therapeutic anti-SIRPα antibody. To prevent this, BYON4228 was designed with an IgG1 Fc tail containing L234A/L235A mutations in the Fc tail (abbreviated as 'LALA'-tail). As expected, BYON4228 displayed strongly decreased binding to FcγRs when compared with its counterpart with wild type (WT) IgG1 backbone without the LALA mutations (IgG1) (online supplemental table S2). Consistent with this, BYON4228 was unable to induce macrophage-mediated phagocytosis of the SIRPα-expressing acute myeloid leukemia (AML) tumor cell line OCI-AML2, whereas the WT IgG1 variant (BYON5664) and anti-CD47 WT IgG1 clearly induced phagocytosis (figure 6A–C). Notably, SIRPAB-11, which contains an IgG1-tail with the K322A modification (designed for reduction of complement activation[58]), also induced ADCP of the OCI-AML2 cells. In line with its inability to induce phagocytosis of SIRPα-positive cells, BYON4228 did not induce NK cell-mediated ADCC of SIRPα-expressing target cells, whereas NK cell induced ADCC was observed by the IgG1 variant (online supplemental figure S6A). Both BYON4228 and its IgG1 variant did not induce CDC of the SIRPα-expressing cell lines U937 and MOLM-13, whereas anti-CD47 (IgG1) induced potent lysis of these cells after incubation with active serum (online supplemental figure S6B). Overall, these data show that the silent Fc tail of BYON4228 prevents destruction of SIRPα-expressing cells by different immune-mediated mechanisms.

Optimal enhancement of anti-TAA-induced ADCC and ADCP by BYON4228 is independent of its Fc functionality

For optimal efficacy, it was suggested previously that the Fc tail of SIRPα-blocking antibodies should not be able to bind to FcγRs on myeloid effector cells in cis to avoid competition with the tumor-opsonizing antibody-FcγR interaction and hence reduced tumor cell destruction, a phenomenon also known as the 'scorpion effect'.[51 59] To examine the influence of the Fc tail for BYON4228

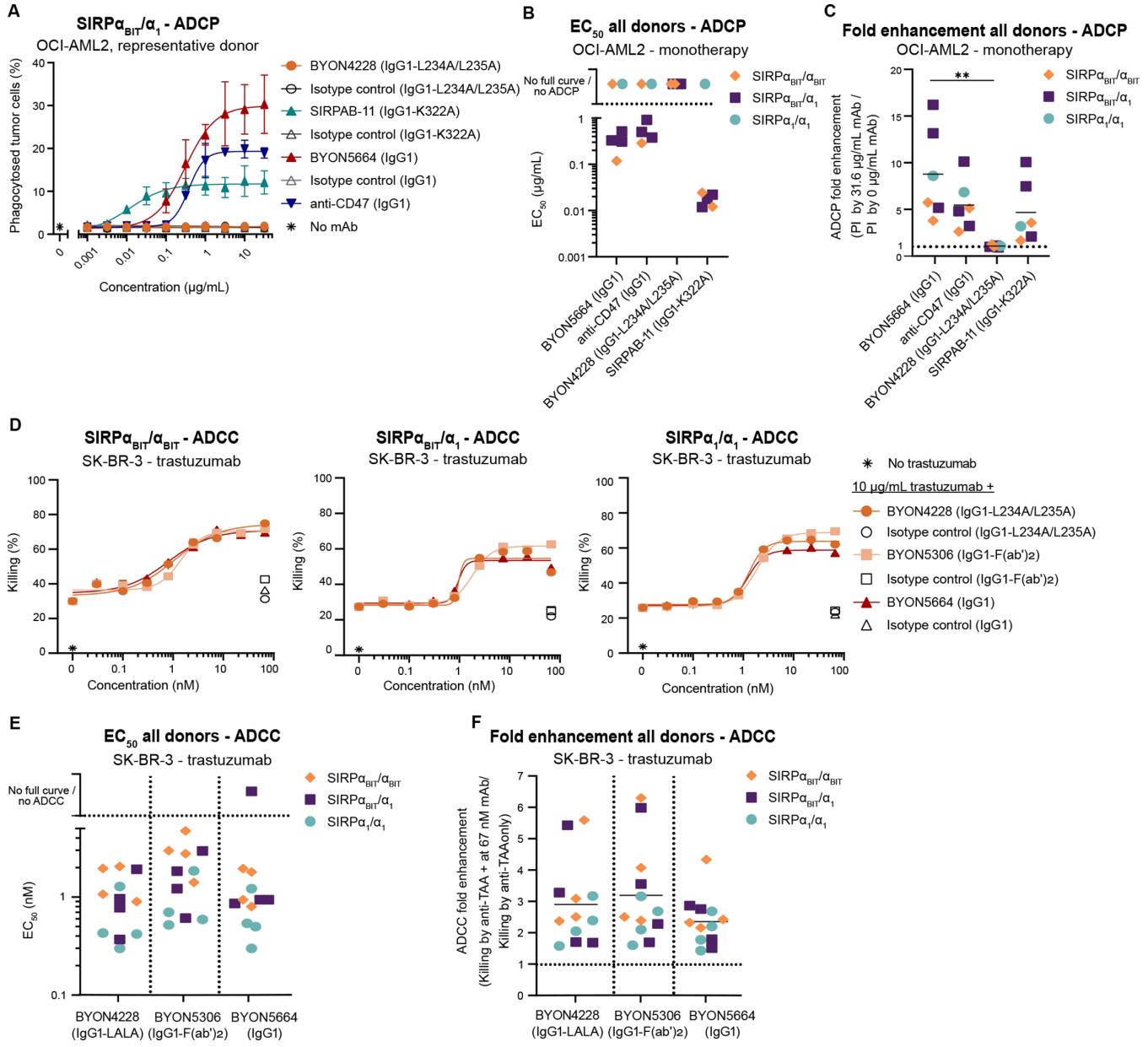

Figure 6 Potent and efficacious enhancement of anti-TAA-induced ADCC and ADCP with BYON4228 having a hIgG1-L234A/L235A Fc tail. (A–C) Macrophage mediated ADCP measured using the live-cell imaging pHrodo ADCP assay after incubation of target cells (OCI-AML2) and effector cells (macrophages) in the presence of a concentration range of indicated antibodies or respective isotype controls. BYON5664 contains the variable domains of BYON4228 but has a wildtype IgG1 constant domain with wildtype effector functions. Donors tested: Two SIRPα$_{BIT}$/α$_{BIT}$, three SIRPα$_{BIT}$/α$_1$, and one SIRPα$_1$/α$_1$ donors. (A) Results show % phagocytosed tumor cells by macrophages from a representative donor. No mAb=effector+target cells only. (B) ADCP EC$_{50}$ values of all donors. No EC$_{50}$ values could be calculated from donors with incomplete curve saturation, no response or incorrect curve-fitting as indicated in the graph. (C) The ADCP fold enhancement of all donors. The means are depicted. The fold enhancement=(% phagocytosed cells at 31.6 µg/mL anti-SIRP)/(% phagocytosed cells at effector+target). (D–F) Neutrophil-mediated ADCC measured using the Cr-51 release assay after 4 hours incubation of target cells (SK-BR-3) and effector cells (primary granulocyte-macrophage colony-stimulating factor activated neutrophils) in the presence of a fixed dose of trastuzumab (10 µg/mL) and a concentration range of indicated antibodies or respective isotype controls. BYON5306 is the F(ab')$_2$ fragment of BYON4228. Donors tested: four SIRPα$_{BIT}$/α$_{BIT}$, four SIRPα$_{BIT}$/α$_1$, and four SIRPα$_1$/α$_1$ donors. (D) Results show % killing of SK-BR-3 cells by activated neutrophils of representative donors with indicated SIRPα genotypes. (E) SIRP-mAb or -F(ab')$_2$ induced ADCC EC$_{50}$ values of all donors. No EC$_{50}$ values could be calculated from donors with incomplete curve saturation, no response or incorrect curve-fitting as indicated in the graph. (F) SIRP-mAb induced ADCC fold enhancement of all donors. The means are depicted. The fold enhancement=(% killing at 10 µg/mL trastuzumab+67 nM anti-SIRPα mAb)/(% killing at 10 µg/mL trastuzumab). For C and F, *p<0.05, **p<0.01, ***p<0.001; p>0.05 is not indicated. P values were calculated by one-way analysis of variance (ANOVA) followed by Tukey's multiple comparisons test. ADCC, antibody-dependent cellular cytotoxicity; ADCP, antibody-dependent cellular phagocytosis; AML, acute myeloid leukemia; mAb, monoclonal antibody; SIRP, signal-regulatory protein; TAA, tumor-associated antigen.

for optimal in vitro ADCC and ADCP, we generated a fragment antigen-binding region ($F(ab')_2$) version of BYON4228, which was still able to block CD47-SIRPα axis signaling to the same extent as intact BYON4228 (online supplemental figure S6C). We performed similar side-by-side comparisons to determine enhancement of anti-TAA-induced neutrophil ADCC. BYON4228 was able to enhance trastuzumab-induced ADCC of SK-BR-3 cells with a similar potency and efficacy when the Fc tail was lacking (figure 6D–F). Even when the Fc tail of BYON4228 was replaced with a human WT IgG1 tail (IgG1), ADCC potency and efficacy of enhancement were similar (figure 6D–F). Similar results were also obtained when the BYON4228 variants were tested for enhancement of cetuximab-induced ADCC of A431 cells (online supplemental figure S6D–F). The $F(ab')_2$ fragment of BYON4228 was compared with BYON4228 in the rituximab-induced macrophage ADCP assay. Here again, the ability to enhance rituximab-induced phagocytosis of Raji cells was essentially indistinguishable from that of BYON4228 (online supplemental figure S7A–C). Finally, daratumumab-induced ADCP enhancement of Daudi cells was identical for BYON4228 or its $F(ab')_2$ (online supplemental figure S7D–F). Overall, these data show that neither BYON4228 nor its WT IgG1 variant suffer from the 'scorpion effect', and therefore BYON4228 provides optimal enhancement of antibody-dependent tumor cell destruction by both neutrophils and macrophages.

BYON4228 improves the efficacy of rituximab in human SIRPα$_{BIT}$-scid mice in vivo

Like most anti-human SIRPα blocking antibodies, BYON4228 does not cross-react with mouse SIRPα (data not shown). To study efficacy of BYON4228 in vivo, we generated mice that expressed human SIRPα$_{BIT}$ from the Rosa26 promotor only in myeloid cells due to Cre-mediated excision of a STOP cassette (Rosa26-stop^{flox}human SIRPα$_{BIT}$ × *Cebpa*$^{Cre/+}$,[60] named huSIRPα$_{BIT}$ mice). Western blot analysis confirmed the presence of the human SIRPα glycoprotein in *Cebpa*$^{Cre/+}$ mice in conjunction with the endogenous mouse SIRPα (online supplemental figure S8A). Flow cytometry analysis showed that the mice indeed expressed human SIRPα$_{BIT}$ on monocytes and neutrophils (online supplemental figure S8B,C). Furthermore, murine neutrophils that expressed human SIRPα$_{BIT}$ enhanced trastuzumab-induced ADCC of SK-BR-3 cells in presence of an anti-SIRPα antibody (online supplemental figure S8D,E), demonstrating proper functionality of the huSIRPα$_{BIT}$ transgene in mice.

First, BYON4228 pharmacokinetic (PK) studies were performed in C57Bl/6 mice and in huSIRPα$_{BIT}$ mice. In C57Bl/6 mice, a low clearance of BYON4228 was noted, while in huSIRPα$_{BIT}$ mice, a threefold higher clearance (based on area under the curve $(AUC)_{last}$) was observed after intravenous or IP administration of a low dose (3 mg/kg) BYON4228 (online supplemental figure S8F,G and online supplemental table S3 and S4). This difference in drug clearance is most likely due to target-mediated drug disposition (TMDD). In huSIRPα$_{BIT}$ mice, the drug elimination via TMDD could be saturated by high doses (intravenous) or repeat dosing (IP) of BYON4228, leading to prolonged high plasma BYON4228 levels (online supplemental figure S8F–H).

Next, antitumor efficacy of rituximab alone or in combination with BYON4228 was studied in huSIRPα$_{BIT}$-scid mice SC xenografted with Raji tumors. No significant effects of BYON4228 alone on tumor growth were observed (one experiment, N=9 mice/group, data not shown). Rituximab treatment at 1 mg/kg significantly inhibited growth of Raji cells in huSIRPα$_{BIT}$-scid mice and this effect could be enhanced by combination treatment with BYON4228 at 5 mg/kg (figure 7A), one of two independent studies shown, N=11 mice/group). These results show that the huSIRPα$_{BIT}$-scid mouse model can be employed to study efficacy of anti-SIRPα antibodies in

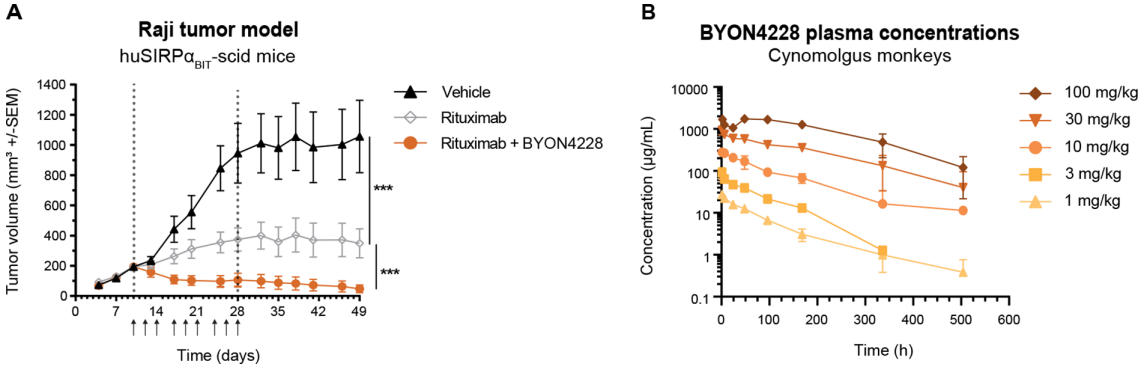

Figure 7 BYON4228 potentiates the antitumor activity of rituximab in vivo and pharmacokinetic evaluation of BYON4228 in cynomolgus monkeys. (A) Growth curve of Raji cells (subcutaneous) in female huSIRPα$_{BIT}$-scid mice treated IP with vehicle, rituximab monotherapy, or rituximab in combination with BYON4228. All compounds were administered IP three times a week (indicated by arrows between dotted lines). Rituximab was used at 1 mg/kg for monotherapy and in combination with 5 mg/kg BYON4228. N=11 per group. Statistical analysis of area under the curve from randomization to end of study; *** p<0.001, Dunnett's multiple comparison test. (B) Mean BYON4228 plasma concentrations in cynomolgus monkey after a single intravenous infusion of BYON4228 (N=2 (one female and one male) ±SD/dose group). IP, intraperitoneal; SIRP, signal-regulatory protein; scid, severe combined immunodeficiency.

vivo and, most importantly, that BYON4228 can improve tumor clearance when combined with rituximab. These data are in line with Murata *et al*, who demonstrated enhancement of the inhibitory effect of rituximab by anti-human SIRPα antibody on the growth of tumors formed by Raji cells in other human SIRPα transgenic mice.[61]

BYON4228 has a favorable preclinical safety profile

We assessed the safety of BYON4228 in vitro. BYON4228 did not display hemolytic activity, it did not induce red blood cell (RBC) clumping and it was compatible with human plasma in vitro (data not shown). At concentrations of 1 up to 100 µg/mL, BYON4228 did not induce any biologically significant increases in a panel of 18 cytokines/chemokines measured (data not shown). A toxicological evaluation of BYON4228 was performed in cynomolgus monkeys. We noticed that BYON4228 displayed potent binding to SIRPα-positive granulocytes of most cynomolgus monkeys (online supplemental figure S9A,B). Individual monkeys that displayed no or very poor BYON4228 binding were deselected for toxicity studies. The selected individuals had an average 3.5-fold more potent binding (3.5-fold lower EC_{50}) compared with that in man (0.03 µg/mL, online supplemental figure S9B vs 0.09 µg/mL, figure 1D), supporting the relevance of cynomolgus monkey for the human risk assessment of BYON4228. Intravenous infusion of BYON4228 was well tolerated as a single dose up to 100 mg/kg. PK profiles in monkeys showed almost dose linear increase in exposure. One week after dosing, variability is observed in the PK curves due to the induction of immunogenicity as was confirmed by the observation of anti-drug antibodies (figure 7B, online supplemental table S5 and data not shown). In the 5-cycle repeated dose toxicity study in monkey, where 3, 10 or 30 mg/kg BYON4228 was infused intravenously one time a week, BYON4228 showed comparable PK profiles and was well tolerated with no adverse effects on body weight and no clinical evidence of toxicity including safety pharmacology endpoints (cardiovascular, respiratory, and central nervous system) (data not shown). In addition, no effects on hemoglobin levels, RBC count or platelets were noted (online supplemental figure S9C–E). When comparing the measured SIRPα receptor occupancy (RO) data with the observed exposure levels, the data show that >80%–90% RO (needed for 100% efficacy in ADCC and ADCP assays in vitro, data not shown) can be reached at plasma concentrations around 2 µg/mL BYON4228 based on limited data. The mean C_{trough} of BYON4228 following the first dose in the 5-cycle toxicity study ranged from 15.8 µg/mL to 285 µg/mL for the 3–30 mg/kg doses indicating that the >80% RO had been reached over the entire dosing interval. Based on the 5-cycle study, the No Adverse Effect Level (NOAEL) was considered to be the highest dose tested, 30 mg/kg. At this repeated dose, the exposure is 165,000 hours × µg/mL for males and 179,000 hours × µg/mL for females.

DISCUSSION/CONCLUSION

The CD47-SIRPα myeloid immune checkpoint has been identified as a promising therapeutic target to promote tumor destruction in combination with anti-TAAs and other therapeutics.[9 38] Blockade of CD47-SIRPα signaling can stimulate destruction of antibody-opsonized cancer cells by innate immune cells, in particular by macrophage ADCP and neutrophil ADCC. Furthermore, disruption of CD47-SIRPα interactions triggers adaptive T cell-mediated anticancer immunity, probably, at least in part, by enhancing cross-presentation by SIRPα-expressing dendritic cells. Currently, a number of agents targeting CD47 or SIRPα are in clinical development. The vast majority of these agents are targeting CD47 and the most advanced ones have already shown encouraging safety/efficacy profiles in early clinical studies.[36 37 39 41] Nevertheless, as outlined above there are a number of disadvantages of targeting CD47, and this may therefore not be the most optimal and selective way to antagonize CD47-SIRPα interactions therapeutically. Notably, the disruption of CD47-SIRPγ interactions, which are critical for T-cell extravasation and activation,[34 46–48] might curtail durable adaptive antitumor immunity.

As an alternative strategy, therapeutic agents have been developed that target SIRPα[29 34 49–53 55] and at present four of such drugs are, or have been, in early clinical development. Preclinical data of HEFLB, SIRPAB-11, and 1H9, most likely corresponding to BI 765063 (formerly OSE-172), BMS-986351 (anzurstobart, formerly CC-95251), and GS-0189 (formerly FSI-189) (table 1), respectively, have been reported.[34 49 58] However, we have shown here that these SIRPα blocking antibodies, like several others that have been reported,[50–53 55] either fail to recognize both of the two SIRPα polymorphic variants present in the human population, or they cross-react with SIRPγ.

Here we preclinically characterize BYON4228, a novel anti-SIRPα antibody, and perform direct in vitro comparisons with HEFLB, SIRPAB-11, and 1H9. Our results identify BYON4228 as a highly differentiating antibody, which recognizes both of the two polymorphic variants $SIRP\alpha_{BIT}$ and $SIRP\alpha_1$. BYON4228 efficiently inhibits CD47 binding to primary myeloid cells from individuals with all three genotypes (ie, $SIRP\alpha_{BIT}$-homozygotes and $SIRP\alpha_1$-homozygotes and $SIRP\alpha_{BIT}$/$SIRP\alpha_1$-heterozygotes). The antagonistic activity of BYON4228 can be explained by direct competition with CD47 binding, as the BYON4228 epitope strongly overlaps with the previously described CD47 binding site on both of the SIRPα variants.[21] In line with this, BYON4228 prevents inhibitory signaling via the CD47-SIRPα axis, and promotes neutrophil ADCC and macrophage ADCP using immune effector cells from individuals of all three SIRPα genotypes. In contrast, HEFLB lacks binding to $SIRP\alpha_1$ and, as a consequence, the ability to reduce CD47 binding to $SIRP\alpha_1$ homozygous myeloid cells, and clearly fails to enhance ADCC and ADCP by $SIRP\alpha_1$ homozygous myeloid immune effector cells. Notably, HEFLB also appears to be only a partial inhibitor of CD47 binding by $SIRP\alpha_{BIT}$/$SIRP\alpha_1$

heterozygote myeloid cells, and, if anything, only a weak stimulator of ADCC and ADCP, mediated by, respectively, neutrophils and macrophages from such heterozygous individuals. These findings are also supported by previous reports.[51 55] These properties will likewise compromise the applicability of BI 765063/OSE-172, the probable corresponding agent of HEFLB in clinical development, in more than half (range: 51–88%) of all major ethnic patient populations.[50] Surprisingly, and in contrast to its reported pan-allelic functionality,[49] our data revealed that 1H9, and likewise its putative clinical equivalent GS-0189/FSI-189, exhibits only weak binding to SIRPα$_1$ on primary myeloid cells and it displays only partial inhibition of CD47 binding to SIRPα$_1$/α$_1$ homozygote cells accordingly. In contrast to this, Liu *et al* reported comparable binding of 1H9 to plate-coated soluble SIRPα$_1$-Fc and SIRPα$_{BIT}$ -Fc proteins. Indeed, we also noted similar binding potency of 1H9 to SIRPα$_1$ and SIRPα$_{BIT}$ expressed on ExpiCHO-S cells at high levels. However, the poor binding of 1H9 to SIRPα$_1$ become apparent when using primary human monocytes. Consistent with this, we noted limited potency of 1H9 when using SIRPα$_1$-homozygous cells in ADCC/ADCP assays using various target cell lines and anti-TAA combinations with many different donors, while Liu *et al* showed enhancement of cetuximab-induced ADCP of HT-29 cells by macrophages derived from SIRPα$_1$/α$_1$ donors, although only two donors were reported. The first-in-human study with GS-0189/FSI-189 (NCT04502706) was terminated after inclusion of a limited number of patients.

We also studied binding of the different mAbs to SIRPγ, a closely related homolog of SIRPα. BYON4228 lacked binding to SIRPγ, nor did affect CD47 binding to SIRPγ-expressing T cells. This may, as indicated, be instrumental to preserve optimal antitumor T-cell immunity. Instead, SIRPAB-11 and 1H9, and likewise their respective putative clinical equivalents BMS-986351/CC-95251 and GS-0189/FSI-189, clearly recognize SIRPγ, and also inhibit CD47 binding to primary T cells. While 1H9 was described not to bind to T cells,[49] only a narrow window of detection for the positive control was evident in the reported ELISA, possibly explaining the discrepancy with our findings.

BYON4228 was engineered with a modified L234A/L235A IgG1 Fc tail with strongly reduced Fc receptor binding to avoid non-desirable immune-mediated elimination of SIRPα-expressing myeloid cells,[62] which could both undermine the antitumor promoting effects of the drug, as well as cause toxicity, for instance by increasing susceptibility to infections. Indeed, the L234A/L235A modification prevented macrophage ADCP and NK ADCC towards SIRPα-positive cells in the presence of BYON4228 as a single agent. In contrast, SIRPAB-11, which has been modified to reduce complement activation, but exhibits normal Fc receptor binding[63] (and data not shown), demonstrates macrophage ADCP of SIRPα-positive cells. This may also be relevant in vivo in human patients, as the first results reported with the corresponding BMS-986351/anzurstobart/CC-95251 have demonstrated treatment-related ≥grade 3 neutropenia in 9 of 17 (53%) resistant/refractory patients with non-Hodgkin's lymphoma treated with escalating doses of the antibody.[64] It seems reasonable to assume that this is related to the high Fc receptor binding capacity of this particular anti-SIRPα antibody.

For some anti-SIRPα antibodies it has been reported that having a functional Fc region also compromises their ability to promote anti-TAA-dependent elimination of tumor cells.[51 55] In particular, it was postulated that the Fc tail of these SIRPα-bound antibodies have interactions with Fc receptors on myeloid effector cells in cis and therefore compete with anti-TAA Fc receptor binding, a phenomenon also known as the 'Scorpion-effect'.[51 59 65] Interestingly, the IgG1-L234A/L235A modification of BYON4228 was not necessary for optimal functionality, since a version equipped with a WT IgG1 Fc was equally potent and efficacious to enhance neutrophil ADCC. Moreover, complete elimination of the Fc effector functions using BYON4228 F(ab')$_2$ did not improve the performance of BYON4228 either. Thus, the Fc tail of BYON4228 has an optimal design for enhancing anti-TAA-dependent cancer cell destruction, while ensuring preservation of the normal myeloid immune effector cell populations.

Apart from the above in vitro properties our results also demonstrate efficacy of BYON4228 in an in vivo Raji B-cell lymphoma xenograft model in scid mice engineered to express human SIRPα$_{BIT}$ on myeloid cells. In particular, BYON4228 enhanced the antitumor activity of the anti-CD20 mAb rituximab. These results are in line with other studies with anti-SIRPα antibodies.[61] BYON4228 also displayed a favorable toxicity profile. Treatment of cynomolgus monkeys with BYON4228 up to 100 mg/kg (single dose) and up to 30 mg/kg (repeated dosing), which demonstrated complete RO on SIRPα-positive blood cells did not show any adverse effects, including the absence of anemia and thrombocytopenia. The latter contrasts with results obtained for several of the more advanced CD47-targeting agents, including magrolimab, in both preclinical toxicity studies and clinical studies, where anemia and thrombocytopenia were clearly observed.[36 39 66 67]

Collectively, these data show that BYON4228 is a highly differentiating pan-allelic blocking anti-SIRPα antibody, which specifically lacks reactivity with SIRPγ on T cells. In doing so, BYON4228 has the principal features to potentially become a best-in-class drug. Our preclinical functional ADCC and/or ADCP experiments with a variety of target cancer cells and clinically available therapeutic anti-TAAs, including trastuzumab, cetuximab, panitumumab, rituximab and daratumumab, underline the broad potential applicability of BYON4228. This may also extend to other non-anti-TAA combinations, such as other checkpoint inhibitors,[33 34 41 49] chemotherapy[68] and radiotherapy.[35 69] First-in-human clinical studies with BYON4228 are scheduled to start in 2023.

Acknowledgements We thank the Byondis cell line development team and the downstream processing team for generation and purification of critical reagents. We thank Jos van den Crommert, Jenny Vermeer, Tinie van Boekel, Myrthe Rouwette, and Benno Ingelse from Byondis for their assistance with the conception, design and analysis of experiments. We thank Professor Dr I.P. Touw for providing the *Cebpa*$^{Cre/Cre}$ mice.

Contributors MJvH and TKvdB wrote the manuscript with input from all authors. MJvH, SAZ, RJA, HLM, KF, EM-H, DHRFG, DEJWvW, JS, WAK, DvdD, MT, RU, GJAR, GV, MMCvdL, WHAD and TKvdB contributed to the conception and development of the project. SAZ, IMJR-B, MCBCP, LD-E, KdL-A, DD, EWHS-L, DWJvK, IL, HO, HLM, KF, EM-H, MEMS, PJB and BdW performed experiments and analyzed data. DHRFG, DEHWvW, LJ-S and JS generated antibodies (fragments), recombinant proteins and cell lines. RJA, MvdV, JWHS, WAK, DvdD and RU coordinated in vivo studies and (PK) analysis. All authors read and approved the final version of the manuscript. MJvH is responsible for the overall content as guarantor.

Funding The study was sponsored by Byondis BV.

Competing interests TKvdB is inventor on WO 2009/131453; GV, GJAR, RJA, TKvdB, HLM and KF are inventors on WO 2018/210793; GV is inventor on WO 2020/099653.

Patient consent for publication Not applicable.

Ethics approval Not applicable.

Provenance and peer review Not commissioned; externally peer reviewed.

Data availability statement Data are available upon reasonable request.

ORCID iD

Mary J van Helden http://orcid.org/0000-0002-4506-4943

REFERENCES

1 Glennie MJ, van de Winkel JGJ. Renaissance of cancer therapeutic antibodies. *Drug Discov Today* 2003;8:503–10.
2 Strome SE, Sausville EA, Mann D. A mechanistic perspective of monoclonal antibodies in cancer therapy beyond target-related effects. *Oncologist* 2007;12:1084–95.
3 Derer S, Beurskens FJ, Rosner T, *et al*. Complement in antibody-based tumor therapy. *Crit Rev Immunol* 2014;34:199–214.
4 Albanesi M, Mancardi DA, Jönsson F, *et al*. Neutrophils mediate antibody-induced antitumor effects in mice. *Blood* 2013;122:3160–4.
5 Matlung HL, Babes L, Zhao XW, *et al*. Neutrophils kill antibody-opsonized cancer cells by trogoptosis. *Cell Rep* 2018;23:3946–59.
6 Gül N, Babes L, Siegmund K, *et al*. Macrophages eliminate circulating tumor cells after monoclonal antibody therapy. *J Clin Invest* 2014;124:812–23.
7 DiLillo DJ, Ravetch JV. Differential fc-receptor engagement drives an anti-tumor vaccinal effect. *Cell* 2015;161:1035–45.
8 Barclay AN, Van den Berg TK. The interaction between signal regulatory protein alpha (SIRPα) and CD47: structure, function, and therapeutic target. *Annu Rev Immunol* 2014;32:25–50.
9 Matlung HL, Szilagyi K, Barclay NA, *et al*. The CD47-sirpα signaling axis as an innate immune checkpoint in cancer. *Immunol Rev* 2017;276:145–64.
10 Chao MP, Alizadeh AA, Tang C, *et al*. Anti-CD47 antibody synergizes with rituximab to promote phagocytosis and eradicate non-Hodgkin lymphoma. *Cell* 2010;142:699–713.
11 Zhao XW, van Beek EM, Schornagel K, *et al*. CD47-Signal regulatory protein-α (SIRPα) interactions form a barrier for antibody-mediated tumor cell destruction. *Proc Natl Acad Sci U S A* 2011;108:18342–7.
12 Kamber RA, Nishiga Y, Morton B, *et al*. Inter-cellular CRISPR screens reveal regulators of cancer cell phagocytosis. *Nature* 2021;597:549–54.
13 Fujioka Y, Matozaki T, Noguchi T, *et al*. A novel membrane glycoprotein, SHPS-1, that binds the SH2-domain-containing protein tyrosine phosphatase SHP-2 in response to mitogens and cell adhesion. *Mol Cell Biol* 1996;16:6887–99.
14 Adams S, van der Laan LJ, Vernon-Wilson E, *et al*. Signal-regulatory protein is selectively expressed by myeloid and neuronal cells. *J Immunol* 1998;161:1853–9.
15 Veillette A, Thibaudeau E, Latour S. High expression of inhibitory receptor SHPS-1 and its association with protein-tyrosine phosphatase SHP-1 in macrophages. *J Biol Chem* 1998;273:22719–28.
16 Kharitonenkov A, Chen Z, Sures I, *et al*. A family of proteins that inhibit signalling through tyrosine kinase receptors. *Nature* 1997;386:181–6.
17 van Beek EM, Cochrane F, Barclay AN, *et al*. Signal regulatory proteins in the immune system. *J Immunol* 2005;175:7781–7.
18 Jiang P, Lagenaur CF, Narayanan V. Integrin-associated protein is a ligand for the P84 neural adhesion molecule. *J Biol Chem* 1999;274:559–62.
19 Vernon-Wilson EF, Kee WJ, Willis AC, *et al*. CD47 is a ligand for rat macrophage membrane signal regulatory protein SIRP (OX41) and human SIRPalpha 1. *Eur J Immunol* 2000;30:2130–7.
20 Seiffert M, Cant C, Chen Z, *et al*. Human signal-regulatory protein is expressed on normal, but not on subsets of leukemic myeloid cells and mediates cellular adhesion involving its counterreceptor CD47. *Blood* 1999;94:3633–43.
21 Hatherley D, Graham SC, Turner J, *et al*. Paired receptor specificity explained by structures of signal regulatory proteins alone and complexed with CD47. *Mol Cell* 2008;31:266–77.
22 Lindberg FP, Gresham HD, Schwarz E, *et al*. Molecular cloning of integrin-associated protein: an immunoglobulin family member with multiple membrane-spanning domains implicated in alpha v beta 3-dependent ligand binding. *J Cell Biol* 1993;123:485–96.
23 Oldenborg PA, Zheleznyak A, Fang YF, *et al*. Role of CD47 as a marker of self on red blood cells. *Science* 2000;288:2051–4.
24 Abram CL, Roberge GL, Pao LI, *et al*. Distinct roles for neutrophils and dendritic cells in inflammation and autoimmunity in motheaten mice. *Immunity* 2013;38:489–501.
25 Abram CL, Lowell CA. Shp1 function in myeloid cells. *J Leukoc Biol* 2017;102:657–75.
26 Myers DR, Abram CL, Wildes D, *et al*. Shp1 loss enhances macrophage effector function and promotes anti-tumor immunity. *Front Immunol* 2020;11:576310.
27 Chen J, Zhong M-C, Guo H, *et al*. SLAMF7 is critical for phagocytosis of haematopoietic tumour cells via Mac-1 integrin. *Nature* 2017;544:493–7.
28 Veillette A, Chen J. SIRPα-CD47 immune checkpoint blockade in anticancer therapy. *Trends Immunol* 2018;39:173–84.
29 Ring NG, Herndler-Brandstetter D, Weiskopf K, *et al*. Anti-SIRPα antibody immunotherapy enhances neutrophil and macrophage antitumor activity. *Proc Natl Acad Sci USA* 2017;114:E10578–85.
30 Weiskopf K, Ring AM, Ho CCM, *et al*. Engineered SIRPα variants as immunotherapeutic adjuvants to anticancer antibodies. *Science* 2013;341:88–91.
31 Liu X, Pu Y, Cron K, *et al*. CD47 blockade triggers T cell-mediated destruction of immunogenic tumors. *Nat Med* 2015;21:1209–15.
32 Xu MM, Pu Y, Han D, *et al*. Dendritic cells but not macrophages sense tumor mitochondrial DNA for cross-priming through signal regulatory protein α signaling. *Immunity* 2017;47:363–73.
33 Sockolosky JT, Dougan M, Ingram JR, *et al*. Durable antitumor responses to CD47 blockade require adaptive immune stimulation. *Proc Natl Acad Sci USA* 2016;113.
34 Gauttier V, Pengam S, Durand J, *et al*. Selective SIRPα blockade reverses tumor T cell exclusion and overcomes cancer immunotherapy resistance. *J Clin Invest* 2020;130:6109–23.
35 Bian Z, Shi L, Kidder K, *et al*. Intratumoral sirpα-deficient macrophages activate tumor antigen-specific cytotoxic T cells under radiotherapy. *Nat Commun* 2021;12:3229.
36 Advani R, Flinn I, Popplewell L, *et al*. Cd47 blockade by hu5F9-G4 and rituximab in non-Hodgkin's lymphoma. *N Engl J Med* 2018;379:1711–21.
37 Sikic BI, Lakhani N, Patnaik A, *et al*. First-in-human, first-in-class phase I trial of the anti-CD47 antibody hu5f9-G4 in patients with advanced cancers. *J Clin Oncol* 2019;37:946–53.

38 Behrens LM, van den Berg TK, van Egmond M. Targeting the CD47-SIRPα innate immune checkpoint to potentiate antibody therapy in cancer by neutrophils. *Cancers (Basel)* 2022;14:3366.
39 Ansell SM, Maris MB, Lesokhin AM, *et al*. Phase I study of the CD47 blocker TTI-621 in patients with relapsed or refractory hematologic malignancies. *Clin Cancer Res* 2021;27:2190–9.
40 Querfeld C, Thompson JA, Taylor MH, *et al*. Intralesional TTI-621, a novel biologic targeting the innate immune checkpoint CD47, in patients with relapsed or refractory mycosis fungoides or Sézary syndrome: a multicentre, phase 1 study. *Lancet Haematol* 2021;8:e808–17.
41 Lakhani NJ, Chow LQM, Gainor JF, *et al*. Evorpacept alone and in combination with pembrolizumab or trastuzumab in patients with advanced solid tumours (ASPEN-01): a first-in-human, open-label, multicentre, phase 1 dose-escalation and dose-expansion study. *Lancet Oncol* 2021;22:1740–51.
42 Brown EJ, Frazier WA. Integrin-associated protein (CD47) and its ligands. *Trends Cell Biol* 2001;11:130–5.
43 Kaur S, Martin-Manso G, Pendrak ML, *et al*. Thrombospondin-1 inhibits VEGF receptor-2 signaling by disrupting its association with CD47. *J Biol Chem* 2010;285:38923–32.
44 Soto-Pantoja DR, Stein EV, Rogers NM, *et al*. Therapeutic opportunities for targeting the ubiquitous cell surface receptor CD47. *Expert Opin Ther Targets* 2013;17:89–103.
45 Brooke G, Holbrook JD, Brown MH, *et al*. Human lymphocytes interact directly with CD47 through a novel member of the signal regulatory protein (SIRP) family. *J Immunol* 2004;173:2562–70.
46 Stefanidakis M, Newton G, Lee WY, *et al*. Endothelial CD47 interaction with sirpgamma is required for human T-cell transendothelial migration under shear flow conditions in vitro. *Blood* 2008;112:1280–9.
47 Piccio L, Vermi W, Boles KS, *et al*. Adhesion of human T cells to antigen-presenting cells through sirpbeta2-CD47 interaction costimulates T-cell proliferation. *Blood* 2005;105:2421–7.
48 Dehmani S, Nerrière-Daguin V, Néel M, *et al*. SIRPγ-CD47 interaction positively regulates the activation of human T cells in situation of chronic stimulation. *Front Immunol* 2021;12:732530.
49 Liu J, Xavy S, Mihardja S, *et al*. Targeting macrophage checkpoint inhibitor SIRPα for anticancer therapy. *JCI Insight* 2020;5:e134728.
50 Sim J, Sockolosky JT, Sangalang E, *et al*. Discovery of high affinity, pan-allelic, and pan-mammalian reactive antibodies against the myeloid checkpoint receptor SIRPα. *MAbs* 2019;11:1036–52.
51 Voets E, Paradé M, Lutje Hulsik D, *et al*. Functional characterization of the selective pan-allele anti-SIRPα antibody ADU-1805 that blocks the sirpα-CD47 innate immune checkpoint. *J Immunother Cancer* 2019;7:340.
52 Wu Z-H, Li N, Mei X-F, *et al*. Preclinical characterization of the novel anti-sirpα antibody BR105 that targets the myeloid immune checkpoint. *J Immunother Cancer* 2022;10:e004054.
53 Andrejeva G, Capoccia BJ, Hiebsch RR, *et al*. Novel SIRPα antibodies that induce single-agent phagocytosis of tumor cells while preserving T cells. *J Immunol* 2021;206:712–21.
54 Poirier NM, Van-Hove B, Gauttier V, *et al*. OSE immunotherapeutics, assignee. new anti-sirpa antibodies and their therapeutic applications. 2017.
55 Kuo TC, Chen A, Harrabi O, *et al*. Targeting the myeloid checkpoint receptor SIRPα potentiates innate and adaptive immune responses to promote anti-tumor activity. *J Hematol Oncol* 2020;13:160.
56 Hatherley D, Lea SM, Johnson S, *et al*. Polymorphisms in the human inhibitory signal-regulatory protein α do not affect binding to its ligand CD47. *J Biol Chem* 2014;289:10024–8.
57 Seiffert M, Brossart P, Cant C, *et al*. Signal-Regulatory protein alpha (SIRPalpha) but not SIRPbeta is involved in T-cell activation, binds to CD47 with high affinity, and is expressed on immature CD34 (+) CD38 (-) hematopoietic cells. *Blood* 2001;97:2741–9.
58 Abbasian MC, Escoubet L, Fenalti G, *et al*. SIRPα binding proteins and methods of use thereof. 2020.
59 Kurlander RJ. Blockade of Fc receptor-mediated binding to U-937 cells by murine monoclonal antibodies directed against a variety of surface antigens. *J Immunol* 1983;131:140–7.
60 Koentgen F, Lin J, Katidou M, *et al*. Exclusive transmission of the embryonic stem cell-derived genome through the mouse germline. *Genesis* 2016;54:326–33.
61 Murata Y, Tanaka D, Hazama D, *et al*. Anti-Human SIRPα antibody is a new tool for cancer immunotherapy. *Cancer Sci* 2018;109:1300–8.
62 Leabman MK, Meng YG, Kelley RF, *et al*. Effects of altered FcγR binding on antibody pharmacokinetics in cynomolgus monkeys. *MAbs* 2013;5:896–903.
63 Hezareh M, Hessell AJ, Jensen RC, *et al*. Effector function activities of a panel of mutants of a broadly neutralizing antibody against human immunodeficiency virus type 1. *J Virol* 2001;75:12161–8.
64 Strati P, Hawkes E, Ghosh N, *et al*. Interim results from the first clinical study of CC-95251, an anti-signal regulatory protein-alpha (SIRPα) antibody, in combination with rituximab in patients with relapsed and/or refractory non-hodgkin lymphoma (R/R NHL). *Blood* 2021;138:2493.
65 Hogarth PM, Pietersz GA. Fc receptor-targeted therapies for the treatment of inflammation, cancer and beyond. *Nat Rev Drug Discov* 2012;11:311–31.
66 Liu J, Wang L, Zhao F, *et al*. Pre-clinical development of a humanized anti-CD47 antibody with anti-cancer therapeutic potential. *PLoS One* 2015;10:e0137345.
67 Petrova PS, Viller NN, Wong M, *et al*. TTI-621 (sirpαfc): a CD47-blocking innate immune checkpoint inhibitor with broad antitumor activity and minimal erythrocyte binding. *Clin Cancer Res* 2017;23:1068–79.
68 Wang C, Sallman DA. Targeting the cluster of differentiation 47/signal-regulatory protein alpha axis in myeloid malignancies. *Curr Opin Hematol* 2022;29:44–52.
69 Hsieh RC-E, Krishnan S, Wu R-C, *et al*. Atr-Mediated CD47 and PD-L1 up-regulation restricts radiotherapy-induced immune priming and abscopal responses in colorectal cancer. *Sci Immunol* 2022;7:eabl9330.
70 Poirier N, Gauttier V, Mary C, *et al*. Use of anti-human SIRPA V1 antibodies and method for producing anti-SIRPA V1 antibodies. 2019.
71 Events and presentations. n.d. Available: https://ir.fortyseveninc.com/events-and-presentations
72 Treffers LW, van Houdt M, Bruggeman CW, *et al*. FcγRIIIb restricts antibody-dependent destruction of cancer cells by human neutrophils. *Front Immunol* 2018;9:3124.

Figure S1

A

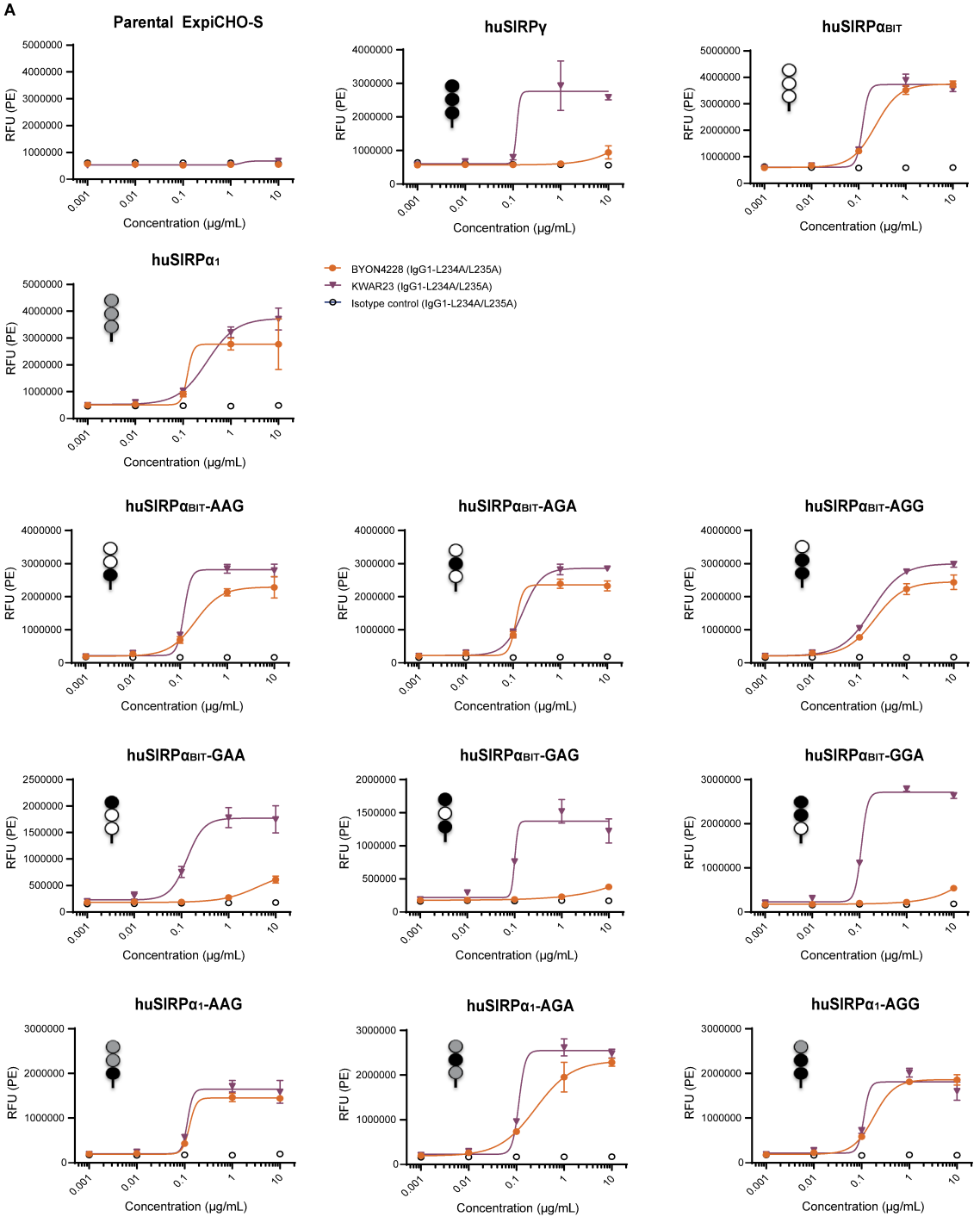
Parental ExpiCHO-S
huSIRPγ
huSIRPαBIT
huSIRPα1
huSIRPαBIT-AAG
huSIRPαBIT-AGA
huSIRPαBIT-AGG
huSIRPαBIT-GAA
huSIRPαBIT-GAG
huSIRPαBIT-GGA
huSIRPα1-AAG
huSIRPα1-AGA
huSIRPα1-AGG
RFU (PE)
Concentration (µg/mL)
BYON4228 (IgG1-L234A/L235A)
KWAR23 (IgG1-L234A/L235A)
Isotype control (IgG1-L234A/L235A)

Figure S1

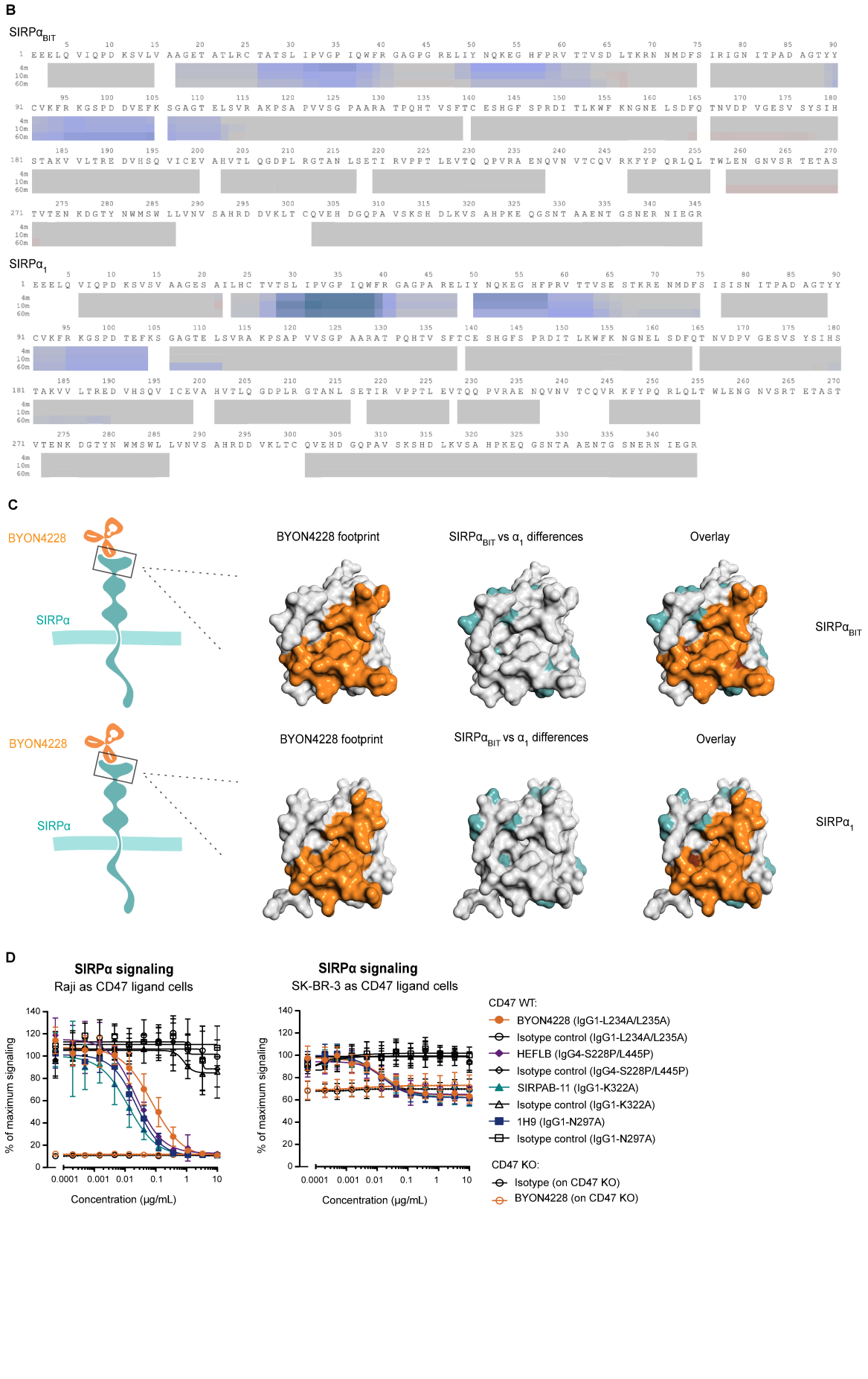
B
SIRPα$_{BIT}$
1 EEELQ VIQPD KSVLV AAGET ATLRC TATSL IPVGP IQWFR GAGPG RELIY NQKEG HFPRV TTVSD LTKRN NMDFS IRIGN ITPAD AGTYY
91 CVKFR KGSPD DVEFK SGAGT ELSVR AKPSA PVVSG PAARA TPQHT VSFTC ESHGF SPRDI TLKWF KNGNE LSDFQ TNVDP VGESV SYSIH
181 STAKV VLTRE DVHSQ VICEV AHVTL QGDPL RGTAN LSETI RVPPT LEVTQ QPVRA ENQVN VTCQV RKFYP QRLQL TWLEN GNVSR TETAS
271 TVTEN KDGTY NWMSW LLVNV SAHRD DVKLT CQVEH DGQPA VSKSH DLKVS AHPKE QGSNT AAENT GSNER NIEGR
SIRPα$_{1}$
1 EEELQ VIQPD KSVSV AAGES AILHC TVTSL IPVGP IQWFR GAGPA RELIY NQKEG HFPRV TTVSE STKRE NMDFS ISISN ITPAD AGTYY
91 CVKFR KGSPD TEFKS GAGTE LSVRA KPSAP VVSGP AARAT PQHTV SFTCE SHGFS PRDIT LKWFK NGNEL SDFQT NVDPV GESVS YSIHS
181 TAKVV LTRED VHSQV ICEVA HVTLQ GDPLR GTANL SETIR VPPTL EVTQQ PVRAE NQVNV TCQVR KFYPQ RLQLT WLENG NVSRT ETAST
271 VTENK DGTYN WMSWL LVNVS AHRDD VKLTC QVEHD GQPAV SKSHD LKVSA HPKEQ GSNTA AENTG SNERN IEGR
C
BYON4228
SIRPα
BYON4228 footprint
SIRPα$_{BIT}$ vs α$_{1}$ differences
Overlay
SIRPα$_{BIT}$
BYON4228
SIRPα
BYON4228 footprint
SIRPα$_{BIT}$ vs α$_{1}$ differences
Overlay
SIRPα$_{1}$
D
SIRPα signaling
Raji as CD47 ligand cells
SIRPα signaling
SK-BR-3 as CD47 ligand cells
% of maximum signaling
Concentration (μg/mL)
CD47 WT:
BYON4228 (IgG1-L234A/L235A)
Isotype control (IgG1-L234A/L235A)
HEFLB (IgG4-S228P/L445P)
Isotype control (IgG4-S228P/L445P)
SIRPAB-11 (IgG1-K322A)
Isotype control (IgG1-K322A)
1H9 (IgG1-N297A)
Isotype control (IgG1-N297A)
CD47 KO:
Isotype (on CD47 KO)
BYON4228 (on CD47 KO)

Figure S2

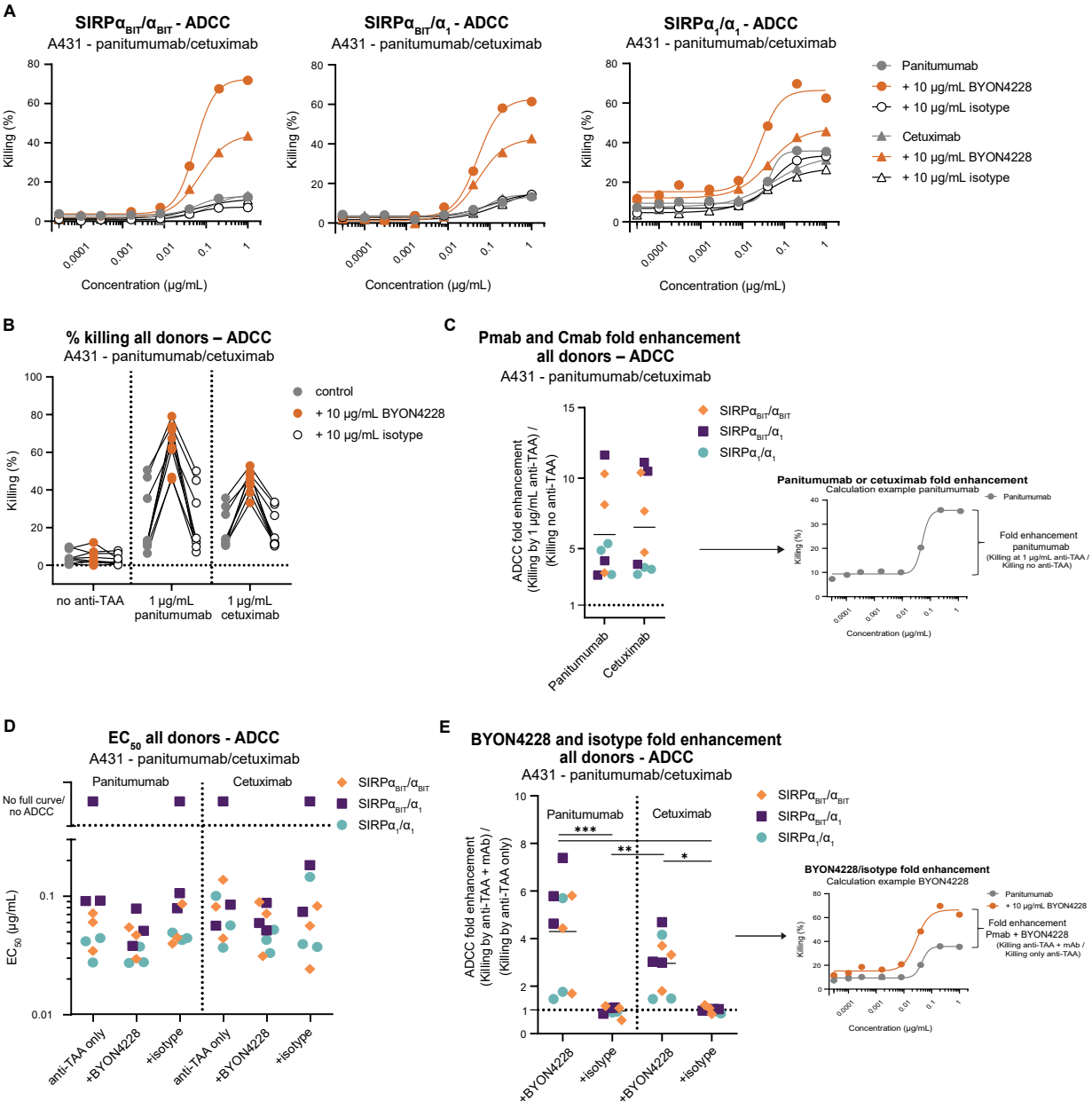
A
SIRPα$_{BIT}$/α$_{BIT}$ - ADCC
SIRPα$_{BIT}$/α$_{1}$ - ADCC
SIRPα$_{1}$/α$_{1}$ - ADCC
A431 - panitumumab/cetuximab
Killing (%)
Concentration (µg/mL)
Panitumumab
+ 10 µg/mL BYON4228
+ 10 µg/mL isotype
Cetuximab
+ 10 µg/mL BYON4228
+ 10 µg/mL isotype
B
% killing all donors – ADCC
A431 - panitumumab/cetuximab
control
+ 10 µg/mL BYON4228
+ 10 µg/mL isotype
no anti-TAA
1 µg/mL panitumumab
1 µg/mL cetuximab
C
Pmab and Cmab fold enhancement all donors – ADCC
A431 - panitumumab/cetuximab
ADCC fold enhancement (Killing by 1 µg/mL anti-TAA) / (Killing no anti-TAA)
Panitumumab
Cetuximab
Panitumumab or cetuximab fold enhancement
Calculation example panitumumab
Fold enhancement panitumumab (Killing at 1 µg/mL anti-TAA / Killing no anti-TAA)
D
EC$_{50}$ all donors - ADCC
A431 - panitumumab/cetuximab
No full curve/ no ADCC
EC$_{50}$ (µg/mL)
anti-TAA only
+BYON4228
+isotype
E
BYON4228 and isotype fold enhancement all donors - ADCC
A431 - panitumumab/cetuximab
ADCC fold enhancement (Killing by anti-TAA + mAb) / (Killing by anti-TAA only)
***
**
*
BYON4228/isotype fold enhancement
Calculation example BYON4228
Fold enhancement Pmab + BYON4228 (Killing anti-TAA + mAb / Killing only anti-TAA)

Figure S3

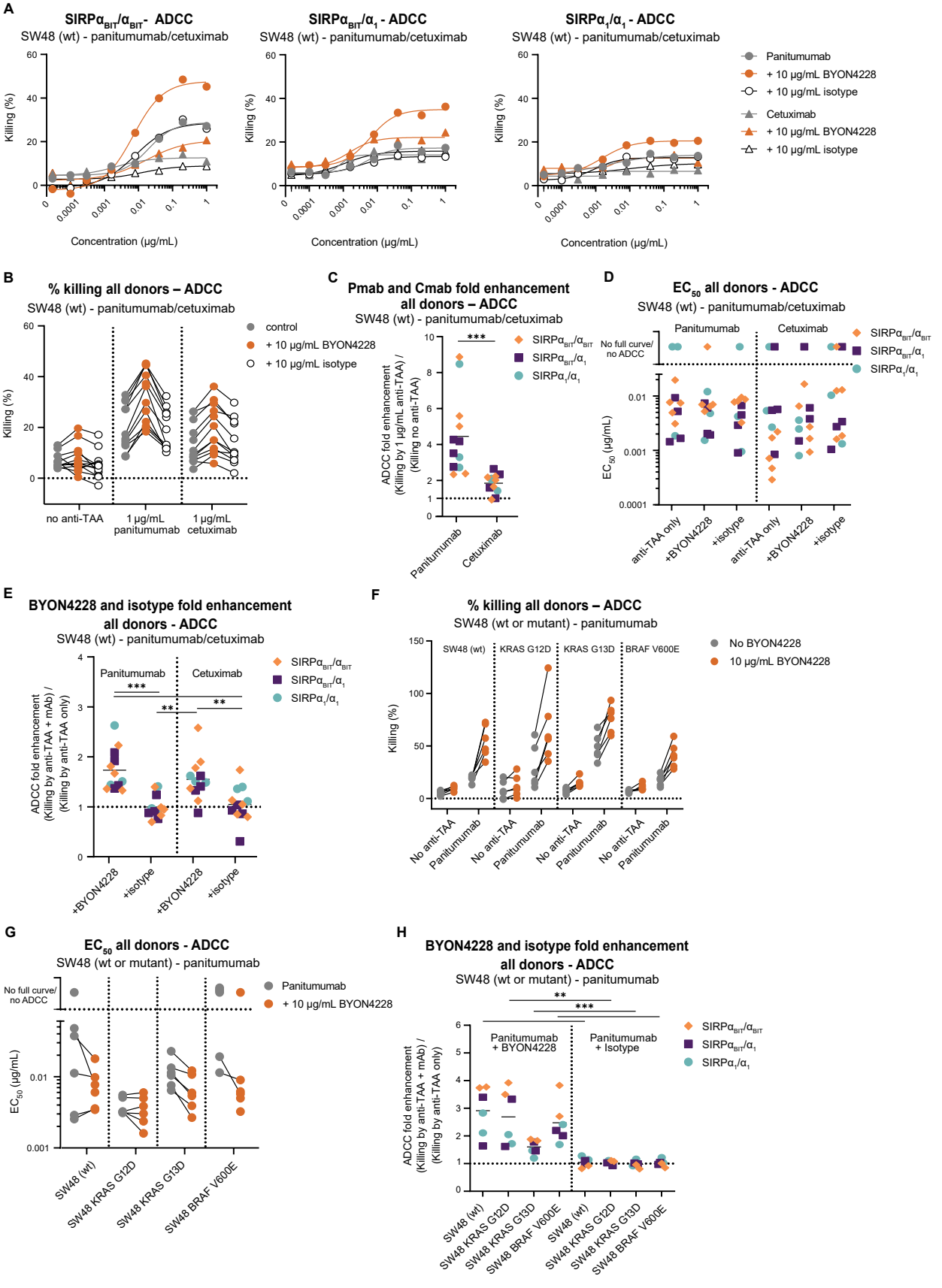
A
SIRPα$_{BIT}$/α$_{BIT}$- ADCC
SW48 (wt) - panitumumab/cetuximab
SIRPα$_{BIT}$/α$_1$ - ADCC
SW48 (wt) - panitumumab/cetuximab
SIRPα$_1$/α$_1$ - ADCC
SW48 (wt) - panitumumab/cetuximab
Killing (%)
Concentration (µg/mL)
Panitumumab
+ 10 µg/mL BYON4228
+ 10 µg/mL isotype
Cetuximab
+ 10 µg/mL BYON4228
+ 10 µg/mL isotype
B
% killing all donors – ADCC
SW48 (wt) - panitumumab/cetuximab
control
+ 10 µg/mL BYON4228
+ 10 µg/mL isotype
no anti-TAA
1 µg/mL panitumumab
1 µg/mL cetuximab
C
Pmab and Cmab fold enhancement all donors – ADCC
SW48 (wt) - panitumumab/cetuximab
ADCC fold enhancement (Killing by 1 µg/mL anti-TAA) / (Killing no anti-TAA)
Panitumumab
Cetuximab
D
EC$_{50}$ all donors - ADCC
SW48 (wt) - panitumumab/cetuximab
No full curve/ no ADCC
EC$_{50}$ (µg/mL)
anti-TAA only
+BYON4228
+isotype
E
BYON4228 and isotype fold enhancement all donors - ADCC
SW48 (wt) - panitumumab/cetuximab
ADCC fold enhancement (Killing by anti-TAA + mAb) / (Killing by anti-TAA only)
F
% killing all donors – ADCC
SW48 (wt or mutant) - panitumumab
SW48 (wt)
KRAS G12D
KRAS G13D
BRAF V600E
No BYON4228
10 µg/mL BYON4228
No anti-TAA
Panitumumab
G
EC$_{50}$ all donors - ADCC
SW48 (wt or mutant) - panitumumab
SW48 (wt)
SW48 KRAS G12D
SW48 KRAS G13D
SW48 BRAF V600E
H
BYON4228 and isotype fold enhancement all donors - ADCC
SW48 (wt or mutant) - panitumumab
Panitumumab + BYON4228
Panitumumab + Isotype

Supplementary Table S1: *SIRPα, CD47 and EGFR expression levels on indicated cells expressed as the mean specific antibody binding capacity (sABC). N indicates the number of tests performed.*

Cell line / Receptor	SIRPα		CD47		EGFR (panitumumab)		EGFR (cetuximab)	
	Mean sABC	N	Mean sABC	N	Mean sABC	N	Mean sABC	N
SW48 (006)	< 3300[$]	2	53681	5	104416	5	118262	5
SW48 (115)	< 3300[$]	2	56096	5	98710	5	126366	5
SW48 BRAF V600E	< 3300[$]	2	71094	2	47841	2	68095	2
SW48 KRAS G12D	< 3300[$]	2	70397	2	74716	2	125488	2
SW48 KRAS G13D	< 3300[$]	2	77390	2	143566	2	186522	2

$: Receptor expression is below the lowest calibration point of the Human IgG calibrator kit, namely 3300 receptors/cell.

Supplementary Table S2: *Observed affinities (K_D-obs) for BYON4228-IgG1-L234A/L235A and BYON4228-IgG1 binding to Fcγ Receptors.*

Ligand	BYON4228-IgG1-L234A/L235A Observed affinities (K_D-obs)	SYD5664-IgG1* Observed affinities (K_D-obs)
Human FcγRIIIa (CD16a)	15.1 µM	2.6 µM
Human FcγRIIIb (CD16b)	> 16.7 µM	7.4 µM
Human FcγRIIa (CD32a H131 or R131)	> 16.7 µM	1.4 or 1.6 µM
Human FcγRIIb (CD32b)	> 16.7 µM	6.5 µM
Human FcγRI (CD64)	> 1.67 µM	2.5 nM

* SYD5664 contains the variable domains of BYON4228 but has a wildtype IgG1 constant domain with wildtype effector functions.

Supplementary Table S3: *BYON4228 PK in mice after single IV dose.*

	huSIRPα$_{BIT}$ mice			C57BL/6 mice
Parameter	**3 mg/kg**	**10 mg/kg**	**30 mg/kg**	**3 mg/kg**
C_{max} (µg/mL)	44.2	197	581	45.2
AUC_{last} (h*µg/mL)	1340	9810	36700	3390

Last sample taken at 168 h

Supplementary Table S4: *BYON4228 PK in mice after single IP dose.*

	huSIRPα$_{BIT}$ mice			C57BL/6 mice
Parameter	**3 mg/kg**	**10 mg/kg**	**30 mg/kg**	**3 mg/kg**
C_{max} (µg/mL)	21.9	78.5	311	29.8
AUC_{last} (h*µg/mL)	940	8720	33400	3730

Last sample taken at 168 h

Supplementary Table S5: *BYON4228 PK in monkey after a single IV dose*

Parameters	1 mg/kg BYON4228	3 mg/kg BYON4228	10 mg/kg BYON4228	30 mg/kg BYON4228	100 mg/kg BYON4228
$t_{½}$ (h)	105	66.8	95.6	109	100
C_{max} (µg/mL)	27.2	90.5	278	930	1740
AUC_{last} (h*µg/mL)	2010	5520	29100	131000	426000
AUC_{inf} (h*µg/mL)	2080	6190	30400	143000	449000
CL (mL/h/kg)	0.496	0.485	0.329	0.218	0.229
V_{ss} (mL/kg)	55.8	47.0	44.2	37.6	41.5

Cynomolgus monkeys after single IV infusion of BYON4228, animals sampled for 3 weeks following dosing. Values are means of n=2, with one male and one female animal per dose group.

Supplementary Movies: Real-time phagocytosis was visualized using live-cell imaging. Panitumumab-opsonized (40 ng/mL) HT-29 tumor cells were labeled with pHrodo and co-incubated with unlabeled macrophages and BYON4228 (10 µg/mL). Images were taken every 3 minutes for 4 hours. The light-red tumor cells become bright red upon phagocytosis by macrophages.

Figure S4

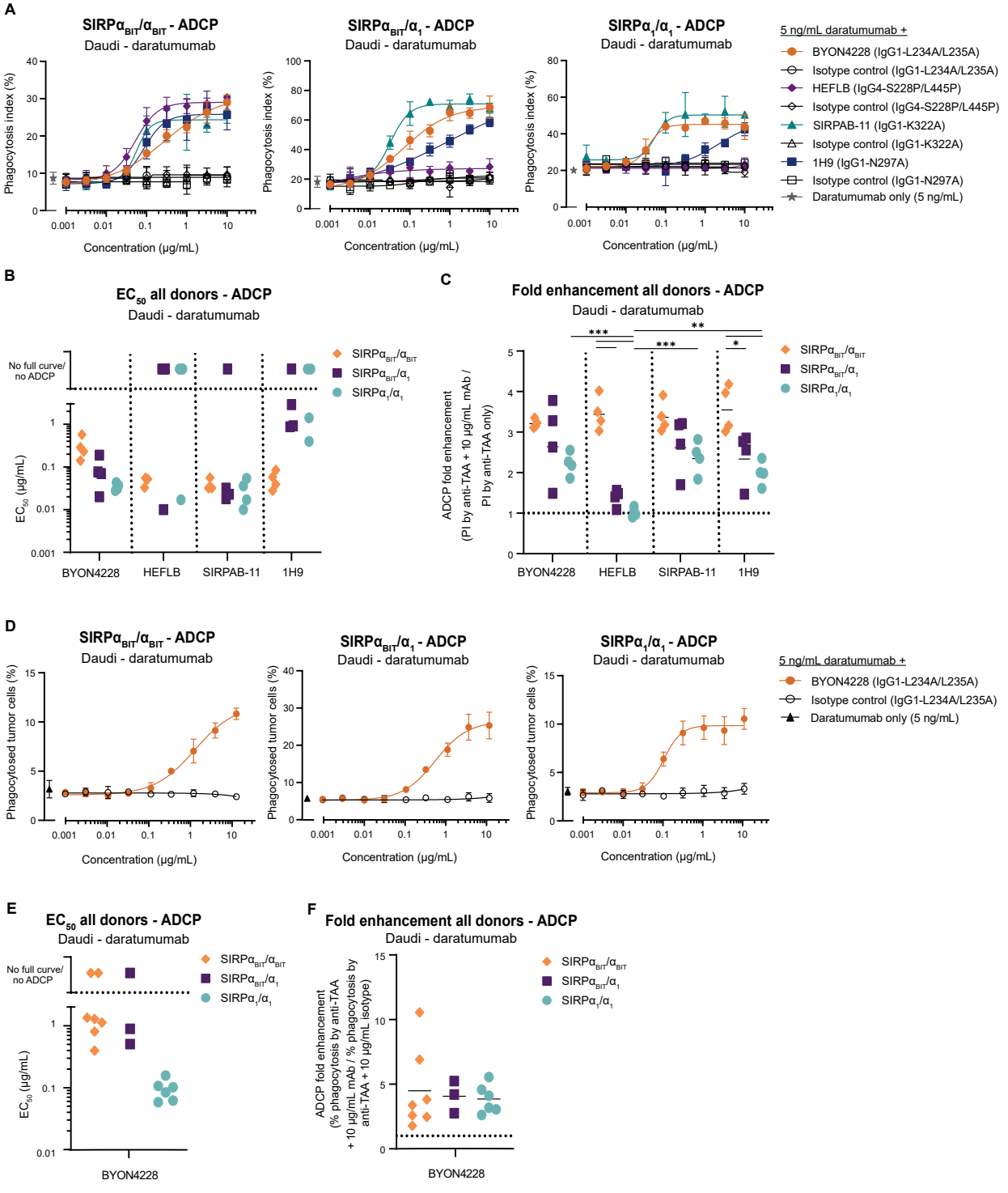
A
SIRPα$_{BIT}$/α$_{BIT}$ - ADCP
Daudi - daratumumab
SIRPα$_{BIT}$/α$_1$ - ADCP
Daudi - daratumumab
SIRPα$_1$/α$_1$ - ADCP
Daudi - daratumumab
Phagocytosis index (%)
Concentration (µg/mL)
5 ng/mL daratumumab +
BYON4228 (IgG1-L234A/L235A)
Isotype control (IgG1-L234A/L235A)
HEFLB (IgG4-S228P/L445P)
Isotype control (IgG4-S228P/L445P)
SIRPAB-11 (IgG1-K322A)
Isotype control (IgG1-K322A)
1H9 (IgG1-N297A)
Isotype control (IgG1-N297A)
Daratumumab only (5 ng/mL)
B
EC$_{50}$ all donors - ADCP
Daudi - daratumumab
No full curve/ no ADCP
EC$_{50}$ (µg/mL)
BYON4228
HEFLB
SIRPAB-11
1H9
SIRPα$_{BIT}$/α$_{BIT}$
SIRPα$_{BIT}$/α$_1$
SIRPα$_1$/α$_1$
C
Fold enhancement all donors - ADCP
Daudi - daratumumab
ADCP fold enhancement (PI by anti-TAA + 10 µg/mL mAb / PI by anti-TAA only)
***
***
**
*
D
SIRPα$_{BIT}$/α$_{BIT}$ - ADCP
Daudi - daratumumab
SIRPα$_{BIT}$/α$_1$ - ADCP
Daudi - daratumumab
SIRPα$_1$/α$_1$ - ADCP
Daudi - daratumumab
Phagocytosed tumor cells (%)
Concentration (µg/mL)
5 ng/mL daratumumab +
BYON4228 (IgG1-L234A/L235A)
Isotype control (IgG1-L234A/L235A)
Daratumumab only (5 ng/mL)
E
EC$_{50}$ all donors - ADCP
Daudi - daratumumab
No full curve/ no ADCP
EC$_{50}$ (µg/mL)
BYON4228
SIRPα$_{BIT}$/α$_{BIT}$
SIRPα$_{BIT}$/α$_1$
SIRPα$_1$/α$_1$
F
Fold enhancement all donors - ADCP
Daudi - daratumumab
ADCP fold enhancement (% phagocytosis by anti-TAA + 10 µg/mL mAb / % phagocytosis by anti-TAA + 10 µg/mL isotype)
BYON4228
SIRPα$_{BIT}$/α$_{BIT}$
SIRPα$_{BIT}$/α$_1$
SIRPα$_1$/α$_1$

Figure S5

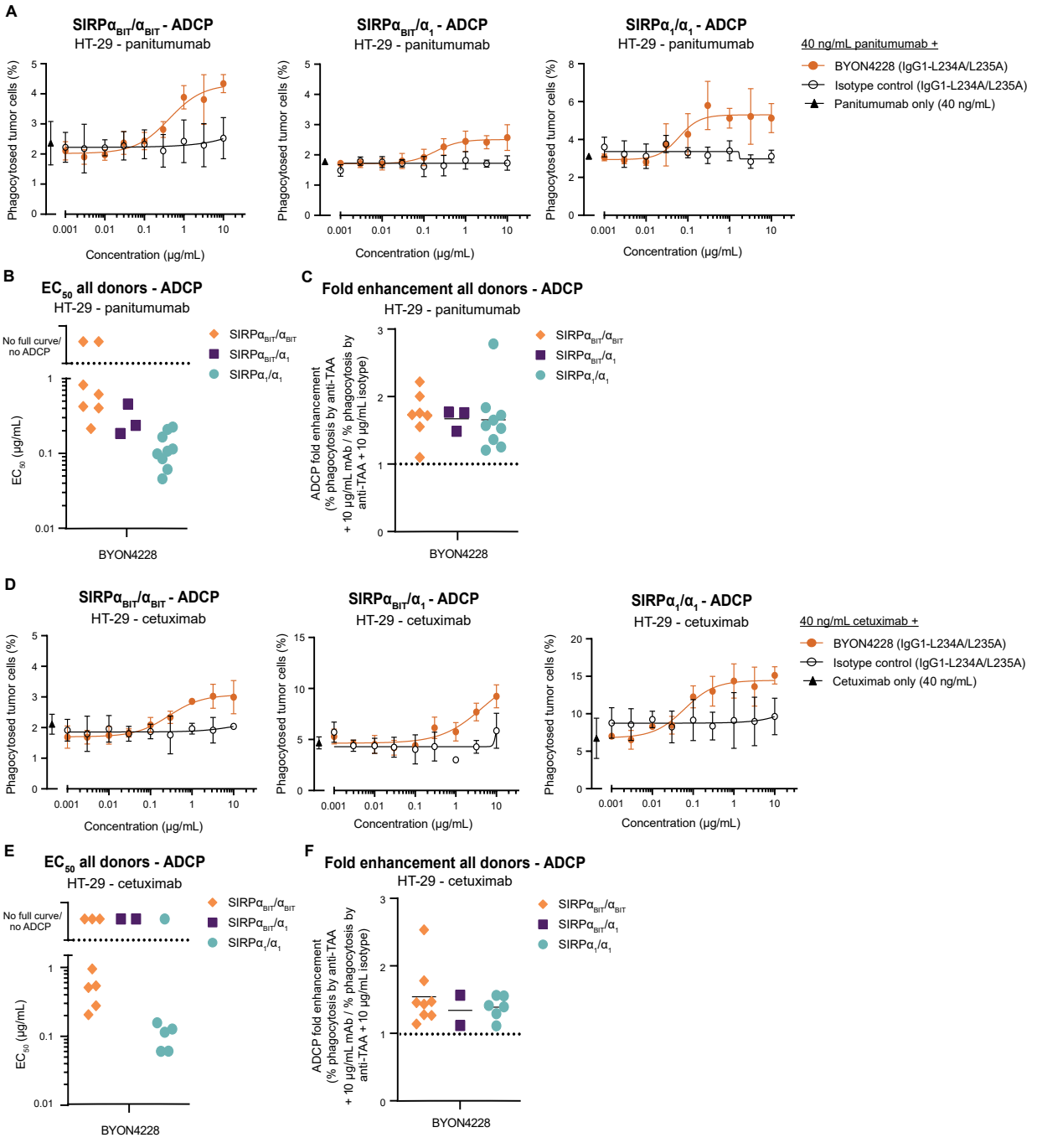
A
SIRPα$_{BIT}$/α$_{BIT}$ - ADCP
HT-29 - panitumumab
SIRPα$_{BIT}$/α$_{1}$ - ADCP
HT-29 - panitumumab
SIRPα$_{1}$/α$_{1}$ - ADCP
HT-29 - panitumumab
Phagocytosed tumor cells (%)
Concentration (µg/mL)
40 ng/mL panitumumab +
BYON4228 (IgG1-L234A/L235A)
Isotype control (IgG1-L234A/L235A)
Panitumumab only (40 ng/mL)
B
EC$_{50}$ all donors - ADCP
HT-29 - panitumumab
No full curve/ no ADCP
EC$_{50}$ (µg/mL)
BYON4228
C
Fold enhancement all donors - ADCP
HT-29 - panitumumab
ADCP fold enhancement (% phagocytosis by anti-TAA + 10 µg/mL mAb / % phagocytosis by anti-TAA + 10 µg/mL isotype)
D
SIRPα$_{BIT}$/α$_{BIT}$ - ADCP
HT-29 - cetuximab
SIRPα$_{BIT}$/α$_{1}$ - ADCP
HT-29 - cetuximab
SIRPα$_{1}$/α$_{1}$ - ADCP
HT-29 - cetuximab
40 ng/mL cetuximab +
BYON4228 (IgG1-L234A/L235A)
Isotype control (IgG1-L234A/L235A)
Cetuximab only (40 ng/mL)
E
EC$_{50}$ all donors - ADCP
HT-29 - cetuximab
F
Fold enhancement all donors - ADCP
HT-29 - cetuximab

Figure S6

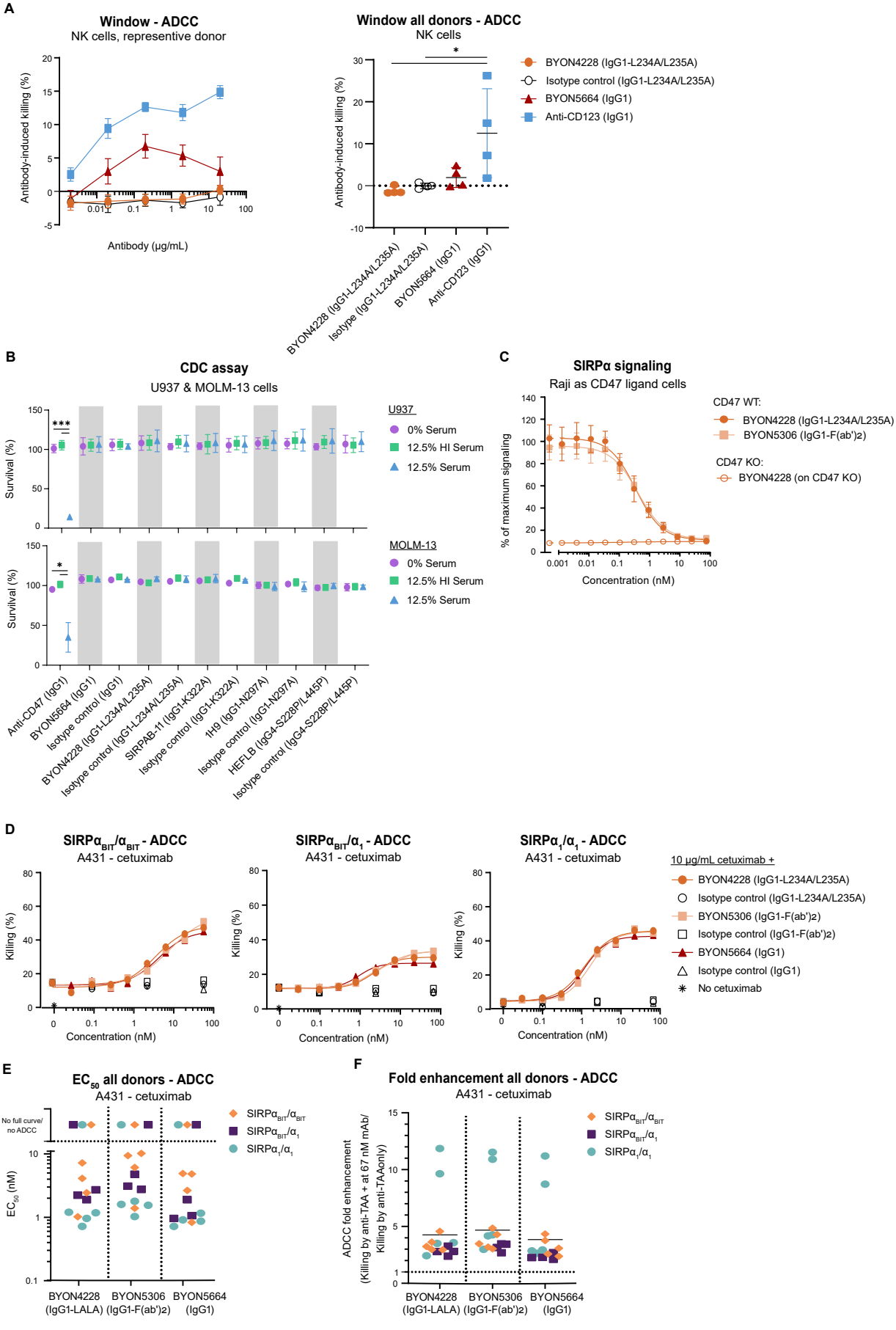
A
Window - ADCC
NK cells, representive donor
Antibody-induced killing (%)
Antibody (µg/mL)
Window all donors - ADCC
NK cells
Antibody-induced killing (%)
BYON4228 (IgG1-L234A/L235A)
Isotype control (IgG1-L234A/L235A)
BYON5664 (IgG1)
Anti-CD123 (IgG1)
B
CDC assay
U937 & MOLM-13 cells
Survival (%)
U937
0% Serum
12.5% HI Serum
12.5% Serum
MOLM-13
Anti-CD47 (IgG1)
BYON5664 (IgG1)
Isotype control (IgG1)
BYON4228 (IgG1-L234A/L235A)
Isotype control (IgG1-L234A/L235A)
SIRPAB-11 (IgG1-K322A)
Isotype control (IgG1-K322A)
1H9 (IgG1-N297A)
Isotype control (IgG1-N297A)
HEFLB (IgG4-S228P/L445P)
Isotype control (IgG4-S228P/L445P)
C
SIRPα signaling
Raji as CD47 ligand cells
% of maximum signaling
Concentration (nM)
CD47 WT:
BYON4228 (IgG1-L234A/L235A)
BYON5306 (IgG1-F(ab')2)
CD47 KO:
BYON4228 (on CD47 KO)
D
SIRPα$_{BIT}$/α$_{BIT}$ - ADCC
SIRPα$_{BIT}$/α$_1$ - ADCC
SIRPα$_1$/α$_1$ - ADCC
A431 - cetuximab
Killing (%)
Concentration (nM)
10 µg/mL cetuximab +
BYON4228 (IgG1-L234A/L235A)
Isotype control (IgG1-L234A/L235A)
BYON5306 (IgG1-F(ab')2)
Isotype control (IgG1-F(ab')2)
BYON5664 (IgG1)
Isotype control (IgG1)
No cetuximab
E
EC$_{50}$ all donors - ADCC
A431 - cetuximab
No full curve/ no ADCC
EC$_{50}$ (nM)
SIRPα$_{BIT}$/α$_{BIT}$
SIRPα$_{BIT}$/α$_1$
SIRPα$_1$/α$_1$
BYON4228 (IgG1-LALA)
BYON5306 (IgG1-F(ab')2)
BYON5664 (IgG1)
F
Fold enhancement all donors - ADCC
A431 - cetuximab
ADCC fold enhancement (Killing by anti-TAA + at 67 nM mAb/ Killing by anti-TAAonly)

Figure S7

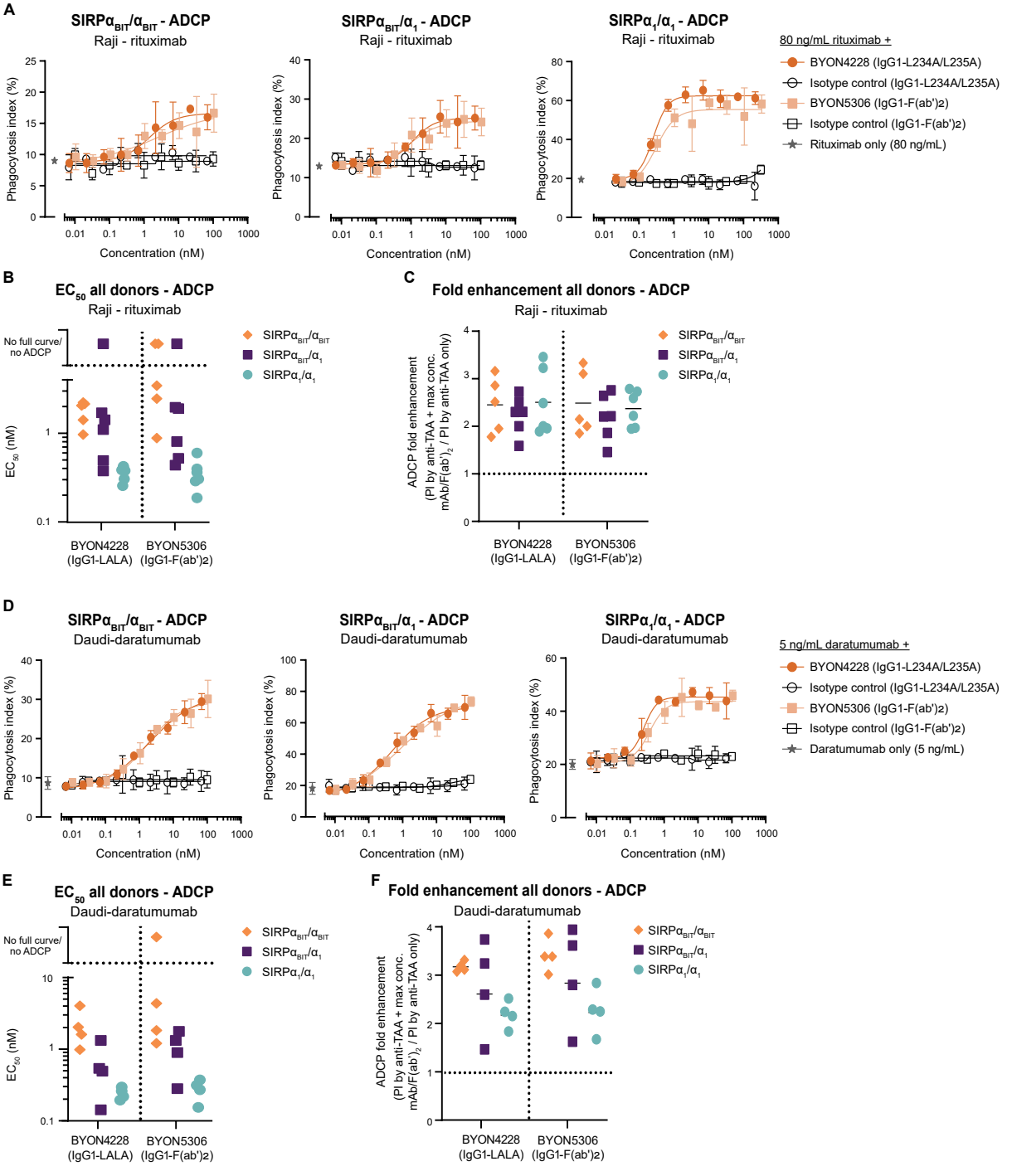
A
SIRPα$_{BIT}$/α$_{BIT}$ - ADCP
Raji - rituximab
SIRPα$_{BIT}$/α$_{1}$ - ADCP
Raji - rituximab
SIRPα$_{1}$/α$_{1}$ - ADCP
Raji - rituximab
Phagocytosis index (%)
Concentration (nM)
80 ng/mL rituximab +
BYON4228 (IgG1-L234A/L235A)
Isotype control (IgG1-L234A/L235A)
BYON5306 (IgG1-F(ab')2)
Isotype control (IgG1-F(ab')2)
Rituximab only (80 ng/mL)
B
EC$_{50}$ all donors - ADCP
Raji - rituximab
No full curve/ no ADCP
EC$_{50}$ (nM)
BYON4228 (IgG1-LALA)
BYON5306 (IgG1-F(ab')2)
SIRPα$_{BIT}$/α$_{BIT}$
SIRPα$_{BIT}$/α$_{1}$
SIRPα$_{1}$/α$_{1}$
C
Fold enhancement all donors - ADCP
Raji - rituximab
ADCP fold enhancement (PI by anti-TAA + max conc. mAb/F(ab')$_2$ / PI by anti-TAA only)
D
SIRPα$_{BIT}$/α$_{BIT}$ - ADCP
Daudi-daratumumab
SIRPα$_{BIT}$/α$_{1}$ - ADCP
Daudi-daratumumab
SIRPα$_{1}$/α$_{1}$ - ADCP
Daudi-daratumumab
5 ng/mL daratumumab +
BYON4228 (IgG1-L234A/L235A)
Isotype control (IgG1-L234A/L235A)
BYON5306 (IgG1-F(ab')2)
Isotype control (IgG1-F(ab')2)
Daratumumab only (5 ng/mL)
E
EC$_{50}$ all donors - ADCP
Daudi-daratumumab
F
Fold enhancement all donors - ADCP
Daudi-daratumumab

Figure S8

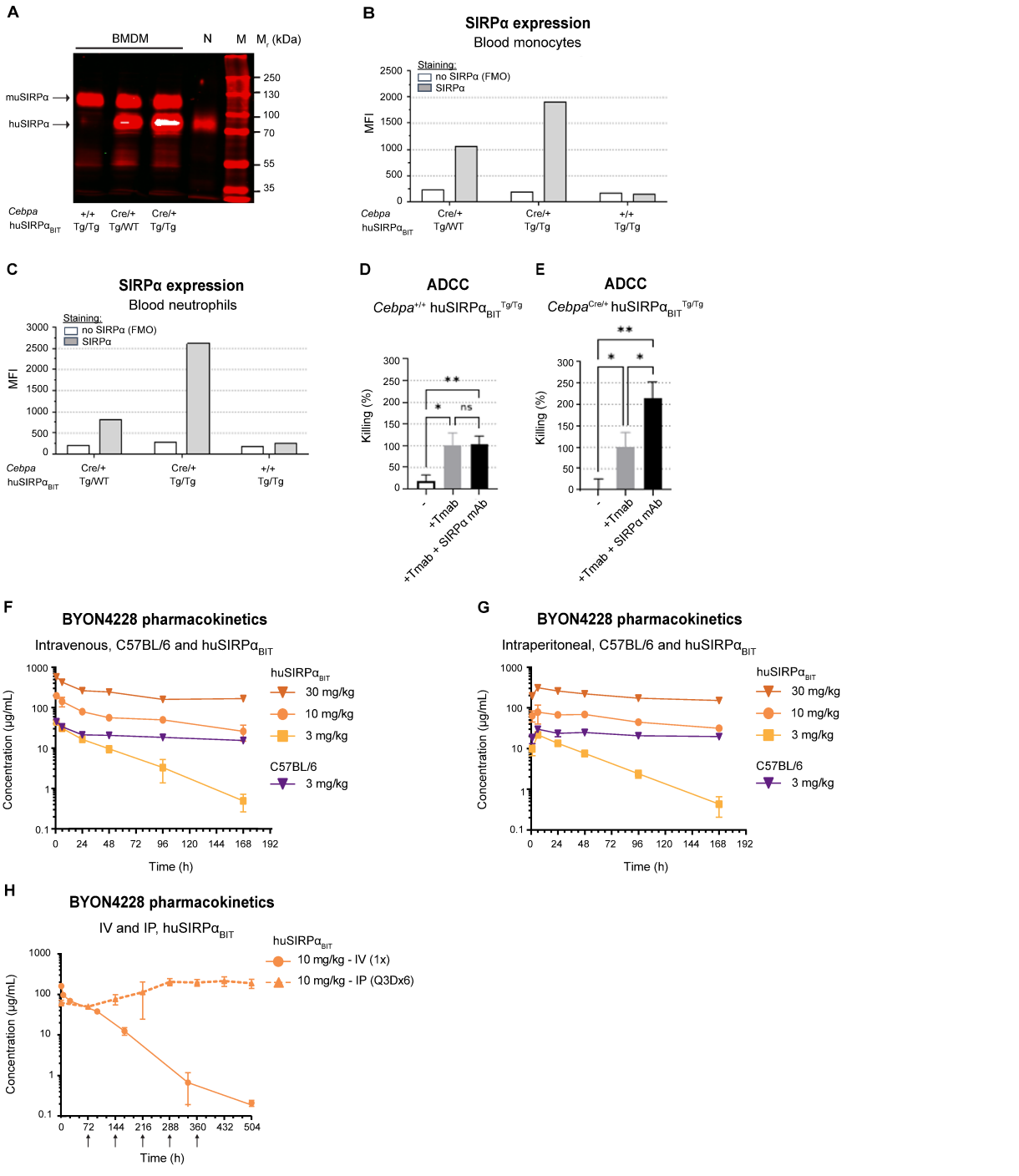
A
BMDM
N
M
Mr (kDa)
muSIRPα
huSIRPα
250
130
100
70
55
35
Cebpa
huSIRPαBIT
+/+ Tg/Tg
Cre/+ Tg/WT
Cre/+ Tg/Tg
B
SIRPα expression
Blood monocytes
Staining:
no SIRPα (FMO)
SIRPα
MFI
C
SIRPα expression
Blood neutrophils
D
ADCC
Cebpa+/+ huSIRPαBIT Tg/Tg
Killing (%)
ns
-
+Tmab
+Tmab + SIRPα mAb
E
ADCC
CebpaCre/+ huSIRPαBIT Tg/Tg
F
BYON4228 pharmacokinetics
Intravenous, C57BL/6 and huSIRPαBIT
Concentration (µg/mL)
Time (h)
huSIRPαBIT
30 mg/kg
10 mg/kg
3 mg/kg
C57BL/6
3 mg/kg
G
BYON4228 pharmacokinetics
Intraperitoneal, C57BL/6 and huSIRPαBIT
H
BYON4228 pharmacokinetics
IV and IP, huSIRPαBIT
10 mg/kg - IV (1x)
10 mg/kg - IP (Q3Dx6)

Figure S9

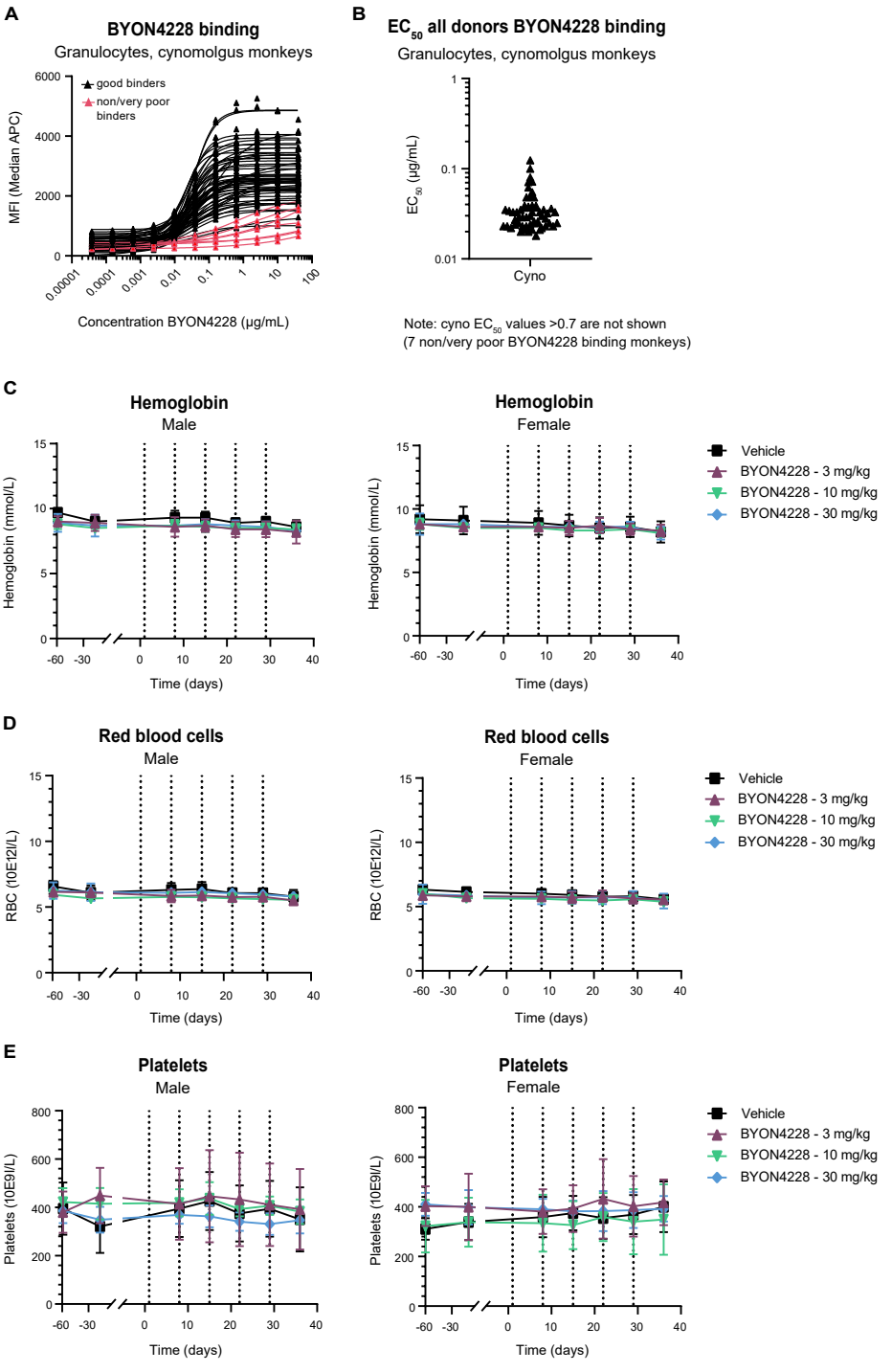
A
BYON4228 binding
Granulocytes, cynomolgus monkeys
good binders
non/very poor binders
MFI (Median APC)
Concentration BYON4228 (µg/mL)
B
EC50 all donors BYON4228 binding
Granulocytes, cynomolgus monkeys
EC50 (µg/mL)
Cyno
Note: cyno EC50 values >0.7 are not shown
(7 non/very poor BYON4228 binding monkeys)
C
Hemoglobin
Male
Female
Hemoglobin (mmol/L)
Time (days)
Vehicle
BYON4228 - 3 mg/kg
BYON4228 - 10 mg/kg
BYON4228 - 30 mg/kg
D
Red blood cells
Male
Female
RBC (10E12/L)
Time (days)
E
Platelets
Male
Female
Platelets (10E9/L)
Time (days)

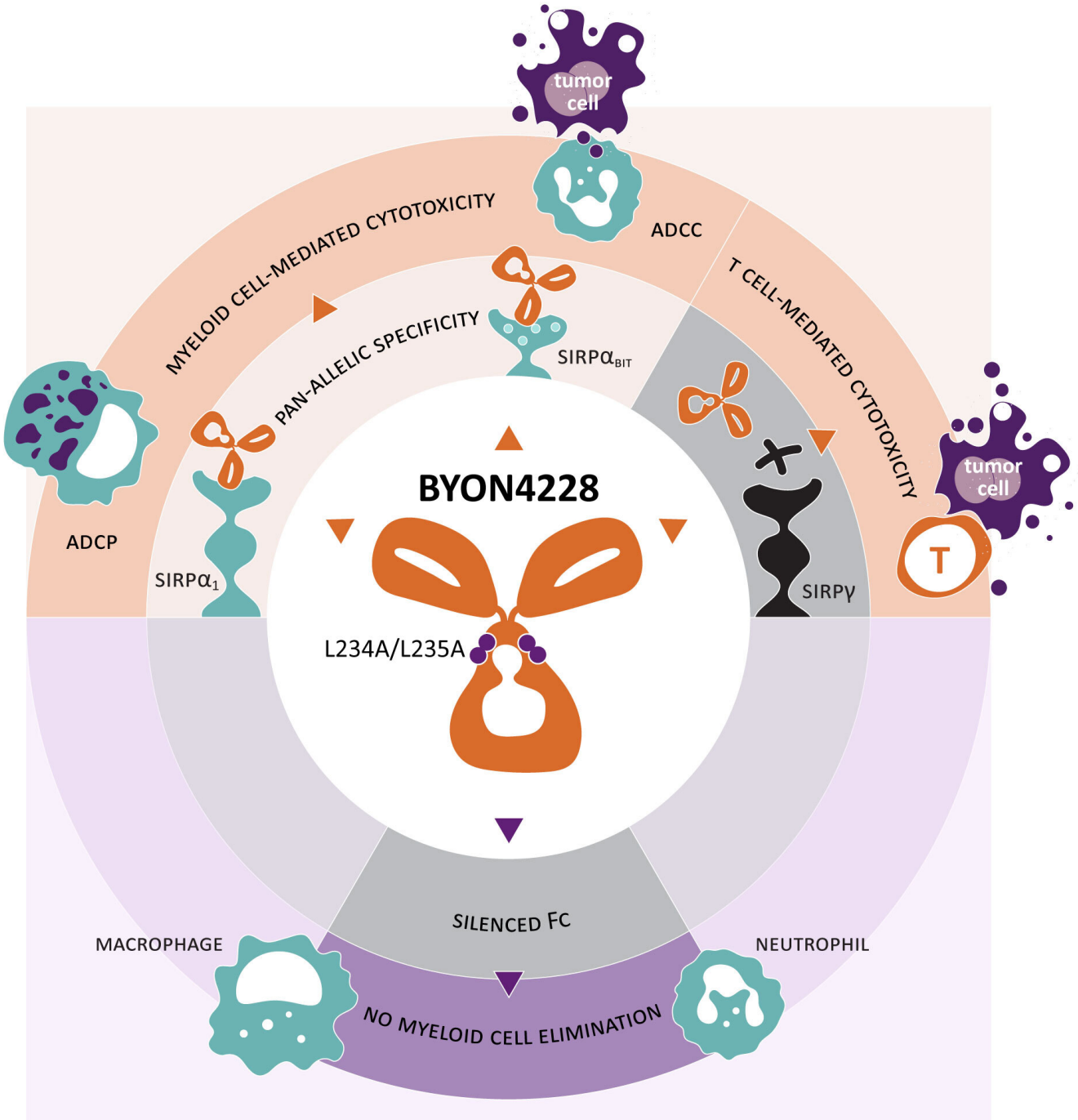
tumor cell
MYELOID CELL-MEDIATED CYTOTOXICITY
ADCC
T CELL-MEDIATED CYTOTOXICITY
PAN-ALLELIC SPECIFICITY
SIRPα$_{BIT}$
ADCP
SIRPα$_1$
BYON4228
L234A/L235A
SIRPγ
tumor cell
T
SILENCED FC
MACROPHAGE
NEUTROPHIL
NO MYELOID CELL ELIMINATION

Supplementary Figure Legends and Movie Legend

Figure S1. BYON4228 binds to a conserved epitope on the CD47-binding domain of SIRPα and blocked signaling

(A) BYON4228 (IgG1-L234A/L235A), KWAR23 (1) (IgG1-L234A/L235A) and isotype control (IgG1-L234A/L235A) binding to ExpiCHO-S cells that transiently expressed indicated (chimeric) SIRPα/γ molecules or not. Pictures visualize the composition of the chimeric SIRP molecules; $SIRP\alpha_{BIT}$, $SIRP\alpha_1$ and SIRPγ domains are represented in white, grey and black, respectively. The A/G letter abbreviation depicts the origin of a certain domain (SIRPα or SIRPγ); AAG means domain 1 and 2 from SIRPα, domain 3 from SIRPγ. Results depict the mean relative fluorescence unit +/- SD. (B) Differential heatmaps of differences in deuterium incorporation in antigens $SIRP\alpha_{BIT}$ (top) and $SIRP\alpha_1$ (bottom) alone and in the presence of BYON4228. Darker blue signifies a lower incorporation of deuterium in the presence of BYON4228 and suggests an interaction site between BYON4228 and antigen. (C) The BYON4228 epitope was mapped using hydrogen deuterium exchange mass spectrometry (HDX-MS) on the N-terminal Ig-like CD47-binding domain of $SIRP\alpha_{BIT}$ (top) and $SIRP\alpha_1$ (bottom). Projection of the BYON4228 footprint (orange, left). Indicated are the amino acid differences between $SIRP\alpha_1$ and $SIRP\alpha_{BIT}$ (turquoise blue, middle) and the overlap between the two (brown, right). (D) SIRPα signaling measured using the PathHunter Jurkat SIRPα signaling reporter cell line (DiscoverX), after co-incubation with indicated CD47-expressing or knock-out (KO) cells, in presence of a concentration-range of indicated antibodies. Results are shown as mean +/- SD of N=6 independent experiments.

Figure S2. BYON4228 augmented panitumumab- and cetuximab-induced ADCC of A431 cells

Neutrophil-mediated ADCC measured using the Cr-51 release assay after 4 hours incubation of target cells (A431) and effector cells (primary GM-CSF activated neutrophils) in the presence of a fixed dose of BYON4228 (10 µg/mL), isotype control (10 µg/mL) or nothing and a concentration range of panitumumab or cetuximab. Donors tested: 3 $SIRP\alpha_{BIT}/\alpha_{BIT}$, 3 $SIRP\alpha_{BIT}/\alpha_1$, and 3 $SIRP\alpha_1/\alpha_1$ donors. (A) Results show % killing of A431 cells by activated neutrophils of representative donors with indicated SIRPα genotypes. (B) Summary of ADCC results of all donors by plotting the % killing of A431 cells in presence or absence of BYON4228 or isotype control at 0 or 1 µg/mL anti-TAA (panitumumab or cetuximab). Results from the same donor are connected by lines. (C) Panitumumab (Pmab)- or cetuximab (Cmab)-induced ADCC fold enhancement of all donors (in absence of BYON4228 or isotype control). The fold enhancement ([% killing at 1 µg/mL anti-TAA]/[% killing without anti-TAA]) of anti-TAA-induced ADCC was calculated. The right graph illustrates how the fold enhancement was calculated. The left graph depicts the results of all donors. The lines indicate the mean values. (D) ADCC EC_{50} values of all donors of panitumumab and cetuximab in absence and presence of BYON4228 or isotype control. No EC_{50} values could be calculated from donors with incomplete curve saturation, no response or incorrect curve-fitting as indicated in the graph. (E) BYON4228 and isotype ADCC fold enhancement of all donors. The fold enhancement ([% killing at 1 µg/mL panitumumab or cetuximab + 10 µg/mL anti-SIRPα mAb or isotype]/ [% killing at 1 µg/mL panitumumab or cetuximab]) of panitumumab- or cetuximab-induced ADCC enhancement was calculated. The right graph illustrates how the fold enhancement was calculated. The left graph depicts the results of all donors. The lines

indicate the mean values. For C and E, * *P*<0.05, ** *P*<0.01, *** *P*<0.001; *P*>0.05 is not indicated. *P* values were calculated by a two-tailed t-test (C) and an one-way ANOVA followed by Tukey's multiple comparisons test (E).

Figure S3. BYON4228 augmented panitumumab-induced ADCC of the CRC cell line SW48 regardless of mutations downstream the EGFR signaling pathway

(A-E) Neutrophil-mediated ADCC measured using the Cr-51 release assay after 20 hours incubation of target cells (SW48) and effector cells (primary GM-CSF activated neutrophils) in the presence of a fixed dose of BYON4228 (10 µg/mL), isotype control (10 µg/mL) or nothing and a concentration range of panitumumab or cetuximab. Donors tested: 5 SIRP$\alpha_{BIT}/\alpha_{BIT}$, 4 SIRP$\alpha_{BIT}/\alpha_1$, and 3 SIRP$\alpha_1/\alpha_1$ donors. (A) Results show % killing of SW48 cells by activated neutrophils of representative donors with indicated SIRPα genotypes. (B) Summary of ADCC results of all donors by plotting the % killing of SW48 cells in presence or absence of BYON4228 or isotype control at 0 or 1 µg/mL panitumumab or cetuximab. Results from the same donor are connected by lines. (C) Panitumumab (Pmab)- or cetuximab (Cmab)-induced ADCC fold enhancement of all donors (in absence of BYON4228 or isotype control). The fold enhancement ([% killing at 1 µg/mL anti-TAA]/ [% killing without anti-TAA]) of anti-TAA-induced ADCC was calculated. The lines indicate the mean values. (D) ADCC EC_{50} values of panitumumab and cetuximab of all donors in absence and presence of BYON4228 or isotype control. No EC_{50} values could be calculated from donors with incomplete curve saturation, no response or incorrect curve-fitting as indicated in the graph. (E) BYON4228 and isotype ADCC fold enhancement of all donors. The fold enhancement ([% killing at 1 µg/mL anti-TAA + anti-SIRPα mAb or isotype]/ [% killing at 1 µg/mL anti-TAA]) of panitumumab- or cetuximab-induced ADCC enhancement was calculated. The lines indicate the mean values. (F-I) Neutrophil-mediated ADCC measured using the Cr-51 assay after 20 hours incubation of target cells (SW48 cells and isogenic SW48 mutant cells) and effector cells (primary GM-CSF activated neutrophils) in the presence of a fixed dose of BYON4228 (10 µg/mL) or nothing and a concentration range of panitumumab. Cell lines tested are SW48 (WT) (= parental cell line), SW48 KRAS exon 2 G12D, SW48 KRAS exon 2 G13D and SW48 BRAF V600E. Donors tested: 2 SIRP$\alpha_{BIT}/\alpha_{BIT}$, 2 SIRP$\alpha_{BIT}/\alpha_1$, and 2 SIRP$\alpha_1/\alpha_1$ donors. (F) Summary of ADCC results of all donors by plotting the % killing of SW48 cells in presence of BYON4228 at 0 or 10 µg/mL with or without 1 µg/mL panitumumab. Results from the same donor are connected by lines. (G) ADCC EC_{50} values of panitumumab for all donors in presence of absence of BYON4228. Results from the same donor are connected by a line. No EC_{50} values could be calculated from donors with incomplete curve saturation, no response or incorrect curve-fitting as indicated in the graph. (H) BYON4228 or isotype ADCC fold enhancements of all donors. The fold enhancement ([% killing at 1 µg/mL anti-TAA + anti-SIRPα mAb or isotype]/ [% killing at 1 µg/mL anti-TAA]) of panitumumab-induced ADCC enhancement was calculated. The lines indicate the mean values. For C, E and H, * *P*<0.05, ** *P*<0.01, *** *P*<0.001; *P*>0.05 is not indicated. *P* values were calculated by two-tailed t-tests (C: panitumumab vs cetuximab, H: for each cell line panitumumab + BYON4228 versus panitumumab + isotype) and one-way ANOVA followed by Tukey's multiple comparisons test (E).

Figure S4. BYON4228 enhanced daratumumab-induced ADCP of Daudi cells in a pan-allelic fashion

(A-C) Macrophage mediated ADCP measured using confocal microscopy after 3 hours incubation of target cells (Daudi) and effector cells (macrophages) in the presence of a fixed dose of daratumumab (5 ng/mL) and a concentration range of indicated antibodies or respective isotype controls. Donors tested: 4 SIRP$\alpha_{BIT}/_{BIT}$, 4 SIRPα_{BIT}/α_1, and 4 SIRPα_1/α_1 donors. (A) Results show phagocytosis index (PI) of macrophages from representative donors with indicated SIPRα genotypes. (B) SIRP-mAb induced ADCP EC_{50} values of all donors. No EC_{50} values could be calculated from donors with incomplete curve saturation, no response or incorrect curve-fitting as indicated in the graph. (C) SIRP-mAb induced ADCP fold enhancement of all donors. The means are depicted. The fold enhancement= [PI at 5 ng/mL daratumumab + 10 µg/mL anti-SIRP mAb]/ [PI at 5 ng/mL daratumumab]. (D-F) Macrophage mediated ADCP measured using the live-cell imaging pHrodo ADCP assay after up to 8 hours incubation of target cells (Daudi) and effector cells (macrophages) in the presence of a fixed dose of daratumumab (5 ng/mL) and a concentration range of indicated antibodies or respective isotype controls. Donors tested: 7 SIRP$\alpha_{BIT}/_{BIT}$, 3 SIRPα_{BIT}/α_1, and 6 SIRPα_1/α_1 donors. (D) Results show % phagocytosed tumor cells by macrophages from representative donors with indicated SIPRα genotypes. (E) SIRP-mAb induced ADCP EC_{50} values of all donors. No EC_{50} values could be calculated from donors with incomplete curve saturation, no response or incorrect curve-fitting as indicated in the graph. (F) SIRP-mAb induced ADCP fold enhancement of all donors. The means are depicted. The fold enhancement= [PI at 5 ng/mL daratumumab + 10 µg/mL anti-SIRP mAb]/ [PI at 5 ng/mL daratumumab]. For C and F, * P<0.05, ** P<0.01, *** P<0.001; P>0.05 is not indicated. P values were calculated by one-way ANOVA for each genotype (comparing the different mAbs) and for each mAb (comparing the different genotypes) followed by Tukey's multiple comparisons test (C) and an one-way ANOVA followed by Tukey's multiple comparisons test (F).

Figure S5. BYON4228 enhanced panitumumab and cetuximab-induced ADCP of HT-29 CRC cells in a pan-allelic fashion

Macrophage mediated ADCP measured using the live-cell imaging pHrodo ADCP assay after up to 8 hours incubation of target cells (HT-29) and effector cells (macrophages) in the presence of a fixed dose of panitumumab (A-C) or cetuximab (D-F) (both fixed at 40 ng/mL) and a concentration range of indicated antibodies or respective isotype controls. Donors tested (A-C): 7 SIRP$\alpha_{BIT}/_{BIT}$, 3 SIRPα_{BIT}/α_1, and 9 SIRPα_1/α_1 donors. Donors tested (D-F): 8 SIRP$\alpha_{BIT}/_{BIT}$, 2 SIRPα_{BIT}/α_1, and 6 SIRPα_1/α_1 donors. (A, D) Results show % phagocytosed tumor cells by macrophages from representative donors with indicated SIPRα genotypes. (B, E) SIRP-mAb induced ADCP EC_{50} values of all donors. No EC_{50} values could be calculated from donors with incomplete curve saturation, no response or incorrect curve-fitting as indicated in the graph. (C, F) SIRP-mAb induced ADCP fold enhancement of all donors. The means are depicted. The fold enhancement= [% phagocytosed cells at 40 ng/mL panitumumab or cetuximab + 10 µg/mL anti-SIRP mAb]/ [% phagocytosed cells at 40 ng/mL panitumumab or cetuximab]. For C and F, * P<0.05, ** P<0.01, *** P<0.001; P>0.05 is not indicated. P values were calculated by one-way ANOVA followed by Tukey's multiple comparisons test.

Figure S6. BYON4228 does not induce Fc dependent immune effector activation and Fc tail variants all potently enhance cetuximab-induced ADCC

(A) NK-mediated ADCC: Purified NK cells were incubated for 24 hours with indicated antibodies and MOLM-13 cells (effector: target = 4:1) and antibody-induced killing was determined. BYON5664 contains the variable domains of BYON4228 but has a wildtype IgG constant domain with wildtype effector functions. Left: representative donor. Right: results of N=4 donors using 20 µg/mL antibody. (B) CDC: U937 or MOLM-13 cells were opsonized with indicated antibodies and then treated with 0% baby rabbit serum, 12.5% heat inactivated (HI) baby rabbit serum or 12.5% baby rabbit serum. % survival was measured using CellTiter-Glo (CTG) luminescent assay. Data show the percentage of survival +/- SD of three independent experiments. (C) Blocking of CD47-induced SIRPα-mediated signal transduction: SIRPα signaling measured using the PathHunter Jurkat SIRPα signaling reporter cell line (DiscoverX), after co-incubation with CD47-expressing or knock-out (KO) Raji cells, in presence of a concentration-range of BYON4228 (IgG1-L234A/L235A) or BYON5306 which is a $F(ab')_2$ of BYON4228. Results are shown as mean +/- SD of N=6 independent experiments. (D-F) Neutrophil-mediated ADCC measured using the Cr-51 release assay after 4 hours incubation of target cells (A431) and effector cells (primary GM-CSF activated neutrophils) in the presence of a fixed dose of cetuximab (10 µg/mL) and a concentration range of indicated antibodies or respective isotype controls. Donors tested: 5 $SIRP\alpha_{BIT}/\alpha_{BIT}$, 4 $SIRP\alpha_{BIT}/\alpha_1$, and 5 $SIRP\alpha_1/\alpha_1$ donors. (D) Results show % killing of A431 cells by activated neutrophils of representative donors with indicated SIRPα genotypes. (E) SIRP-mAb induced ADCC EC_{50} values of all donors. No EC_{50} values could be calculated from donors with incomplete curve saturation, no response or incorrect curve-fitting as indicated in the graph. (F) SIRP-mAb induced ADCC fold enhancement of all donors. The means are depicted. The fold enhancement = [% killing at 10 µg/mL cetuximab + 67 nM anti-SIRPα mAb]/ [% killing at 10 µg/mL cetuximab]. For A, B and F, * $P<0.05$, ** $P<0.01$, *** $P<0.001$; $P>0.05$ is not indicated. *P* values were calculated by one-way ANOVA for each mAb (comparing the different treatment conditions) followed by Tukey's multiple comparisons test (B) and an one-way ANOVA followed by Tukey's multiple comparisons test (A, F).

Figure S7. BYON4228 and BYON4228-$F(ab')_2$ induce potent enhancement of rituximab and daratumumab-induced ADCP

Macrophage mediated ADCP was measured using confocal microscopy after 3 hours incubation of target cells (Raji, A-C or Daudi, D-F) and effector cells (macrophages) in the presence of a fixed dose of rituximab (80 ng/mL, A-C) or daratumumab (5 ng/mL, D-F) and a concentration range of indicated antibodies or respective isotype controls. BYON5306 is a $F(ab')_2$ fragment of BYON4228. Donors tested (A-C): 5 $SIRP\alpha_{BIT}/_{BIT}$, 6 $SIRP\alpha_{BIT}/\alpha_1$, and 6 $SIRP\alpha_1/\alpha_1$ donors, (D-F): 4 $SIRP\alpha_{BIT}/_{BIT}$, 4 $SIRP\alpha_{BIT}/\alpha_1$, and 4 $SIRP\alpha_1/\alpha_1$ donors. (A, D) Results show phagocytosis index (PI) of macrophages from representative donors with indicated SIPRα genotypes. (B, E) SIRP-mAb or -$F(ab')_2$ induced ADCP EC_{50} values of all donors. No EC_{50} values could be calculated from donors with incomplete curve saturation, no response or incorrect curve-fitting as indicated in the graph. (C, F) SIRP-mAb or -$F(ab')_2$ induced ADCP fold enhancement of all donors. The means are depicted. The fold enhancement= [PI at 80 ng/mL rituximab or 5 ng/mL daratumumab + maximum concentration of anti-SIRP mAb/$F(ab')_2$]/ [PI at 80 ng/mL rituximab or 5 ng/mL daratumumab]. For C and F, * $P<0.05$, ** $P<0.01$, *** $P<0.001$; $P>0.05$ is not indicated. *P* values were calculated by one-way

ANOVA for each mAb (comparing the different genotypes) followed by Tukey's multiple comparisons test and two-tailed t-tests for each genotype (comparing the different mAbs).

Figure S8. Characterization of huSIRPα$_{BIT}$ transgenic mice and BYON4228 pharmacokinetic studies in mice

(A) Western blotting of bone marrow-derived macrophages (BMDM) samples from *Cebpa*$^{+/+}$huSIRPα$_{BIT}$$^{Tg/Tg}$ or *Cebpa*$^{Cre/+}$huSIRPα$_{BIT}$$^{Tg/WT}$ or *Cebpa*$^{Cre/+}$huSIRPα$_{BIT}$$^{Tg/Tg}$ mice as indicated, or of human primary neutrophils (N). Indicated is murine (mu) SIRPα and human (hu) SIRPα. (B, C) FACS analysis for SIRPα expression on blood monocytes (B) and neutrophils (C) of indicated mice. FMO is fluorescence minus one. (D, E) ADCC (normalized to trastuzumab) by neutrophils of trastuzumab opsonized SK-BR-3 cells in absence or presence of an anti-SIRPα blocking mAb in *Cebpa*$^{+/+}$huSIRPα$_{BIT}$$^{Tg/Tg}$ (D) and *Cebpa*$^{Cre/+}$huSIRPα$_{BIT}$$^{Tg/Tg}$ (E) mice. * P<0.05 , ** P<0.01 Tukey's multiple comparison test, ns; not significant. (F-H) Pharmacokinetic (PK) of BYON4228 in C57Bl/6 mice (purple line) and huSIRPα$_{BIT}$ mice (*Cebpa*$^{Cre/+}$huSIRPα$_{BIT}$$^{Tg/Tg}$ or *Cebpa*$^{Cre/Cre}$huSIRPα$_{BIT}$$^{Tg/Tg}$) (orange/yellow lines) after single IV (F, H, solid line) or IP (G) dosing, or repeated IP dosing every 3 days for 6 times (H, dashed line). Concentration mean +/- SD, N=3 per time-point. Arrows in (H) indicate timepoints of dosing.

Figure S9. BYON4228 administration to cynomolgus monkeys does not induce anemia or thrombocytopenia

(A,B) Cellular binding of BYON4228 to human or cynomolgus granulocytes and the EC_{50} summary (N=65). (C-E) Measurement of hemoglobin levels, red blood cells and platelets after repeated administration of BYON4228 or vehicle to cynomolgus monkeys as indicated with the dotted lines at indicated doses (N=5, +/- SEM).

Supplementary Movies Legend. Visualization of real-time phagocytosis using live-cell imaging

Panitumumab-opsonized (40 ng/mL) HT-29 tumor cells were labeled with pHrodo and co-incubated with unlabeled macrophages and BYON4228 (10 µg/mL). Images were taken every 3 minutes for 4 hours. The light-red tumor cells become bright red upon phagocytosis by macrophages. Two representative movies are shown.

References

1. Ring NG, Herndler-Brandstetter D, Weiskopf K, Shan L, Volkmer JP, George BM, et al. Anti-SIRPalpha antibody immunotherapy enhances neutrophil and macrophage antitumor activity. Proc Natl Acad Sci U S A. 2017;114(49):E10578-E85.

Supplementary Methods

BYON4228 antibody development and humanization

First, rabbit antibodies were generated. After immunization of rabbits (MAB Discovery GmbH, Neuried, Germany) with the ECDs of different human SIRPα allelic variants, cell culture supernatants derived from individual B cells were tested in enzyme-linked immunosorbent assays (ELISA) for binding to various SIRP family members from different species (human, mouse, monkey), and for interference with CD47-SIRPα binding. Selected clonal B cell cultures were used to obtain the heavy and light chain sequences for the corresponding antibodies and used to generate rabbit-human chimeric mAbs. After further selection (e.g. in the ADCC assay), the chimeric mAbs were further humanized by replacing amino acids present in antibodies with demonstrated high production levels in mammalian cells and low immunogenicity in humans.

HEFLB, SIRPAB-11-K322A and 1H9 antibody sequences

HEFLB: antibody amino acid sequences identical to those described in patent application WO 2017/178653 HEFLB (1):

>HEFLB_heavy_chain
EVQLVQSGAEVKKPGESLRISCKASGYSFTSYWVHWVRQMPGKGLEWMGNIDPSDSDTHYSPSFQGH
VTLSVDKSISTAYLQLSSLKASDTAMYYCVRGGTGTLAYFAYWGQGTLVTVSSASTKGPSVFPLAPCSRSTS
ESTAALGCLVKDYFPEPVTVSWNSGALTSGVHTFPAVLQSSGLYSLSSVVTVPSSSLGTKTYTCNVDHKPS
NTKVDKRVESKYGPPCPPCPAPEFLGGPSVFLFPPKPKDTLMISRTPEVTCVVVDVSQEDPEVQFNWYVD
GVEVHNAKTKPREEQFNSTYRVVSVLTVLHQDWLNGKEYKCKVSNKGLPSSIEKTISKAKGQPREPQVYT
LPPSQEEMTKNQVSLTCLVKGFYPSDIAVEWESNGQPENNYKTTPPVLDSDGSFFLYSRLTVDKSRWQEG
NVFSCSVMHEALHNHYTQKSLSLSPGK
>HEFLB_light_chain
DVVMTQSPLSLPVTLGQPASISCRSSQSLVHSYGNTYLYWFQQRPGQSPRLLIYRVSNRFSGVPDRFSGS
GSGTDFTLKISRVEAEDVGVYYCFQGTHVPYTFGGGTKVEIKRTVAAPSVFIFPPSDEQLKSGTASVVCLLN
NFYPREAKVQWKVDNALQSGNSQESVTEQDSKDSTYSLSSTLTLSKADYEKHKVYACEVTHQGLSSPVTK
SFNRGEC

SIRPAB-11-K322A: The antibody amino acid sequences of antibody SIRPAB-11 as made at Byondis are identical to those described in patent application WO 2020/068752 SIRPAB-11-K322A (2):

> SIRPAB-11-K322A _heavy_chain
QVQLVQSGAEVKKPGASVKVSCKASGYTFRGYGISWVRQAPGQGLEWMGWISAYGGETNYAQKLQG
RVTMTTDTSTSTAYMELRSLRSDDTAVYYCAREAGSSWYDFDLWGRGTLVTVSSASTKGPSVFPLAPSSK
STSGGTAALGCLVKDYFPEPVTVSWNSGALTSGVHTFPAVLQSSGLYSLSSVVTVPSSSLGTQTYICNVNH
KPSNTKVDKKVEPKSCDKTHTCPPCPAPELLGGPSVFLFPPKPKDTLMISRTPEVTCVVVDVSHEDPEVKF
NWYVDGVEVHNAKTKPREEQYNSTYRVVSVLTVLHQDWLNGKEYKCAVSNKALPAPIEKTISKAKGQPR
EPQVYTLPPSREEMTKNQVSLTCLVKGFYPSDIAVEWESNGQPENNYKTTPPVLDSDGSFFLYSKLTVDKS
RWQQGNVFSCSVMHEALHNHYTQKSLSLSPGK
> SIRPAB-11-K322A _light_chain
DIQMTQSPSSVSASVGDRVTITCRASQGISSWLAWYQQKPGKAPKLLIYAASNLQSGVPSRFSGSGSGTD
FTLTISSLQPEDFATYYCQQGASFPITFGGGTKVEIKRTVAAPSVFIFPPSDEQLKSGTASVVCLLNNFYPRE
AKVQWKVDNALQSGNSQESVTEQDSKDSTYSLSSTLTLSKADYEKHKVYACEVTHQGLSSPVTKSFNRGE
C

Preclinical characterization of the pan-allelic SIRPα-blocking antibody BYON4228

1H9: The antibody amino acid sequences of antibody 1H9 as made at Byondis are identical to those described in patent application WO 2019/023347 humanized 1H9 (3), with a G1m17,1 allotype:

>1H9_heavy_chain
QVQLVQSGAEVKKPGASVKVSCKASGYTFTSYWITWVKQAPGQGLEWIGDIYPGSGSTNHIEKFKSKATL
TVDTSISTAYMELSRLRSDDTAVYYCATGYGSSYGYFDYWGQGTLVTVSSASTKGPSVFPLAPSSKSTSGG
TAALGCLVKDYFPEPVTVSWNSGALTSGVHTFPAVLQSSGLYSLSSVVTVPSSSLGTQTYICNVNHKPSNT
KVDKKVEPKSCDKTHTCPPCPAPELLGGPSVFLFPPKPKDTLMISRTPEVTCVVVDVSHEDPEVKFNWYV
DGVEVHNAKTKPREEQYASTYRVVSVLTVLHQDWLNGKEYKCKVSNKALPAPIEKTISKAKGQPREPQVY
TLPPSRDELTKNQVSLTCLVKGFYPSDIAVEWESNGQPENNYKTTPPVLDSDGSFFLYSKLTVDKSRWQQ
GNVFSCSVMHEALHNHYTQKSLSLSPGK
>1H9_light_chain
DIQMTQSPSSLSASVGDRVTITCRASENIYSYLAWYQQKPGKAPKLLIYTAKTLAEGVPSRFSGSGSGTDFT
LTISSLQPEDFATYYCQHQYGPPFTFGQGTKLEIKRTVAAPSVFIFPPSDEQLKSGTASVVCLLNNFYPREAK
VQWKVDNALQSGNSQESVTEQDSKDSTYSLSSTLTLSKADYEKHKVYACEVTHQGLSSPVTKSFNRGEC

Sequences of WT and domain swap SIRP variants, used for expression on ExpiCHO-S cells and soluble expression

Full-length human SIRPα_1 (CAA71403), human SIRPα_{BIT} (NP_542970), human SIRPβ1v1 (O00241), human SIRPβ1v2 (Q5TFQ8) and human SIRPγ (Q9P1W8), including three ECDs, a transmembrane domain and an intracellular domain were expressed by using their germline signal peptide sequences. Also, domain swap SIRP variants were made and used to identify binding specificity of subjected antibodies to either the first, second or third domain of human SIRPα_1, human SIRPα_{BIT}, or human SIRPγ. The boundaries of each of the domains were based on UniProt annotations. The chimeric SIRP variants were assembled by either replacing human SIRPα_{BIT} or human SIRPα_1 domains by the human SIRPγ domain while retaining the human SIRPα membrane anchor.

Human SIRPα_{BIT} ECD, human SIRPα_1 ECD, human SIRPβ1v1 ECD and human SIRPβ1v2 ECD were expressed as fusion protein, all containing an Avi-tag, a Factor Xa (FXa) cleavage site and an Fc tail for purification. The ECD of human CD47 (Q08722) was expressed as fusion protein using an Fc tail and Avi-tag only and human SIRPγ ECD was fused to the combination of an Avi-tag and a C-tag.

>hSIRPα_{BIT} ECD_AviTag_FXa_Fc
EEELQVIQPDKSVLVAAGETATLRCTATSLIPVGPIQWFRGAGPGRELIYNQKEGHFPRVTTVSDLTKRNN
MDFSIRIGNITPADAGTYYCVKFRKGSPDDVEFKSGAGTELSVRAKPSAPVVSGPAARATPQHTVSFTCES
HGFSPRDITLKWFKNGNELSDFQTNVDPVGESVSYSIHSTAKVVLTREDVHSQVICEVAHVTLQGDPLRG
TANLSETIRVPPTLEVTQQPVRAENQVNVTCQVRKFYPQRLQLTWLENGNVSRTETASTVTENKDGTYN
WMSWLLVNVSAHRDDVKLTCQVEHDGQPAVSKSHDLKVSAHPKEQGSNTAAENTGSNERNGGGLND
IFEAQKIEWHEIEGRDKTHTCPPCPAPELLGGPSVFLFPPKPKDTLMISRTPEVTCVVVDVSHEDPEVKFN
WYVDGVEVHNAKTKPREEQYNSTYRVVSVLTVLHQDWLNGKEYKCKVSNKALPAPIEKTISKAKGQPRE
PQVYTLPPSREEMTKNQVSLTCLVKGFYPSDIAVEWESNGQPENNYKTTPPVLDSDGSFFLYSKLTVDKSR
WQQGNVFSCSVMHEALHNHYTQKSLSLSPGK

>hSIRPα_1 ECD_AviTag_FXa_Fc

Preclinical characterization of the pan-allelic SIRPα-blocking antibody BYON4228

3

EEELQVIQPDKSVSVAAGESAILHCTVTSLIPVGPIQWFRGAGPARELIYNQKEGHFPRVTTVSESTKREN
MDFSISISNITPADAGTYYCVKFRKGSPDTEFKSGAGTELSVRAKPSAPVVSGPAARATPQHTVSFTCESH
GFSPRDITLKWFKNGNELSDFQTNVDPVGESVSYSIHSTAKVVLTREDVHSQVICEVAHVTLQGDPLRGT
ANLSETIRVPPTLEVTQQPVRAENQVNVTCQVRKFYPQRLQLTWLENGNVSRTETASTVTENKDGTYN
WMSWLLVNVSAHRDDVKLTCQVEHDGQPAVSKSHDLKVSAHPKEQGSNTAAENTGSNERNGGGLND
IFEAQKIEWHEIEGRDKTHTCPPCPAPELLGGPSVFLFPPKPKDTLMISRTPEVTCVVVDVSHEDPEVKFN
WYVDGVEVHNAKTKPREEQYNSTYRVVSVLTVLHQDWLNGKEYKCKVSNKALPAPIEKTISKAKGQPRE
PQVYTLPPSREEMTKNQVSLTCLVKGFYPSDIAVEWESNGQPENNYKTTPPVLDSDGSFFLYSKLTVDKSR
WQQGNVFSCSVMHEALHNHYTQKSLSLSPGK

>huSIRPβ1v1 ECD AviTag_FXa_Fc
EDELQVIQPEKSVSVAAGESATLRCAMTSLIPVGPIMWFRGAGAGRELIYNQKEGHFPRVTTVSELTKRN
NLDFSISISNITPADAGTYYCVKFRKGSPDDVEFKSGAGTELSVRAKPSAPVVSGPAVRATPEHTVSFTCES
HGFSPRDITLKWFKNGNELSDFQTNVDPAGDSVSYSIHSTARVVLTRGDVHSQVICEIAHITLQGDPLRGT
ANLSEAIRVPPTLEVTQQPMRAENQANVTCQVSNFYPRGLQLTWLENGNVSRTETASTLIENKDGTYN
WMSWLLVNTCAHRDDVVLTCQVEHDGQQAVSKSYALEISAHQKEHGSDITHEAALAPTAPLGGGLNDI
FEAQKIEWHEIEGRDKTHTCPPCPAPELLGGPSVFLFPPKPKDTLMISRTPEVTCVVVDVSHEDPEVKFNW
YVDGVEVHNAKTKPREEQYNSTYRVVSVLTVLHQDWLNGKEYKCKVSNKALPAPIEKTISKAKGQPREPQ
VYTLPPSREEMTKNQVSLTCLVKGFYPSDIAVEWESNGQPENNYKTTPPVLDSDGSFFLYSKLTVDKSRW
QQGNVFSCSVMHEALHNHYTQKSLSLSPGK

>huSIRPβ1v2 ECD AviTag_FXa_Fc
EEELQVIQPDKSISVAAGESATLHCTVTSLIPVGPIQWFRGAGPGRELIYNQKEGHFPRVTTVSDLTKRNN
MDFSIRISNITPADAGTYYCVKFRKGSPDHVEFKSGAGTELSVRAKPSAPVVSGPAARATPQHTVSFTCES
HGFSPRDITLKWFKNGNELSDFQTNVDPAGDSVSYSIHSTAKVVLTREDVHSQVICEVAHVTLQGDPLRG
TANLSETIRVPPTLEVTQQPVRAENQVNVTCQVRKFYPQRLQLTWLENGNVSRTETASTLTENKDGTYN
WMSWLLVNVSAHRDDVKLTCQVEHDGQPAVSKSHDLKVSAHPKEQGSNTAPGPALASAAPLGGGLN
DIFEAQKIEWHEIEGRDKTHTCPPCPAPELLGGPSVFLFPPKPKDTLMISRTPEVTCVVVDVSHEDPEVKFN
WYVDGVEVHNAKTKPREEQYNSTYRVVSVLTVLHQDWLNGKEYKCKVSNKALPAPIEKTISKAKGQPRE
PQVYTLPPSREEMTKNQVSLTCLVKGFYPSDIAVEWESNGQPENNYKTTPPVLDSDGSFFLYSKLTVDKSR
WQQGNVFSCSVMHEALHNHYTQKSLSLSPGK

>huSIRPγ ECD AviCtag
EEELQMIQPEKLLLVTVGKTATLHCTVTSLLPVGPVLWFRGVGPGRELIYNQKEGHFPRVTTVSDLTKRNN
MDFSIRISSITPADVGTYYCVKFRKGSPENVEFKSGPGTEMALGAKPSAPVVLGPAARTTPEHTVSFTCES
HGFSPRDITLKWFKNGNELSDFQTNVDPTGQSVAYSIRSTARVVLDPWDVRSQVICEVAHVTLQGDPLR
GTANLSEAIRVPPTLEVTQQPMRVGNQVNVTCQVRKFYPQSLQLTWSENGNVCQRETASTLTENKDGT
YNWTSWFLVNISDQRDDVVLTCQVKHDGQLAVSKRLALEVTVHQKDQSSDATPKGQDNSADIQHSGG
RSSLEGPRFEGKPIPNPLLGLDSTRTGGGGLNDIFEAQKIEWHEACAAADYKPGGGKPGGEPEA

Vector construction and cloning strategy of mAbs and SIRP variants (for soluble expression and ExpiCHO-S cell based expression)

For expression of antibody chains and SIRP variants the mammalian expression vector pcDNA3.4-TOPO (Thermo Fisher Scientific) was used, which contains an expression cassette consisting of a CMV promoter and a BGHpA poly-adenylation site. Antibody chain amino acid sequences and soluble SIRP and CD47 variants were back-translated into a complementary DNA (cDNA) sequence and codon-optimization was performed for expression in human cells.

Preclinical characterization of the pan-allelic SIRPα-blocking antibody BYON4228

Codon optimization was also performed for cell surface expressed SIRP variant sequences for expression in CHO cells. The antibody chain and SIRP variant cDNAs with flanking AscI and NheI cloning sites were synthesized by assembly of synthetic oligos and/or PCR products (Thermo Fisher Scientific) and individually cloned into the single gene vector pcDNA3.4-TOPO. For co-expression of cell surface expressed SIRP variants and green fluorescent protein (GFP) as reporter double gene vectors (DGV) were constructed. First, the DGV was made by excision of the CMV:BGHpA expression cassette from the pcDNA3.1(-) plasmid (Thermo Fisher Scientific) and re-inserted back into the same original vector (still containing an intact CMV:BGHpA expression cassette), to allow expression of two genes from a single plasmid vector. Next, unique multiple cloning sites (MCS) were created to allow cloning of the synthesized GFP gene into the first MCS using BamHI and DraIII restriction sites. Finally, the resulting vector was digested with AscI and NheI restriction enzymes, and ligated with the SIRP variant cDNA fragment, digested with the same restriction enzymes, and thereby introducing the SIRP variant cDNA into the second MCS. After transfer to *E. coli* K12 DH10B T1R and expansion, large-scale production of the final vectors for transfection was performed using the EndoFree Plasmid Maxi kit according to the manufacturer's instructions (Qiagen).

Antibody expression in Expi293F cells and purification

Expi293F cells were cultured in Expi293 Expression medium and maintained in an incubator at 37 °C, 8% CO_2 and 80% humidity on an orbital shaker platform rotating at 100 rpm with a stroke of 50 mm and according to the manufacturer's instructions (Thermo Fisher Scientific). Expi293F cells were transfected using the transfection agent FectoPRO according to the manufacturer's instructions (Polyplus-transfection). Antibodies were transiently expressed by co-expression of heavy and light chain expression vectors at a 1:1 mass ratio. Six days post transfection, the cell culture supernatant was harvested by centrifugation at 4,000 g for 15 minutes and filtering the clarified harvest over MF75 filters (Nalgene). The antibody concentrations in supernatant were determined by ForteBio Octet QK384 using Protein A Biosensors and trastuzumab as calibrator according to manufacturer's instructions (Sartorius). Antibodies were purified from the clarified harvest using protein A (MabSelect SuRe, Cytiva). After elution with 25 mM NaOAc pH 3.0, the antibodies were rebuffered to 4.2 mM histidine, 50 mM trehalose pH 6.0 for storage. The antibody quality was checked by SDS-PAGE using a Criterion TGX Stain Free Precast Gel of 4-20% (Bio-Rad) and using Size Exclusion Chromatography to determine the level of soluble high molecular weights (HMW).

Expression of SIRP variants on ExpiCHO-S cells

ExpiCHO-S cells were cultured in ExpiCHO Expression medium according to the manual provided by Thermo Fisher Scientific and maintained in an incubator at 37 °C, 8% CO_2 and 80% humidity on an orbital shaker platform rotating at 120 rpm with a stroke of 25 mm. For the generation of batches of cell surface-expressed SIRP variants, ExpiCHO-S cells were transfected using ExpiFectamine CHO as transfection agent according to manufacturers' protocols. For co-expression of the SIRP variants and GFP the DGVs were used. Transfected cell cultures were placed at standard culture conditions for 24 hours before being cryopreserved for later use in binding assays.

Production and purification of soluble SIRP variants and soluble CD47

Soluble SIRP variants and soluble CD47 were produced as Fc fusion variants or with a C-tag.

Preclinical characterization of the pan-allelic SIRPα-blocking antibody BYON4228

The soluble Fc fusion variants were purified from the clarified harvest using protein A (MabSelect SuRe, Cytiva), according to the instruction of the supplier. After elution the antigen-Fc variants were rebuffered to 4.2 mM histidine, 50 mM trehalose pH 6.0 for storage. The antigen-Fc quality was checked by SDS-PAGE using a Criterion TGX Stain Free Precast Gel of 4-20% (Bio-Rad) and using Size Exclusion Chromatography to determine the level of soluble HMW.

The soluble antigen-C-tag variants were purified from the clarified harvest using CaptureSelect C-tagXL resin (Thermo Fisher Scientific) according to the instructions of the supplier. Elution was done with 20 mM tris-HCl, 2 M $MgCl_2$, pH 7.0. After elution product containing fractions were pooled and dialyzed to 4.2 mM histidine, 50 mM trehalose pH 6.0 using dialysis membranes with a MWCO of 10 kDa (Thermo Fisher Scientific). The product was then further concentrated using a Vivaspin Turbo 15 (Satorius) with a 30 kDa molecular weight cut-off.

Removal of the Fc tag and biotinylation of soluble SIRP proteins and CD47; coupling of CD47 to fluorescent beads

The Fc tag was removed by digestion with Factor Xa (FXa). First the purified antigen-Fc variants were rebuffered to 20 mM Tris-HCl, 100 mM NaCl, 2 mM $CaCl_2$ pH 8.0 using a PD10 desalting column (Cytiva). The antigen-Fc variants were incubated with FXa (Biolabs) in a 1:50 (w/w) ratio (FXa : antigen-Fc) and incubated for 23 h at 37 °C. The digestion was followed by SDS-PAGE using a 4-20% gradient Stain-Free gel (Bio-Rad) and upon completion the reaction was stopped with a 10-fold molar excess dansyl-glu-gly-arg-chloromethylketone. The Fc part and undigested antigen-Fc was removed from the antigen using protein A (MabSelect SuRe, Cytiva) . The soluble antigen is found in the flow through of the column while the Fc containing parts are eluted with 25 mM NaOAc pH 3.0. The flow through was then rebuffered to 10 mM Tris-HCl, 0.5 M NaCl pH 8.0 using a PD10 desalting column (Cytiva) and loaded on a Benzamidine FF (High Sub) column (Cytiva). The soluble antigen is found in the flow through while the FXa binds to the Benzamidine FF (High Sub) column. The flow through was then rebuffered to 10 mM Tris-HCl, 5 mM NaCl pH 8.0 for biotinylation. The removal of the FXa was followed by SDS-PAGE using a Criterion TGX Stain-Free Precast Gel of 4-20% (Bio-Rad).

CD47-Fc and soluble SIRP proteins were biotinylated using the BirA500 kit (biotin-protein ligase standard reaction kit, Avidity) according to the manufacturer's protocol. CD47-Fc was then conjugated to FluoSpheresNeurtAvidin-labeled microspheres stock (Thermo Fisher Scientific, F8774) at a final concentration of 50 µg/mL according to manufacturer's instructions.

Generation of F(ab')$_2$ fragments

Protein A purified antibody was rebuffered to 0.2 M NaOAc pH 4.0 using PD10 desalting columns (Cytiva). Pepsin from porcine gastric mucose (Sigma) was dissolved in 10 mM HCl and diluted to 0.1 mg/mL. Pepsin was added to the antibody in a 1:5 molar ratio (pepsin:antibody) and incubated at 37 °C. After 4 hours the digestion was stopped by adding 2 M Tris until a neutral pH. Remaining undigested antibody was removed using protein A (MabSelect SuRe, Cytiva) were the F(ab')$_2$ fragment was found in the flow through of the column. Pepsin was removed from the F(ab')$_2$ fragment and further purified using protein L

(Capto L, Cytiva) in bind and elute mode, where the $F(ab')_2$ fragment was eluted with 0.1 M acetic acid pH 3.0. The $F(ab')_2$ fragment was rebuffered to 4.2 mM histidine, 50 mM trehalose pH 6.0. The quality of the $F(ab')_2$ fragment was checked by SDS-PAGE using a Criterion TGX Stain-Free Precast Gel of 4-20% (Bio-Rad), a single band of about 100 kDa was found.

Cell lines and cell culture

An overview of the cell lines used in this study can be found in Table 4. The generation of SK-BR-3, A431 and Raji CD47-KO cells was described earlier (4-6).

Table 4: Overview of cell lines used and their culture conditions

Cell line	Origin	Cell culture medium
U937	ATCC CRL-1593.2	RPMI-1640 (Gibco)/10% FBS/penicillin-streptomycin (Lonza)
Daudi	DSMZ ACC78	RPMI-1640 (Gibco)/10% FBS/penicillin-streptomycin (Lonza)/GlutaMAX (Gibco
PathHunter cells	DiscoverX	Assay complete cell culture reagent (DiscoverX)
SK-BR-3	ATCC HTB-30	IMDM (Gibco)/20% FBS/2mM L-glutamine/penicillin-streptomycin
A431	DSMZ ACC 91	RPMI-1640 (Gibco)/10% FBS/penicillin-streptomycin (Lonza)
SW48 (WT) = SW48 (006) SW48 BRAF V600E, SW48 KRAS G12D, SW48 KRAS G13D	Horizon Discovery	RPMI-1640 (Gibco)/10% FBS/penicillin-streptomycin (Lonza)
Raji	DSMZ ACC319	RPMI-1640 (Gibco)/10% FBS/penicillin-streptomycin (Lonza)
HT-29	ATCC HTB-38	McCoys 5A (Lonza)/10% FBS/penicillin-streptomycin (Lonza)
OCI-AML2	DSMZ ACC 99	MEM Alpha Eagle (Lonza)/20% FBS/penicillin-streptomycin (Lonza)
MOLM-13	DSMZ ACC 554	RPMI-1640 (Gibco)/10% FBS/penicillin-streptomycin (Lonza)

Origin of healthy donor blood, SIRPα genotyping and phenotyping

SIRPα variant expression (i.e. $SIRP\alpha_{BIT}$ and/or $SIRP\alpha_1$) of donor immune effector cells was determined by either DNA sequencing and/or phenotyping using flow cytometry. SIRPα genotypes of individual donors were determined by Sanger sequencing using genomic DNA isolated from PBMCs of healthy Caucasian donors with the QIAamp kit (Qiagen). SIRPα polymorphic variants, namely $SIRP\alpha_1$ or $SIRP\alpha_{BIT}$, were identified by sequencing the V-Ig domain encoded by the third exon. For PCR amplification and sequencing the following primers were used, located in the introns surrounding exon 3, thus amplifying the whole exon. Forward PCR primer: AACACTTGAGGAAACACAGAG. Reverse PCR primer: CACCTACCACCACACCTGA. Primer used for Sanger sequencing: AAAAAATGACTGCTTTGTGCTCCTTTCC. Phenotyping of donors was performed using a

fluorescent-labeled antibody against SIRPα_{BIT} (clone 4G5, internal production) and a fluorescent-labeled antibody that has preference for binding to SIRPα_1 (internal production).

Affinity measurements

Two different assay setups were used for SIRP ECD binding analysis by surface plasmon resonance (SPR). Data were analyzed using double reference subtraction (DRS): Responses of a sample cycle (Flow $cell_{specific}$ – Flow $cell_{background}$) subtracted with response of a blank cycle (Flow $cell_{specific}$ – Flow $cell_{background}$). All assays were performed at 25 °C.

Antigen on surface

C-terminal Avi-tag biotinylated human SIRPα_1, SIRPα_{BIT}, SIRPβ1v1, SIRPβ1v2 and SIRPγ ECD was captured on a streptavidin surface (Biacore) to a capture level allowing the maximum binding (Rmax) < 50 RU. Responses of a concentration series were used to estimate the K_D-obs by single cycle kinetics (SCK). After DRS, a 1:1 Langmuir model was used to fit the kinetic data.

Antibody on surface

Antibodies were captured on an anti-human-IgG (Fc) surface to a capture level allowing the maximum binding (Rmax) < 50 RU. Responses of a concentration series of human SIRPα_1, SIRPα_{BIT}, SIRPβ1v1, SIRPβ1v2 or SIRPγ ECD was used to estimate the K_D-obs by SCK. After DRS, the data were fitted with a 1:1 Langmuir model.

The assay to estimate the observed binding affinity (K_D-obs) between human FcγRI (Sino Biological, 10256-H27H-B) and BYON4228 consisted of capture of recombinant FcγRI receptor containing a C-terminal biotinylated Avi-tag to a streptavidin sensor surface (Biacore). Binding of 5 increasing concentration of BYON4228 was measured by SPR using SCK. The K_D-obs were estimated from a 1:1 Langmuir interaction model fitted to the measured data.

The assay to estimate a K_D-obs between human FcγRIIIa, FcγRIIIb, FcγRIIa (or FcγRIIb (all from ACRO biosystems) and BYON4228 consisted of capture of each Fcγ receptor containing a C-terminal biotinylated Avi-tag to streptavidin sensor tips. Response of a concentration series of BYON4228 was measured simultaneously on eight sensor tips by bio-layer interferometry (BLI, Octet). The data was evaluated by a steady state affinity model.

Cellular binding to SIRP-expressing ExpiCHO-S cells and primary granulocytes

For cellular binding to ExpiCHO-S cells, transiently transfected ExpiCHO-S cells were rapidly thawed at 37 °C in a water bath. Cells were transferred to a tube containing RPMI-1640 with 10% HI FBS, centrifuged at 250-300xg to remove DMSO and the pellet was resuspended to a concentration of $1x10^6$ cells/mL in ice-cold FACS buffer (PBS + 0.1% v/w BSA + 0.02% v/v Sodium Azide (NaN_3)). Then, $1x10^5$ cells/well were added to 96-well V-shaped plates (100 µL/well), centrifuged at 300xg for 3 minutes, and the supernatant was discarded.

For staining of primary cells, heparinized whole blood samples were obtained from Vietnamese cynomolgus monkeys (Labcorp Drug Development, formerly Covance, Germany) and healthy human donors. One mL whole blood was transferred to a 15 mL tube and samples were lysed with ice-cold 1X BD Pharm Lyse lysing solution (555899), until a color change occurred from opaque red to dark/transparent red. After centrifugation, the pellet was again incubated with 5 mL BD Pharm Lyse lysing solution for 5 minutes, washed twice with 5 mL IMDM (Lonza, BE12-722Q) + 10% HI FBS (10100-147, Gibco), and finally the pellet was resuspended in 5 mL IMDM + 10% FBS. Subsequently, $2x10^5$ cells per well were stained in 96-well round-bottom microtiter plates.

For staining, cells were incubated for 30 minutes with 50 µL serial diluted antibodies in ice-cold FACS buffer, washed three times by centrifugation at 300xg for 3 minutes and resuspended in 50 µL APC-conjugated secondary $F(ab')_2$ goat anti-human IgG (Fc fragment specific, Jackson ImmunoResearch, 109-136-098, 1:500, diluted in FACS buffer), and incubated on ice. After 30 minutes of incubation, the cells were washed twice in FACS buffer and then resuspended in 50 µL ice-cold FACS buffer which contained DAPI (diluted to 0.1 µg/mL) for the ExpiCHO-S binding and analysis was performed using flow cytometry (FACSymphony or FACSVerse, BD Bioscience). For ExpiCHO-S binding, the APC-700 MFI was determined after gating on GFP-positive live, single cells. For the mock transfected cells, gating on GFP-positive cells was not possible and therefore gating was performed on viable, single cells. For primary binding to granulocytes, granulocytes gating was based on FSC-A/SSC-A.

HDX-MS

HDX-MS was performed by the Chemical Proteomics Core Facility of the Karolinska Institutet, Sweden. For this, $hSIRP\alpha_{BIT}$ or $hSIRP\alpha_1$ (Fc tail removed with Factor Xa cleavage) were combined with 1:1 molar ratio mAb BYON4228. The volume of the antigen/mAb and control samples were equalized using a 10 kDa protein concentrator. Samples were analyzed in an automated HDX-MS system (CTC Pal/Biomotif HDX) where samples are automatically labeled, quenched, digested, cleaned and separated at 2 °C. Control and antigen/mAb samples were deuterium labeled in triplicate for 4, 10 and 60 minutes. The labeling reaction was quenched by decreasing the pH to ~2.3 and temperature to ~4 °C by adding a solution containing 6 M Urea, 100 mM tris(2-carboxyethyl)phosphine and 0.5% trifluoroacetic acid. Digestion was performed using an immobilized pepsin column (2.1 × 30 mm) at 60 µL /minute, for 2 minutes followed by an on-line desalting step using a 2 mm I.D x 10 mm length C-18 pre-column (ACE HPLC Columns, Aberdeen, UK) using 0.1% formic acid at 400 µl/minutes for 1 minute. Peptic peptides were then separated by a 18 minutes 8-55 % linear gradient of acetonitrile in 0.1% formic acid using a 2 mm I.D x 50 mm length HALO C18/1.8 µm analytical column operated at 60 µL/minute. Peptides were sequenced using an LTQ Elite Orbitrap mass spectrometer (Thermo Fisher Scientific) operated at 120,000 resolution at m/z 400. All HDX MS data was processed by a HDExaminer Version 2.5.1. Mascot was used for peptide identification using a dedicated database, using a 10 ppm precursor tolerance, 0.05 Da MS/MS mass error. Visualizations of 3D protein structures and overlaying binding sites were rendered by PyMol 2.5.2 (Schrödinger). Protein data bank numbers 4CMM ($SIRP\alpha_1$) and 2JJS ($SIRP\alpha_{BIT}$) were used (7, 8).

CD47-bead and mAb binding to U937 cells and primary cells

Thawed PBMCs (125.000 cells/well) or cultured U937 (50,000 cells/well) cells were stained in a 96-well U-bottom plate with 50 µl diluted AF647-labeled antibodies at the indicated final concentration (Invitrogen, A20186) plus Fc block (Miltenyi, 130-059-901, used for PBMCs only) for 30 minutes at 4 °C and subsequently, 45 µL cell solution (U937) or 40 µL cell solution (PBMCs) was transferred to a new 96-well U-bottom plate containing 5 µL 10% CD47-bead solution or 10 µL 5% CD47-bead solution plus anti-CD3 APC-H7 (BD Pharmingen, 560176, clone SK3, 20x diluted) and anti-CD14 PerCp-Cy5.5 (BD Pharmingen, 550787, clone M5E2, 20x diluted), respectively. This plate was incubated for 30 minutes at 4 °C, the cells were washed twice, resuspended in 100 µL ice-cold FACS buffer containing DAPI (0.1 µg/mL) and analyzed using flow cytometry (FACSVerse, BD Biosciences). MFIs (FITC and AF647) were

determined on DAPI-negative single cells (U937) and DAPI-negative CD3-positive or CD14-positive single cells (PMBCs).

Blocking of CD47-induced signaling (PathHunter)

Jurkat SIRPα_{BIT} signaling cells (DiscoverX) were incubated with a concentration range of anti-SIRP antibody in combination with CD47 ligand cells. Ratio of Jurkat SIRPα_{BIT}:ligand cells used were 1:2 for Raji cells, 1:1.5 for SK-BR-3 cells and 1:2.5 for A431 cells. The assay was performed in a 384-wells plate. 12.5 µL SIRPα_{BIT} signaling cell suspension ($0.8x10^6$ cells/mL) was added to each well followed by 2.5 µL of a 11x concentrated anti-SIRPα antibody solution in PBS-0.1% BSA. The assay was started by adding 12.5 µL CD47 ligand cell suspension ($1.6x10^6$ Raji cells/mL, $1.2x10^6$ SK-BR-3 cells/mL, and $2.0x10^6$ A431 cells/mL). Plates were incubated for 5 hours at 37 °C. After incubation, 2 µL of reagents A (DiscoverX detection kit) in PBS-BSA 0.1% solution was added. Plates were incubated for 30 minutes on a shaker (300 rpm), in the dark, at room temperature (RT). Then, 10 µL of reagents B (DiscoverX detection kit) in PBS-BSA 0.1% solution was added. Plates were incubated for 1 hour on a shaker (300 rpm) in the dark at RT and luminescence was measured (Envision, PerkinElmer).

Complement dependent cytotoxicity (CDC) assay

Cells were incubated with diluted antibodies (final concentration 10 µg/mL) for 15 minutes at RT in a volume of 87.5 µL in a 96-wells plate. Then, 12.5 µL baby rabbit complement serum (BRC; Bio-Rad) or HI BRC (30 minutes at 56 °C) was added and incubated for 1 hour at 37 °C and live cells were determined using CTG (Promega) by measuring luminescence (Envision, PerkinElmer). Percentage survival was calculated by dividing the measured luminescence for each mAb by the measured luminescence of the corresponding no mAb control cells (0% BRC, 12.5% HI BRC or 12.5% BRC) multiplied by 100.

NK cell-based antibody dependent cellular cytotoxicity (NK-ADCC)

NK cells were isolated from buffy coats using the human NK cell isolation kit (Biolegend, 480054) and were used freshly or thawed to determine NK-ADCC. NK cells (effector cells, E) were incubated for 24 hours with 15,000 MOLM-13 cells (target cells, T) and antibodies in 96-well plates in 150 µL at an effector:target ratio of 4:1. Cytotoxicity was determined using the Cytotoxicity detection kit PLUS (LDH, 4744934001, Roche/Merck Life Science) and absorbance was measured (Envision, PerkinElmer). For each sample, the absorbance (A) was calculated as the absorbance at 490 nm minus the background absorbance at 630 nm. The maximally-observed absorbance ($A_{(max\ T)}$) was obtained by chemical lysis of target cells. The % killing = $(A_{(sample)} - A_{(E\ only)} - A_{(T\ only)}) / (A_{(max\ T)} - A_{(T\ only)}) \times 100$. The % antibody-induced killing = $\%\ killing_{(E+T+Ab)} - \%\ killing_{(E+T)}$.

Neutrophil-ADCC

Human polymorphonuclear cells, which are mainly neutrophils, were isolated by density gradient centrifugation and RBC lysis and activated at a concentration of $5x10^6$ cells/mL at 37 °C for 30 minutes with 10 ng/mL of human GM-CSF (Peprotech). Target cells were labeled with 100 µCi Cr-51 (PerkinElmer) for 90 minutes at 37 °C. Then after washing, target cells, effector cells and antibodies were co-cultured for 4 hours or 20 hours (SW48 cells) at 37 °C and 5% CO_2 at an effector: target ratio of 50:1. The supernatant was harvested and analyzed

for radioactivity in a MicroBeta^2 Microplate Counter (PerkinElmer). The percentage of killing was calculated as [(experimental release - spontaneous release)/(total release - spontaneous release)] *x* 100%. The spontaneous release is defined as the release from target cells in absence of neutrophils. The total release is defined as the release from target cells in presence of 0.05% Triton-X100. All conditions were measured in triplicate. Normalization was calculated using the bottom and top values of the fitted curves as '(value –bottom)/(top – bottom) *x* 100%'.

ADCP using confocal microscopy

ADCP using confocal microscopy was performed with CD20-positive target cell lines. Monocytes were isolated from buffy coats using the RosetteSep human monocyte enrichment cocktail (STEMCELL technologies, 15028) according to manufacturer's instructions and frozen. Thawed monocytes were seeded at 30,000 cells/96-well in 100 µL and differentiated to macrophages using 50 ng/mL M-CSF (MACS Miltenyi Biotec) in medium (IMDM without phenol red, + 8.5% HI FBS + penicillin/streptomycin + glutaMAX) for 7 days. On day 3 or 4, the medium was aspirated and fresh medium containing 50 ng/mL M-CSF was added. For the phagocytosis assay, target cells were labeled with 5 µM CellTrace Far Red (CTFR, Live Technologies) for 20 minutes at 37 °C. After washing, target cells were resuspended to 0.6x10^6 cells/mL in assay medium (IMDM without phenol red + 0.5% HI FBS + penicillin/streptomycin + 100 µg/mL Privigen-IVIg). A master plate was generated with assay medium containing anti-TAA (e.g. rituximab or daratumumab) plus serial diluted anti-SIRP-mAb or isotype controls + target cells (30,000/100µL). After aspiration of medium from the macrophages, 100 µL/well of the master plate was directly transferred to the macrophage plate. After 3 hours incubation at 37 °C + 5% CO_2, non-adherent cells were removed by washing twice with PBS and 65 µL fixation solution was added (BD cytofix, BD biosciences) and incubated for 10 minutes on ice and 10 minutes at RT. Cells were washed with PBS, and 100 µl FACS buffer (PBS + 0.1% v/w BSA + 0.02% v/v Sodium Azide (NaN_3) was added. For CD19 staining, FACS buffer was removed and 50 µL FACS buffer containing anti-CD19 PE (1:200, clone REA675, MACS Miltenyi Biotec) + Hoechst 33342 (10 µg/mL) was added and incubated for 30 minutes in the dark at RT. Cells were washed twice with FACS buffer and measured on the ImageXpress (Molecular Devices). Full well single plane fluorescent images were acquired. Data was analyzed using MetaXpress, and the PI was determined. PI = number of phagocytosed tumor cells (CTFR-positive CD19-negative)/total number of macrophages (Hoechst-positive CTFR-negative) *x* 100. The fold enhancement= [PI at 80 ng/mL rituximab or 5 ng/mL daratumumab + maximum concentration of anti-SIRP mAb/F(ab')$_2$]/ [PI at 80 ng/mL rituximab or 5 ng/mL daratumumab].

ADCP using live-cell imaging and pHrodo

ADCP using live-cell imaging and pHrodo was performed for CD20-negative cell lines and Daudi cells. Macrophages were differentiated from monocytes as described in 'ADCP using confocal microscopy'. Target cells were labeled with pHrodo (Sartorius, 0039) for 60 minutes in a 37 °C waterbath. Cells were washed twice and resuspended at 0.6x10^6 cells/mL in assay medium (IMDM without phenol red + 0.5% HI FBS + penicillin/streptomycin + 100µg/mL Privigen IvIg). A master plate was generated with assay medium containing anti-TAA plus serial diluted or a fixed concentration of BYON4228 or isotype controls + target cells (30,000 cells/well). After aspiration of medium from the macrophages, 100 µL/well of the master plate was directly transferred to the macrophage plate. The plate was placed in the IncuCyte

(37 °C + 5% CO_2) for 8 hours. Images were taken every 30 or 60 minutes. Data was analyzed using IncuCyte 2019B rev2 software and phagocytosis was determined by selection of pHrodo bright objects. % phagocytosed tumor cells = number of phagocytosed tumor cells (pHrodo bright)/total number of tumor cells (pHrodo low) *x* 100. ADCP fold enhancement = [% phagocytosed tumor cells at 10 µg/mL anti-SIRP mAb in combination with panitumumab, cetuximab or daratumumab]/ [% phagocytosed tumor cells with panitumumab, cetuximab or daratumumab only or isotype control mAb] or = [% phagocytosed cells at 31.6 µg/mL anti-SIRP]/ [% phagocytosed cells at effector + target].

Generation and characterization of huSIRPα$_{BIT}$-transgenic mice

Mice were generated that expressed human SIRPα$_{BIT}$. A full-length human SIRPα$_{BIT}$ cDNA sequence was inserted into the *Gt(ROSA)26Sor* locus and crossed to *Cebpa*$^{Cre/+}$ mice (9), creating human SIRPα$_{BIT}$-transgenic mice with a selective expression on myeloid cells (Rosa26-stop^{flox}human SIRPα$_{BIT}$ x *Cebpa*$^{Cre/+}$ (9, 10), named huSIRPα$_{BIT}$ mice). These mice where then crossed with scid mice to yield huSIRPα$_{BIT}$-scid mice. Western blotting of bone marrow-derived macrophage samples was performed after cultured for 7 days with CSF-1. Endogenous mouse SIRPα and transgenic human SIRPα were detected simultaneously using rabbit antibodies directed against the SIRPα cytoplasmic domain (Abcam #AB8120). For FACS analysis whole blood was lysed with lysis buffer and blocked with CD16/CD32 blocking antibody clone 2.4G2 for 30 minutes on ice. Cells stained with anti-human SIRPα in 20% normal goat serum containing PBS, washed 1x in PBS + 3% albumin and stained with the mix of directly labelled antibodies F4/80 APC-Cy7, CD19 PerCP-Cy5.5, CD3 Pacific Blue, mouse SIRPα APC, CD11b AF488 and a secondary antibody anti-human IgG AF568. For ADCC assays, bone marrow isolated neutrophils were overnight stimulated with human G-CSF (10 ng/mL) and IFNγ (50 ng/mL). SK-BR-3 target cells were labelled with 100 mCi Cr-51 (PerkinElmer), incubated in RPMI culture medium supplemented with 10% (v/v) fetal calf serum together with stimulated neutrophils in an effector:target ratio of 50:1 in the presence of trastuzumab and anti-SIRPα antibody 12C4 (4). After incubation of target cells and effector cells for 4 hours, supernatant was harvested and analyzed for radioactivity in a gamma counter (Wallac). The percentage of cytotoxicity was calculated as [(experimental cpm-spontaneous cpm)/(total cpm- spontaneous cpm)] *x* 100%. All conditions were measured in triplicate.

PK mouse

BYON4228 was administered by injection into the caudal vein (IV), or injection into the peritoneal cavity (IP) of huSIRPα$_{BIT}$ transgenic mice or C57BL/6mice at doses; 3, 10 or 30 mg/kg. The administration volume was 10 mL/kg. For repeat IP dosing BYON4228 was administered every 3 days for 6 times (Q3Dx6). Blood was collected into collection tubes with anticoagulant (K2 EDTA) and plasma was used for PK analysis. BYON4228 plasma levels were determined as explained in the supplementary method section ‘generic antibody assay for determination of BYON4228 levels in mice and cynomolgus monkeys’.

Raji xenograft in huSIRPα$_{BIT}$ transgenic mice

Tumors were induced by subcutaneous injection of $2x10^7$ Raji cells in RPMI 1640 medium into the flank of female huSIRPα$_{BIT}$-scid transgenic animals. Raji tumor cell implantation was performed 24 to 72 hours after a whole body irradiation with a γ-source (1.44 Gy, 60Co).

BYON4228 was administered IP 3 times a week for 4 weeks ((Q2Dx3) x 4) at a dose of 5 mg/kg. Rituximab was administered at 1 mg/kg IP.

Safety evaluation of BYON4228

BYON4228 was studied *in vitro* for its propensity of hemolysis and RBC clumping in human whole blood as well as precipitate formation in plasma.

A cytokine release assay was performed using heparinized-preserved whole blood obtained from 18 healthy donors who provided informed consent (Immunomonitoring services, Sanquin Pharma & Biotech services). For this, BYON4228 (10 µL) was added to round-bottom 96-well plates, whole blood was added (190 µL) and the plates were incubated overnight at 37 °C in 5% CO_2. The supernatants were assayed for 18 different cytokines and chemokines using The Human ProcartaPlex™ Inflammation Panel on a Luminex FlexMap 3D.

A single dose range toxicity and PK study was conducted in naïve cynomolgus monkeys (*Macaca fascicularis*, 1 animal/sex/group) at 0, 1, 3, 10, 30 and 100 mg/kg BYON4228 via a 30 or 100 minutes IV infusion. All animals were euthanized at day 22 for necropsies.

A 5-cycle toxicity study was performed in which four groups of naïve cynomolgus monkeys (*Macaca fascicularis*, 5 animals/sex/group) received 5 IV, 30 minutes infusions of 0, 3, 10, 30 mg/kg, each 1 week apart. Two animals/sex in the control group and three animals per sex per dose group were sacrificed one week after the last dose, whereas 2 animals per sex per group were allowed an additional recovery period of 7 weeks and were then sacrificed. In-life evaluations included mortality/moribundity, clinical observations, body weight, food consumption, standard neurologic and respiratory/cardiovascular safety, clinical pathology, urinalysis (including urine chemistry) and pharmacokinetics (including ADAs). Upon terminal sacrifice, macroscopic and microscopic evaluation of selected tissues was performed.

Generic antibody assay for determination of BYON4228 levels in mice and cynomologus monkeys

A biotinylated camel single chain domain specifically directed to the constant domains of human IgG (CaptureSelect human IgG-Fc PK Biotin Conjugate, Thermo Fisher Scientific) was used for capturing the analyte. This antibody was coated to a streptavidin-coated ELISA plate (EvenCoat Plate, R&D Systems). An horseradish peroxidase HRP-labeled antibody directed against the constant domains of human IgG (sheep anti-human immunoglobulins (pre-adsorbed with monkey IgG) – peroxidase conjugate, The Binding Site) was used for detection.

Specific antibody assay for determination of BYON4228 levels in cynomologus monkeys A biotinylated anti-idiotype camel single chain domain directed towards the complementarity determining region (CDR) of BYON4228 was used for capturing the analyte. This antibody was coated to a streptavidin-coated ELISA plate (EvenCoat Plate, R&D Systems). A second HRP labeled anti-idiotype camel single chain domain also directed towards the CDR of BYON4228 was used for detection, followed by the addition of 3,3',5,5'-Tetramethylbenzidine (TMB) (TeBu-Bio, Cat. No. TMB100). The color reaction was stopped with H2SO4 and the plate was read at 450 and 630 nm with a plate reader (Varioskan 3001). Each analytical run included appropriate calibrators and quality-control samples.

PK evaluation

PK was evaluated using non-compartmental analysis for IV bolus injection or extravascular injection in Phoenix WinNonlin version 8.2 or higher. Derived PK parameters were rounded to three significant figures. PK figures were made in Graphpad Prism.

References

1. Poirier NM, C.; Van-Hove, B.; Gauttier, V.; Thepenier, V.; Pengam, S., inventor; OSE Immunotherapeutics, assignee. New Anti-SIRPa Antibodies and Their Therapeutic Applications2017.
2. Abbasian MC, H.H.; Escoubet, L.; Fenalti, G.; Hariharan, K., Leung, M.W.L.; Mavromattis, K., Micolon, D.P.; Raymon, H.K.; Santos, C.S.; Sun, J.; Trout, C.V., inventor; Celgene Corporation, assignee. SIRPα Binding Proteins and Methods of Use Thereof2020.
3. Liu J, Volkmer, J.P., inventor; Forty Seven, Inc., assignee. Anti-SIRP-Alpha Antibodies and Related Methods2019.
4. Zhao XW, van Beek EM, Schornagel K, Van der Maaden H, Van Houdt M, Otten MA, et al. CD47-signal regulatory protein-alpha (SIRPalpha) interactions form a barrier for antibody-mediated tumor cell destruction. Proc Natl Acad Sci U S A. 2011;108(45):18342-7.
5. Treffers LW, van Houdt M, Bruggeman CW, Heineke MH, Zhao XW, van der Heijden J, et al. FcgammaRIIIb Restricts Antibody-Dependent Destruction of Cancer Cells by Human Neutrophils. Front Immunol. 2018;9:3124.
6. van Rees DJ, Brinkhaus M, Klein B, Verkuijlen P, Tool ATJ, Schornagel K, et al. Sodium stibogluconate and CD47-SIRPalpha blockade overcome resistance of anti-CD20-opsonized B cells to neutrophil killing. Blood Adv. 2022;6(7):2156-66.
7. Hatherley D, Graham SC, Turner J, Harlos K, Stuart DI, Barclay AN. Paired receptor specificity explained by structures of signal regulatory proteins alone and complexed with CD47. Mol Cell. 2008;31(2):266-77.
8. Hatherley D, Lea SM, Johnson S, Barclay AN. Polymorphisms in the human inhibitory signal-regulatory protein alpha do not affect binding to its ligand CD47. J Biol Chem. 2014;289(14):10024-8.
9. Wolfler A, Danen-van Oorschot AA, Haanstra JR, Valkhof M, Bodner C, Vroegindeweij E, et al. Lineage-instructive function of C/EBPalpha in multipotent hematopoietic cells and early thymic progenitors. Blood. 2010;116(20):4116-25.
10. Koentgen F, Lin J, Katidou M, Chang I, Khan M, Watts J, et al. Exclusive transmission of the embryonic stem cell-derived genome through the mouse germline. Genesis. 2016;54(6):326-33.